1-1-2013

Efficient Regeneration Of Chemical Solvents For Carbon Dioxide Capture By Polymeric Membrane Contactors

Xuefei Zhang

EFFICIENT REGENERATION OF CHEMICAL SOLVENTS FOR CO_2 CAPTURE BY POLYMERIC MEMBRANE CONTACTORS

by

Xuefei Zhang
Bachelor of Engineering, Tianjin University, 2001
Master of Science, The University of Maine, 2007

A Dissertation

Submitted to the Graduate Faculty

of the

University of North Dakota

In partial fulfillment of the requirements

for the degree of

Doctor of Philosophy

Grand Forks, North Dakota
August
2013

This dissertation, submitted by Xuefei Zhang in partial fulfillment of the requirements for the Degree of Doctor of Philosophy from the University of North Dakota, has been read by the Faculty Advisory Committee under whom the work was done, and is hereby approved.

_____
Brian Tande

_____
Steven Benson

_____
Gautham Krishnamoorthy

_____
Alena Kubatova

_____
Qianli Chu

This dissertation is being submitted by the appointed advisory committee as having met all of the requirements of the Graduate School at the University of North Dakota and is hereby approved.

_____
Wayne Swisher
Interim Dean of the Graduate School

Date: _____

PERMISSION

Title Efficient Regeneration of Chemical Solvents for CO_2 Capture by Polymeric Membrane Contactors

Department Chemical Engineering

Degree Doctor of Philosophy

In presenting this dissertation in partial fulfillment of the requirements for a graduate degree from the University of North Dakota, I agree that the library of this University shall make it freely available for inspection. I further agree that permission for extensive copying for scholarly purposes may be granted by the professor who supervised my dissertation work or, in his absence, by the Chairperson of the department or the dean of the Graduate School. It is understood that any copying or publication or other use of this dissertation or part thereof for financial gain shall not be allowed without written consent. It is also understood that due recognition shall be given to me and to the University of North Dakota in any scholarly use which may be made of any material in my dissertation.

_____

Xuefei Zhang

Date 18 July 2013

ACKNOWLEDGMENTS

I give my sincere gratitude to my advisor Dr. Brian Tande for providing me with this research opportunity and support through all these years of study. I appreciate Dr. Steve Benson, Dr. Gautham Krishnamoorthy, Dr. Alena Kubatova and Dr. Qianli Chu for serving as advisory committee members and helping me with my study in class and in research with their expertise. I thank Dr. Wayne Seames for introducing me to this project. I appreciate Dr. Zhengwen Zeng who also served on my committee and encouraged me a lot during his stay at UND.

I appreciate Mr. David Hirschmann, Mr. Harry Feilen, and Mr. Joe Miller of the chemical engineering department at UND for their help in building the experimental system used in this research. I thank my peer graduate students, David James, Hai Wang, Michael Linen, Dennis Sisk, Hassan Sater, Samir Dahal, Alireza Pesaran, for helping in almost every aspect. They shared knowledge, skills, tips and information, as well as many facilitated useful discussions and troubleshooting ideas. Working with them has made this process much easier and more enjoyable.

I am grateful for the financial support provided by the Department of Energy and National Energy Technology Laboratory under grant DE-FE0002196.

ABSTRACT

Although extensive research attention has been drawn to using membranes for carbon dioxide (CO_2) capture from flue gas, the use of membranes for stripping CO_2 solvents has rarely been studied. The technical feasibility of using polymeric membrane based separation technology to recover CO_2 from CO_2 saturated chemical solvents such as monoethanolamine is investigated in the present research. A membrane system was built to study the performance of several common polymeric porous membranes for the recovery of CO_2 from saturated aqueous MEA solution by the thermal swing process. The stripped CO_2 gas was swept by mass flow controlled N_2 reference gas and was measured by a non-dispersive infrared CO_2 analyzer and gas chromatography. Substantial CO_2 permeation flux through the membrane together with superior selectivity suggests the promises of membrane contactors as an alternative stripping configuration for CO_2 recovery.

Parametric screening design of experiments studied parameters of process temperature, retentate flow rate, and sweep gas rate. Process temperature was identified as the only significant factor, which is consistent with individual parametric study results. Heat energy efficiency characterization of this system showed that roughly half of the heat energy was used for the stripping process at 80ºC and above. The membrane material candidates screening experiment results showed that polypropylene and polytetrafluoroethylene porous membranes outperformed polyester, polyamide, polyvinylidene fluoride, polysulfone and cellulose acetate. Compositional, structural and surface morphological characterization was also utilized on the membranes before

and after this process. Mass transfer mechanism study and mass transfer coefficients calculation reveals that the liquid boundary layer resistance is responsible for more than 90% of the overall mass transfer resistance, much greater than either the membrane resistance or gas layer resistance. Membrane wetting and fouling effects were found to deteriorate membrane performance. Polypropylene membranes with different pore size were studied and compared. There was no significantly change of CO_2 flux for membrane pore size from 0.1 μm to 2.5 μm. The membrane with pore size of 0.6 μm was found to have best selectivity. The energy utilization efficiency did not change significantly for membranes with different pore size. Membranes with pore size 2.5 μm and below were found to be not wetted during the course run and membranes with pore size of 5 μm and 10 μm were wetted during the process.

Keywords: *carbon dioxide regeneration, carbon dioxide recovery, carbon dioxide solvent stripping, polymeric membrane contactors, low temperature stripping.*

TABLE OF CONTENTS

LIST OF TABLES

LIST OF FIGURES

NOMENCLATURE

Abbreviations

AMP	2-amino-2-methyl-1-propanol
ATR	Attenuated Total Reflectance
CA	Cellulose Acetate
CE	Cellulose Ester
CFD	Computational Fluid Dynamics
DOE	Department of Energy
DEA	Diethanolamine
DSC	Differential Scanning Calorimetry
EIA	Energy Information Administration
FID	Flame Ionization Deterctor
FTIR	Fourier Transform Infrared Spectroscopy
GC	Gas Chromatography
IR	Infrared
LEPW	Liquid Entry Pressure of Water
MD	Membrane Distillation
MDEA	N-methyldiethanolamine
MEA	Monoethanolamine
NDIR	Non-dispersive Infrared
NGCC	Natural Gas Combined-Cycle
PA	polyamide
PES	polysulfone
PETE	Polyethylene terephthalate
PTFE	Polytetrafluoroethylene
PVDF	polyvinylidene fluoride
SEM	Scanning Electron Microscopy
TPC	Temperature Polarization Coefficient
TCD	Thermal Conductivity Detector
UV-vis	Ultraviolet-visible

Chemical Species

CO	Carbon Monoxide
CO_2	Carbon Dioxide
H_2	Hydrogen
H_2O	Water
HCl	Hydrochloric Acid
He	Helium
N_2	Nitrogen

O_2	Oxygen
Se	Selenium
Zn	Zinc

Symbol and Meaning

A	Absorbance
B	Geometry factor
C	Concentration
c_p	Specific heat
d_p	Diameter of pores
D	Diffusivity coefficient
D_k	Knudsen diffusivity
D_G	Diffusivity in the gas phase
D_E	Combination of Knudsen and molecular diffusivity coefficient
h	Heat transfer coefficient
K	Equilibrium constant
k_B	Boltzman constant
k_L	mass transfer coefficient through melt
k_E	mass transfer coefficient at surface
k_U	mass transfer coefficient through pores
K	Equilibrium constant
L	Length
s	Solubility coefficient
k_G	Gas mass transfer coefficient
k_L	Liquid mass transfer coefficient
k_M	Membrane mass transfer coefficient
k_{OL}	Overall mass transfer coefficient
M_i	Molecular weight of species i
P	Pressure
Q	Amount of heat
R	Gas constant
t	Time
T	Absolute temperature
T_f	Viscous Flow Temperature
T_g	Glass Transition Temperature
T_m	Melting Point
V	Volume

Dimensionles Numbers

E	Enhancement factor
Gr	Grashof number
H	Henry's constant
Nu	Nusselt number
Pr	Prandtl number

Sc	Schmidt number
Sh	Sherwood number
Re	Reynolds number

Greek Symbols

α	CO_2 loading
κ/ε	Lennard-Jones parameter
μ_γ	viscosity
π	3.14159….
ρ	density
σ	collision diameter
ε	Membrane porosity
τ	Membrane tortuosity
θ	Contact angle
λ	Mean free path

1. INTRODUCTION

This chapter overviews the carbon dioxide (CO_2) emission due to the increasing energy demand and identifies coal-fired power plants a large point source for reducing CO_2 emissions. Aqueous amine absorption/stripping is an important technological option. However, it suffers from heavy energy penalty within the regeneration process. Methods for more energy efficient CO_2 regeneration using membrane contactors are proposed. The objectives and scope of this work are addressed.

1.1. Objectives and Scope

Coal-fired power plants are a significant source of atmospheric CO_2 emissions contributing to more than one-third of the anthropogenic CO_2 emissions in the United States (Carapellucci & Milazzo, 2003). With the decline in petroleum and natural gas reserves, coal usage worldwide is expected to increase by 2% per year from 2005 to 2030 (Hrdlicka, Seames, Mann, Muggli, & Horabik, 2008), as an abundant and widely distributed energy resource. Under the conflict of the increasing energy demands and the greenhouse gas driven environmental concerns, the capture and storage of CO_2 is considered one of the potential solutions to alleviate this problem. There is significant interest in developing technologies that allow for the efficient capture of carbon from coal-based power systems.

The overall objective of this study is to research the applicability of polymeric membrane contactors for CO_2 regeneration application. Theoretical predictions and experiments were carried out by analyzing the characteristics of membranes suitable for this application. CO_2 regeneration efficiency was studied with varied process parameters. Specific objectives to address this goal include:

1. Design, construct and validate a continuous lab-scale test system to measure membrane performance.
2. Assess the capability of a range of porous membrane contactors to regenerate chemical solvents for CO_2 capture.
3. Characterize suitable membrane materials for the CO_2 stripping application. This stage proves the concept and explores the potential for commercial application of membrane contactor strippers.
4. Decide appropriate operation window for this process. Study and optimize the CO_2 regeneration efficiency with a parametric study of operating temperatures and pressures, feed solution flow rates, and sweep gas flow rates.
5. Investigate how mass transfer is affected by different chemical compositions and structures of membranes, such as membrane hydrophilicity and hydrophobicity, as well as membrane pore size.
6. Investigate the effects membrane configurations have on the mass transfer process, including both flat sheet configuration and hollow fiber modules. Accumulate experience for more efficient and smarter design.

1.2. Dissertation Outline

The remainder of this dissertation is outlined as follows: Chapter 2 reviews the CO_2 capture technologies, the chemical solvents used for CO_2 capture and regeneration. Advantages and disadvantages of membrane process are outlined. Membrane materials selection criteria and concerns are discussed and potential membrane candidates are provided. Membrane characterization techniques for studying solvent interaction and compatibility are reviewed as well as previous mass transfer models developed.

Chapter 3 presents the detailed design, analytical methods and validation results of the proposed experimental system. Next, chapter 4 details the experimental results of the porous membrane materials screening study and identifies promising membrane candidates. After that, chapter 5 explains results of the parametric study results in different approaches and methodologies. Mass transfer mechanism and energy efficiency analysis are also discussed.

Chapter 6 presents the membrane pore size screening study and offers relatively optimized pore size considerations. Finally, chapter 7 concludes the present work.

2. BACKGROUND AND LITERATURE REVIEW

In this chapter several topics are discussed. First, technological approaches for CO_2 capture are reviewed. Post-combustion approach, especially aqueous amine absorption/stripping as an important option is discussed. Then Section 2.4 reviews alkanolamine solvents, especially MEA. Section 2.5 overviews general membrane technology, outlines its advantages and disadvantages, and reviews membrane research for CO_2 regeneration. Section 2.6 proposes membrane materials selection criteria. Section 2.7 introduces basic techniques that will be used for membrane material characterization in this study. Section 2.8 presents details of a membrane mass transfer model previously developed as well as a mass transfer coefficient calculation methodology.

2.1. CO_2 Capture from Coal-Fired Power Plants

The primary approaches for reducing CO_2 emissions from coal-based energy systems include (1) improving coal-to-electric power conversion and utilization efficiency, (2) utilizing renewable fuel resources and (3) capturing and sequestering the CO_2 emitted from the combustion. Improved coal utilization efficiency alone cannot significantly reduce CO_2 emissions. Renewable energy sources such as wind, solar, and the use of biomass as a fuel only account for a small portion of the current total energy consumption (Figure 2-1). According to the U.S. Energy Information Administration (EIA), energy consumption is far from sufficient to

satisfy future domestic energy demands based on current projections (Figure 2-1). Thus CO_2 capture and sequestration represents an attractive strategy for coal-based power systems.

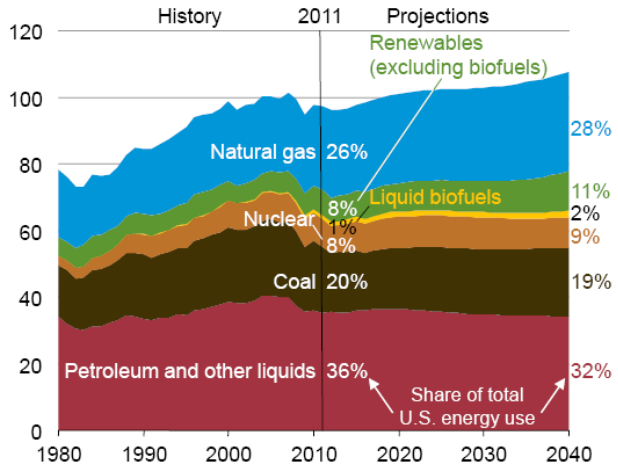

(a)

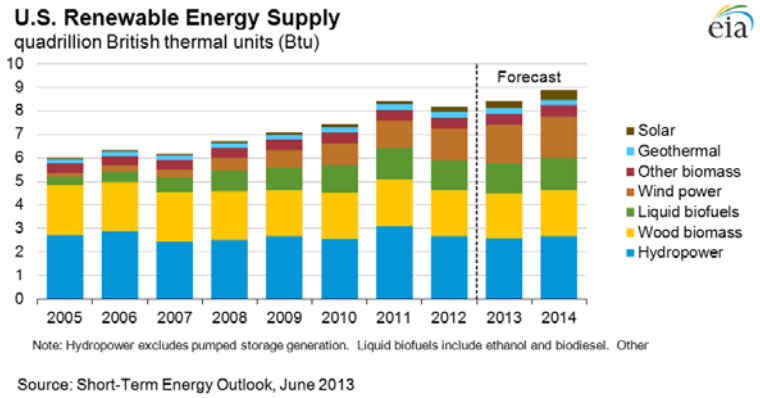

(b)

Figure 2-1 The comparison of renewable energy sources to domestic energy demand (a) primary energy use by fuel, 1980-2040 (quadrillion Btu)(EIA, 2013a); (b) domestic renewable energy supplies(EIA, 2013b)

CO_2 capture involves the separation of CO_2 from anthropogenic emission sources and/or the atmosphere and the recovery of a concentrated stream of CO_2 that is amenable to

sequestration or conversion. Three main approaches and research challenges for CO_2 capture are illustrated in Figure 2-2.

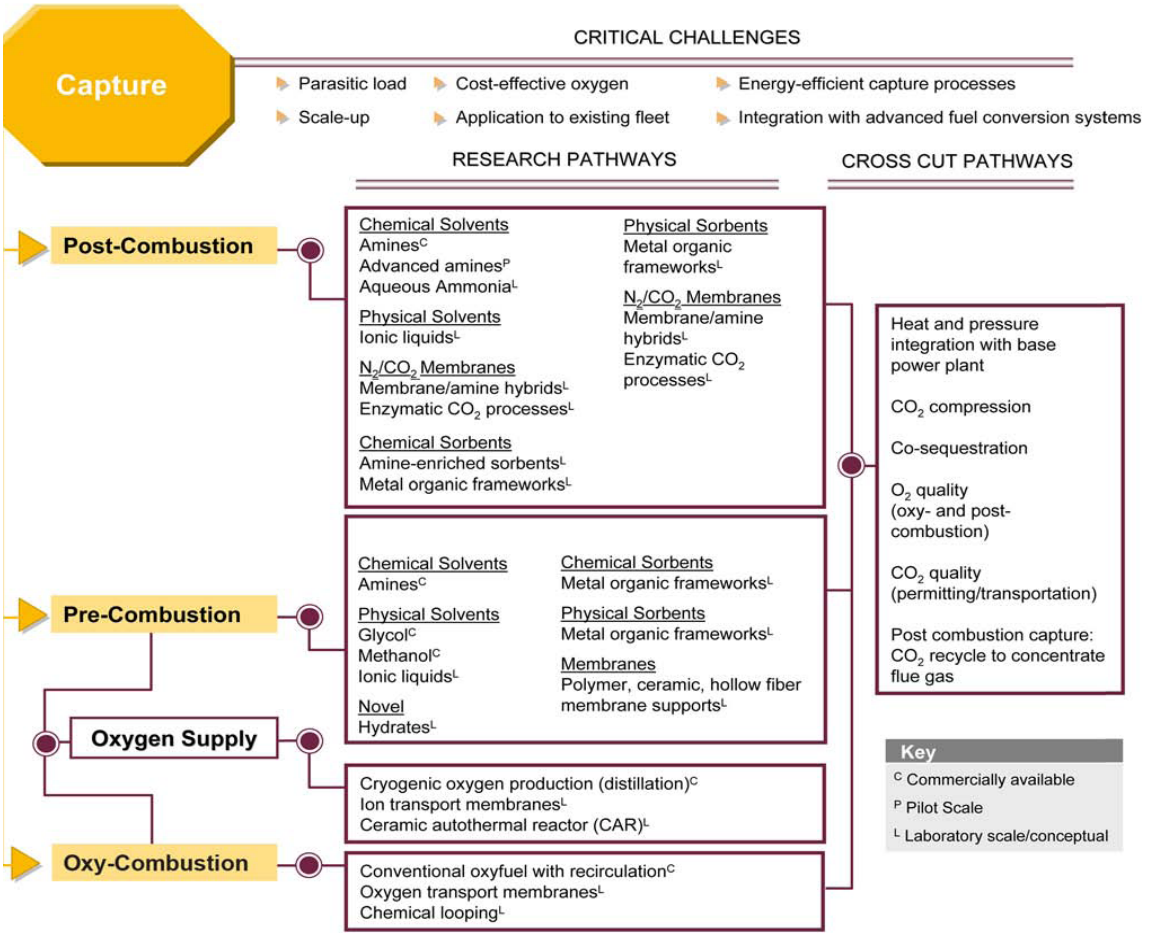

Figure 2-2 CO_2 capture pathways (DOE, 2007)

Post-combustion approach captures the CO_2 by separating it from other constituents in the flue gas. Because of the low concentrations of CO_2 in most pulverized coal (pc)-fired power plants, the easiest way to achieve this is by the use of a liquid solvent. For a modern pc power plant or a natural gas combined-cycle (NGCC) power plant, most proposed post combustion capture systems employ an organic solvent such as monoethanolamine (MEA) in an amine scrubber (Rochelle, 2009).

The pre-combustion process of CO_2 removal involves first gasifying the raw fuel in a reactor at high temperatures with steam and oxygen, creating mainly CO and H_2 (syngas). A shift reactor is then used with more steam to produce a gas stream rich in H_2 and CO_2. The CO_2 in this stream can be separated more easily than CO_2 in a traditional coal combustion flue gas stream because of the higher concentration of CO_2 (generally 15%–60%) and the higher-pressure profiles.

The third approach is known as oxyfuel combustion and it involves replacing the typical combustion air (21% O_2 and 79% N_2) with a CO_2 and O_2. In this concept, an air separation unit is used to produce a pure O_2 stream that is combined with CO_2 and H_2O derived from recycled flue gas. This gas mixture replaces the air used to combust the fuel and results in a flue gas that has very high concentrations of CO_2 (greater than 80%), thereby making the CO_2 easier to capture. Another advantage of this method is the reduction of thermal NO_x by removing N_2 prior to combustion.

2.2. Post-Combustion CO_2 Capture

CO_2 post-combustion capture can be achieved by two steps, (1) the capture of CO_2 from emission sources and/or the atmosphere, and (2) the recovery of a concentrated stream of CO_2 that is amenable to sequestration or conversion. Capture and separation accounts for 60% of the costs for CO_2 sequestration (Yang et al., 2008). Current CO_2 separation processes are technically feasible, but the associated costs, such as solvent regeneration, must be reduced to avoid substantial increases in power generation costs.

Amine absorption/stripping with MEA is state of the art post-combustion CO_2 capture technology. It is the lead mature technology for commercialization and has the fewest hurdles for full-scale implementation. Figure 2-3 shows a typical flow diagram for an MEA absorption/stripping system.

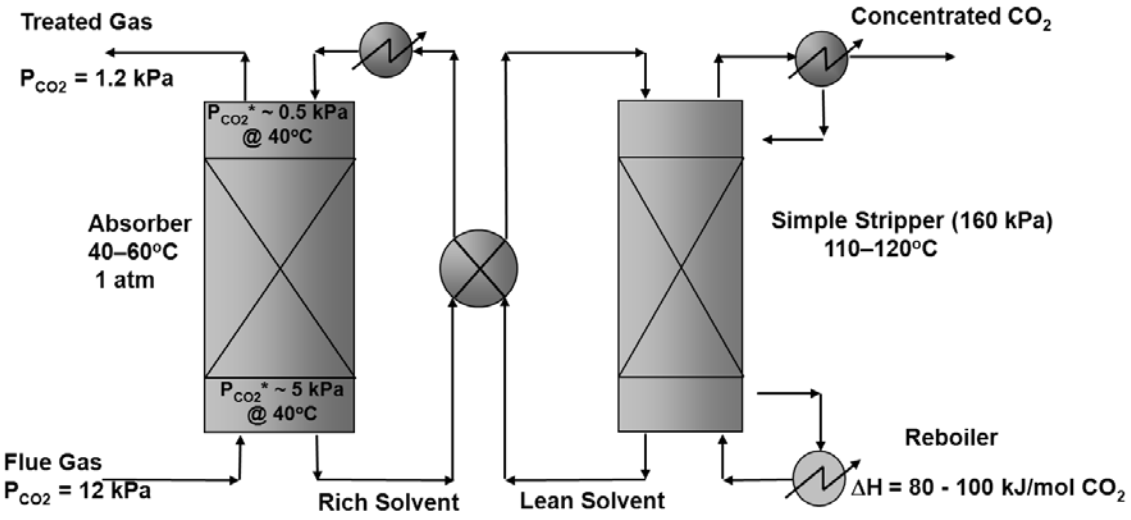

Figure 2-3 Typical process flow diagrams for amine absorption/stripping system (Oyenekan, 2007)

Depending on the process and the fuel feedstock, flue gas contains approximately 10% CO_2. After combustion, it is treated for fly ash and sulfur removal, desiccated and cooled to around 40^{o}C. Then flue gas stream enters at the bottom of the absorber and is counter-currently contacted with a cool CO_2 stripped (usually 0.2-0.4 moles CO_2 per mole MEA) solution with 15-30 wt% MEA in water from the top. The CO_2 captured flue gas, with a base target of 90% CO_2 removal, exits at the top of the absorber and meets a water wash to reduce the amount of MEA loss in the vapor phase. The CO_2 rich (usually 0.4-0.5 moles CO_2 per mole MEA) solution exits the bottom of the column and is preheated in the counter-current heat exchanger by the CO_2 lean amine from the stripper. The CO_2 is liberated from the MEA solution in the stripper by heating

solution temperatures up to approximately 120^{o}C through heat steam addition from the reboiler. Finally, The CO_2 rich gas stream exiting at the top of the stripper is dehydrated and compressed for the subsequent transportation and sequestration. The hot lean amine stream exiting the bottom of the stripper is recycled to the cross-heat exchanger and back to the absorber for continuous run.

In general, amine stripping suffers from high-energy consumption. The absorption of CO_2 is highly exothermic, thus in turn, results in a large heat duty associated with solvent regeneration. The energy needed for regeneration is roughly one third of the steam generated from the plant and results in an 8-13% efficiency loss to the power plant (EIA, 2013a) and is the major economic penalty factor of the process. Large volumes of research have been focused on finding new solvents, sorbents and using membranes for CO_2 absorption (Figueroa, Fout, Plasynski, McIlvried, & Srivastava, 2008), yet not enough research attention has been drawn on the regeneration operation that suffers from heavy energy penalty and usually determines the economic viability of the CO_2 capture technology.

2.3. Stripper Configurations

Oyenekan (Oyenekan, 2007) described three stripper configurations listed in Table 2-1. Generally speaking, these three configurations, operating at high temperatures for a simple stripper, maintaining low pressure for a vacuum stripper, and under a pressure swing to a high pressure for a multi-pressure stripper, are all relatively energy intensive processes. The simple reboiled stripper is the current industrial baseline configuration.

Table 2-1 Comparison of different CO_2 stripper configurations*(Oyenekan, 2007).

	Configuration	**Temperature (^oC)**	**Pressure (kPa)**	**Characteristics**
*Simple stripper	CO_2 and gas vapor leaving at top; Condensate refluxed;	110 to 120	160	Heavy reboiler duty; Significant solvent loss;
*Vacuum stripper	CO_2 and gas vapor leaving at top; Condensate refluxed;	60 to 80	30	Low temperature; Low pressure; Slow mass transfer rate; Additional compression duty
*Multipressure stripper	Three-stage pressure swing from top to bottom; Rich solvent flow from top	94-96	160, 212, 280	Medium temperature; High pressure; More water vapor in CO_2; CO_2 recovered at higher concentration and pressure;
Membrane contactor Stripper	CO_2 and gas vapor as permeates; Solvent stay close looped at retentate side;	80 to 100	103 to 160	Relatively low temperature, Pressure slightly higher than atmospheric; Energy efficient; Additional mass transfer resistance;

An alternative stripper configuration using membrane contactors is proposed and explored in this study. Membrane contactors possess many attractive advantages over the traditiaonal processes. Primarily, it can potentially save substantial amount of energy by providing significantly higher interfacial contact area to improve mass transfer rate. Packed and trayed columns possess ~30-300 m^2/m^3 of interfacial area, while membranes can provide up to 3000 m^2/m^3 (Favre, 2007). Curnow et al. (Curnow, Krumdieck, & Jenkins, 2005) reported that it is possible to lower the temperature for regenerating CO_2-saturated amine by dramatically

increasing the active surface area and the solvent turbulence through the use of a packed bubble reactor. This suggested the membrane usage can possibly lower the regeneration temperature as well by offering even more surface area. Another major advantage of membranes is that solvent loss will be significantly reduced compared with traditional condensate reflux processes due to the circulating close-looped of the retentate side. Moreover, membranes avoid operational issues of a traditional column such as flooding and weeping, thus offering less maintenance for a more compact and robust operation (Mansourizadeh & Ismail, 2011). Each of these advantages makes membrane contactors a desirable alternative CO_2 stripping configuration.

As with any other innovative technology, membrane contactors are not free from drawbacks. Relatively slow mass transfer rate can be expected due to additional membrane resistance. Membrane materials are also susceptible to wetting, fouling, and possible degradation over extended service life. These factors could possibly mitigate operational advantages (Mansourizadeh & Ismail, 2009). In order to take full advantage of membrane merits and minimize drawbacks, research efforts should focus on (1) screening and exploring high performance membrane materials and microstructures; and (2) optimizing membrane module configurations and operating conditions.

2.4. Overview of Alkanolamine Solvent

The basic principle behind chemical solvents used in CO_2 capture is the chemical reaction and bonding of alkali solvents with acidic gases. For example, the capability of alkanolamine to react with CO_2 is attributed to the amine group at one terminus of the molecule. The most common alkanolamine currently in use is MEA. It has been widely used as a CO_2 absorption solvent for over 70 years in natural gas sweetening and gas scrubbing facilities

(Wallace, 2006). Although operations using MEA have been studied and accumulated for so long, some issues are still present and some problems are still not well understood, especially for the solvent behavior at elevated temperatures. Most process designs are still highly empirically based.

Other commonly used Alkanolamines include: 2-amino-2-methyl-1-propanol (AMP), diethanolamine (DEA) and N-methyldiethanolamine (MDEA) (Alvarez, Rendo, Sanjurjo, Sanchez-Vilas, & Navaza, 1998). These amines are usually divided into three main categories–primary, secondary, and tertiary–according to the number of carbon-nitrogen bonds. For example, MDEA is a tertiary amine because it has three carbon-nitrogen bonds; DEA is a secondary amine because it has two carbon-nitrogen bonds whereas MEA is a primary amine as it has only one.

MEA is the alkanolamine with the highest alkalinity (Freeman, Davis, & Rochelle, 2010). It is highly volatile; a hydroxyl group on the molecule makes MEA ready to be dissolved into polar solvents such as water and 10 to 30 wt % MEA is the commonly used form. The basic amine group of an MEA molecule reacts very rapidly with CO_2 to form a carbamate and a proton. This reaction occurs very efficiently below 60°C with an exothermic heat load of 72 kJ per mole of CO_2 absorbed (30 wt % MEA) (Yeh, Pennline, & Resnik, 2001).

Before CO_2 saturation, the rate of reaction with MEA usually determines the overall absorption rate. MEA is favored for complete CO_2 removal due to its fast reaction rate. MEA and CO_2 chemistry (Hook, 1997) is illustrated in Figure 2-4. (Yeh et al., 2001) found no significant difference in absorption ability in the range 38-50°C for a 20 wt% aqueous MEA solution. The principle behind the regeneration process incorporates the fact that the MEA–CO_2 reaction is

reversed by supplying heat to the system to approximately 70°C and higher temepratures. CO_2 regeneration at 120°C requires a heat load of 165 kJ per mole of CO_2 (Yeh et al., 2001). Up to 80 % of the total cost of absorption/desorption can be attributed to the regeneration process even with effective integration of waste heat (Yeh et al., 2001).

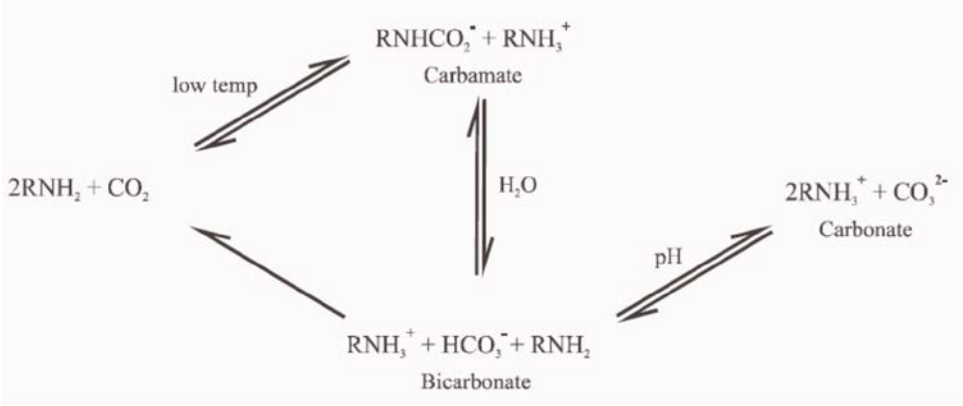

Figure 2-4 MEA-CO_2 chemistry illustration (Wallace, 2006)**,** RNH_2 stands for an amine, where $R=CH_2CH_2OH$ represents MEA

Besides the heavy energy consumption of this process, there are operational issues that arise from using MEA for CO_2 capture. Corrosion of the equipment, oxidative as well as thermal degradation of the solvent represent the major problems (Davis, 2009; Freeman et al., 2010; Kittel et al., 2009). MEA exposed to free O_2 in flue gas streams can react to form corrosive degradation products (Kittel et al., 2009). Inhibitors are often used with MEA to improve solvent performance and stability (Goff & Rochelle, 2006).

Selected physical properties of MEA are summarized and compared with water in Table 2-2.

Table 2-2 selected properties of MEA and water (Wallace, 2006)

Property	MEA	Water	Unit
Molecular Formula	C_2H_7NO	H_2O	N/A
Molecular Weight	61.08	18.02	g/mol
pH	12.5	7	N/A
Density	1012	1000	kg/m^3
Boiling Point	171	100	°C (1atm)
Melting Point	10.5	0	°C (1 atm)
Specific Heat	3200	4182	J/kg.K (25°C)
Thermal Conductivity	0.299	0.598	W/mK (25°C)
Absolute Viscosity	0.021	0.001	Pa.s (25°C)
Surface Tension	0.048	0.073	N/m (25°C)
Vapor Pressure	0.05	2.3	kPa (25°C)
Vapor Pressure	10 (110°C)	101.3 (100°C)	kPa

2.5. Membrane Contactors Overview

2.5.1. Background

Membrane technology is a rapidly developing field for both research and industrial applications. It has been successfully applied in several large-scale industrial fields such as gas purification and water filtration. Some reliable and selective polymeric membranes have been developed for a number of applications. In these processes, separation selectivity is provided by the membrane based on differences in solubility, diffusivity, and/or the size of the molecules to be separated.

The driving force for membrane separation is given by differences in partial pressures of the components on the retentate and the permeate sides of the membrane. This may be achieved by a difference in total pressure or by making use of a sweep gas on the permeate side. If the

permeate is a desired product, a vacuum is usually employed to capture the separated component in highly concentrated form. This will likely be the case in large scale CO_2 capture from flue gas, where the CO_2 is subsequently compressed to the sequestration injection pressure.

The primary advantage that membranes have over other vapor-liquid mass transfer processes is significantly higher interfacial contact area, which potentially could result in a significant reduction in the size of the necessary process equipment. Also, because issues such as flooding and weeping can limit the operational range of a column, membranes have the potential for more robust, lower maintenance operation with fouling and material service life being the most significant factors mitigating these advantages.

The use of membrane systems to strip gases from liquids has been studied for many years and is sometimes referred to as membrane distillation, a term which recognizes the fact that mass transfer is occurring between liquid and gas phases. Previous development of membrane stripping systems has focused on the removal of ammonia and volatile organic compounds from wastewater (Ding, Liu, Li, Ma, & Yang, 2006). Membranes for gas and liquid separations are typically composite or asymmetric with a thin polymeric selective layer and operate on a solution-diffusion mechanism. On the other hand, membrane contactors consist of a thin porous structure without a selective layer may provide even better performance in that CO_2 permeation flux can be more substantial than composite structures. They are used to provide a gas liquid interface and rely on surface tension to reduce the ability of the liquid to pass through the pores. Ideally, only gas phase is able to pass through these porous membranes. For the removal of gases from non-volatile liquid solvents, porous membrane contactors represent a promising opportunity for improved efficiency.

2.5.2. Advantages of Membranes

Membrane contactors have many advantages over conventional column contactors. They include:

Operational flexibility

The membrane contactors provide easier and simpler operation as there are no moving parts involved. It avoided the operating issues such as flooding, foaming. It separate two phases at retentate side and permeate side, thus allowing for independent manipulation of their flow.

Large surface to volume ratio

The manufacture of membranes is capable of dense packing of hollow fibers or spiral wound, resulting in large packing densities and much higher surface to volume ratio.

Economic benefits

Polymeric materials are usually lighter and less expensive than structural and specialty stainless steels. Capital cost can be significantly reduced and installation is much easier. Membrane contactors are considered to be more energy efficient because of their reduced solvent volume as well as solvent loss.

Easy scale-up and down

Membranes are largely produced as modular components of nominal size, the scale-up and down of membrane processes should be relatively easy. This is a desirable and convenient feature when feedstock and upstream processes are subject to change.

Easier design and prediction

Membrane contactors provided separately operation of different phases and avoided issues pertaining to entrainment, flooding, channeling and foaming. Thus the systems are more easily to be designed and modeled. The known interfacial area of membranes also made the prediction of mass transfer rate easier.

Reduced solvent loss

Solvent cost and operational workload can be significantly reduced due to high packing densities and system simplicity that membrane contactors provided. Solvent loss, contamination and degradation problems can be lessened, which is especially favorable for expensive, corrosive or toxic solvents.

2.5.3. Disadvantages of Membranes

On the other hand, membrane contactors also have drawbacks. They include:

Slow mass transfer rate

The membrane is a mass transfer barrier itself causing the resistance of the system. The resistance can be reduced by choosing appropriate pore size and thinner layers, but it is an intrinsic drawback that the membrane process provides relatively slower mass transfer rates compared with traditional columns.

Fouling

Fouling products can be formed through the solvent degradation, precipitation or impurities to the system. Aggregation of fouling products on the membrane surface may block the membrane pores, increase membrane resistance thus deteriorate permeation flux and performance.

Membrane reliability

Membranes are susceptible to degradation and wetting over extended periods of service under the exposure to the solvent, especially chemical progressive ones. This contributes to additional cost associated with membrane replacement. For some membranes, an additional membrane cleaning process is employed to reuse the membranes.

2.5.4. Membrane Technology in CO_2 Regeneration

Unlike the large volume of literature of using membrane contactors for CO_2 capture (Aaron & Tsouris, 2005; Carapellucci & Milazzo, 2003; Li & Chen, 2005), the use of membranes for the regeneration of CO_2 solvents has been studied by only a handful of researchers. Most notably, Kosaraju and others (Kosaraju, Kovvali, Korikov, & Sirkar, 2005) studied an absorption-stripping scheme, which consisted of both absorber and stripper hollow fiber membranes. In this project, an aqueous amine solution was circulated from the tube side of the absorber module to the tube side of the stripper module. Feed and sweep gases were circulated through the shell side of the absorber and stripper modules, respectively. In this system, CO_2 was successfully removed from the amine in the stripper membrane module without

heating, though the authors concluded that more contact area was needed in the stripper than in the absorber.

Koonaphapdeelert et al. (Koonaphapdeelert, Wu, & Li, 2009) have introduced ceramic hollow fiber membrane contactors for CO_2 stripping application with high temperature stability. But on the other hand, ceramic hollow fiber membrane contactor is usually harder and more expensive to manufacture. It also has the drawback of limited surface to volume ratio compared with polymeric membranes.

Khaisri et al. (Khaisri, deMontigny, Tontiwachwuthikul, & Jiraratananon, 2011) used PTFE hollow fiber membranes for this process and studied the gas and liquid velocity, temperature and feed solution concentration effects on desorption flux. Mass transfer co-efficients of liquid, membrane and gas were calculated. Severe membrane pore wetting in the long term was reported but detailed characterization about membrane wetting was not provided.

Naim et al. (Naim, Ismail, & Mansourizadeh, 2012) fabricated microporous PVDF hollow fiber membranes for CO_2 stripping from preloaded aqueous DEA solutions. Membranes were characterized; optimal operation conditions were explored and highest flux and stripping efficiency achieved in the experiments were reported.

Simioni et al. (Simioni, Kentish, & Stevens, 2011) successfully used two types of polymeric flat sheet microporous membranes, PTFE and PES with a hydrophobic coating, to strip CO_2 from 30 wt% potassium carbonate solvent. It was found that the PTFE membranes were not sustained at high temperatures, whereas PES with hydrophobic coating performed

better and survived all the temperatures. The possible reason was attributed to pore wetting caused by solvent intrusion to the membrane.

All the results from previous work were in early proof of concept stage, they indicate that the removal of CO_2 from chemical solvents using membranes may be a feasible approach, however numerous questions remain. The rate of mass transfer from the solvent to the membrane is not known for any of the systems of interest here, and in the case of chemical solvents, it is complicated by the reaction. Understanding this mechanism is critical to determine the necessary amount of membrane area for stripping. Further, the required magnitude of the driving force across the membrane and the optimum conditions on the permeate side of the module are not known.

2.6. Membrane Materials Selection

Membrane regeneration of CO_2 from alkali solvents has a lot similarity with Membrane distillation (MD). The materials selection criteria of CO_2 regeneration could thus employ many principles developed in MD. However, CO_2 regeneration process is operated at elevated temperatures, which requires much higher chemical and mechanical criteria than MD and limits membrane selection.

Selection criteria suitable for MD processes were proposed by several researchers (Adnan, Hoang, Wang, & Xie, 2012; Khayet, 2011; Zhang et al., 2010). Based on those criteria, the following conditions were proposed as membrane selection preferences for CO_2 regeneration:

1. Membrane surface is preferred to be highly hydrophobic. It could be asymmetric membranes with one layer or multilayer of the membrane surface; or symmetric membranes made of materials with low surface energy.
2. Porous membranes are preferred to minimize mass transfer resistance of membranes and ensure high mass transfer flux. Composite membrane with a selective layer is a good choice as well because it can provide better selectivity and make membranes highly resistant to fouling and wetting. However, mass transfer flux may be reduced due to the much larger mass transfer resistance of composite membrane than porous membranes.
3. Membranes should be chemically stable and inert to the process liquid. Membrane materials are preferred to be non-reactive and non-soluble to the process liquids. It should not change the gas-liquid equilibrium of the process liquids. This also makes membrane highly resistant to fouling and wetting and prevents process liquid from degradation.
4. Membranes should be mechanically strong enough to withstand trans-membrane pressure and elevated temperature. It also should has good thermal stability and reliability to ensure long term use.
5. Membranes should have high permeability to CO_2 gas to ensure high mass transfer flux.
6. Membranes with low thermal conductivity are preferred so that convective heat loss can be minimized.
7. Membrane with low thickness is preferred to maximize mass transfer.

8. Membranes with small tortuosity factor (defined as the straightness of the pores) are preferred.

Polymer materials usually are in the forms of completely amorphous or semi-crystalline. Normally, glassy polymers that are hard and rigid will be softened when the temperature exceeds their glass transition temperature (T_g). Beyond T_g, the polymer's physical strength will be significantly changed. Usually, it becomes soft and flexible and shows properties of either an elastomer or a viscous liquid. The elastic modulus of the material can be significantly reduced and the polymer shows little crystallinity or becomes totally amorphous when temperature goes above T_g. For these reasons mentioned above, T_g is a primary consideration when selecting membrane materials for mechanical strength. In addition, the melting temperature (T_m) should also be considered, especially for semi-crystalline polymers because the polymer undergoes a phase change and molts when the temperature is above T_m. Based on above criteria, a number of membrane material candidates from literature were compared and listed in Appendix B.

2.7. Membrane Materials Characterization Methods

Traditional materials characterization techniques can also be used in characterization of membranes. In our study, differential scanning calorimetry (DSC), fourier transform infrared spectroscopy (FTIR), UV-vis spectroscopy, scanning electron microscope (SEM) were employed for membrane characterization.

2.7.1. Differential Scanning Calorimetry (DSC)

Differential scanning calorimetry (DSC) is a powerful thermo-analytical tool to determine the thermal properties of polymers. It measures the heat flow rate between a sample

and an inert reference as a function of time and temperature. For amorphous glass state polymers, the molecular chains begin to move and reach a rubbery state when the temperature goes beyond T_g. When temperature continues rising to a point where the polymer molecules begin to flow, this temperature is called the viscous flow temperature (T_f). The range between T_g and T_f is known as the rubbery state of polymer. All these changes can be characterized by DSC and expressed by the thermal-mechanical curve of a polymer. Some semi-crystalline polymers exhibit both crystalline and amorphous behavior, such as PE, PP, and PTFE. DSC can characterize both T_g of amorphous behavior and T_m of the crystalline behavior. A typical DSC curve for semi-crystalline polymer sample is shown in Figure 2-5.

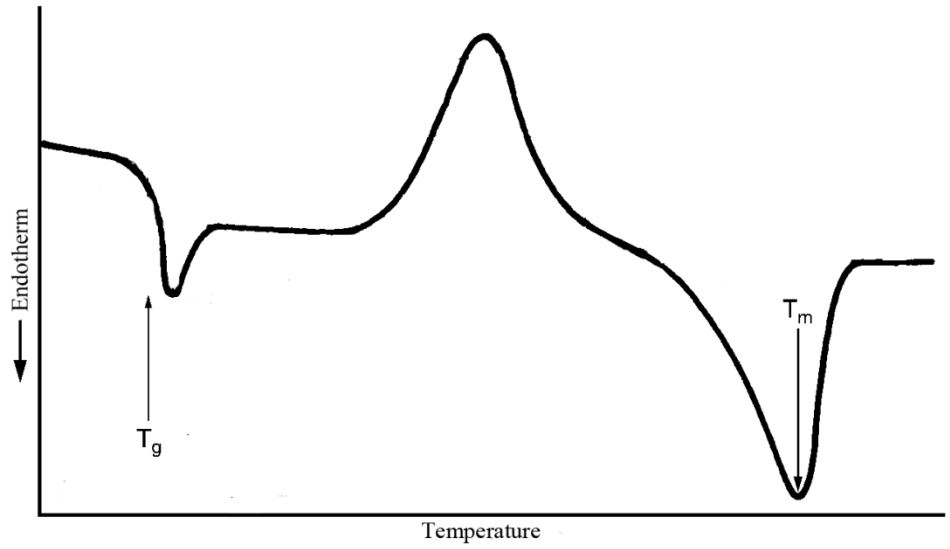

Figure 2-5 Typical DSC curve of semi-crystalline polymer

2.7.2. Fourier Transform Infrared Spectroscopy (FTIR)

FTIR analysis is employed in this study for qualitative analysis of membrane materials. Usually, vibrations of chemical bonds that change the dipole moment of the molecules are sensitive to the light wavelength of Infrared (IR) region. In IR spectroscopy, the light (photon)

with certain wavelength corresponding to the energy difference between atomic levels of the sample molecules is absorbed. Different functional groups have their unique characteristic absorption energy bands, from which the identification of molecules can be recognized. The position of a certain absorption band is specified by its wavenumber ($\bar{\nu}$), which is defined as the inverse of the wavelength and is preferred to be used because it is in linear relationship with photon energy (shown in Equation 2-1).

$$\bar{\nu}\ (\mathrm{cm}^{-1}) = \frac{1}{\lambda\ (\mathrm{cm})}$$

Equation 2-1

FTIR can also be used in quantitative analysis with relevant standards by applying the Beer-Lambert Law. Figure 2-6 shows a typical setup for absorption technique. When radiation beam passing through a sample, the incoming intensity of the beam is denoted by I_0 and the outgoing intensity is denoted as I. If the radiant beam is assumed to be monochromatic, the Beer-Lambert law can be written as:

$$A = -\lg\left(\frac{I}{I_0}\right) = -a \times l \times c$$

Equation 2-2

Where A is the absorbance, c is the concentration of absorbing species, l is the light path length, and a the absorption coefficient or the molar absorptivity of the absorber. This Beer-Lambert law is the principle behind the use of non-dispersive infrared (NDIR) CO_2 analyzer as well. When l and a is fixed, the absorbance is proportional to the concentration of CO_2 in the optical bench (Section 3.2.2).

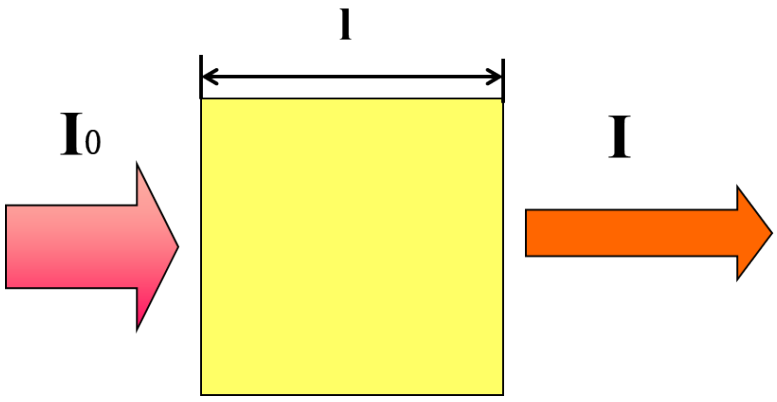

Figure 2-6 Typical experimental direct absorption setup.

2.7.3. Membrane Porosity, Tortuosity and Pore Size

Methods to determine membrane pore size include mercury porosimetry, scanning electron microscopy, bubble point method and so on. These methods were outlined and reviewed in many literatures (Nakao, 1994; Zhao, Zhou, & Yue, 2000). In our study, nominal pore size of membranes was provided by the manufacturer and verified by scanning electron microscope (SEM).

The porosity of the membrane is defined as the ratio of the volume of the pores and the total membrane volume. And tortuosity is a factor to characterize how the molecules travel through the pores (straight or twisted path). These two factors are important parameters when studying the mass transfer of the membrane process. They were calculated in our study using Equation 2-3, which was originally developed by Mackie et al.(Mackie & Meares, 1955). Their study reported that membrane tortuosity and porosity were directly related to the volume fraction of the polymer. This equation applies to most polymers in membrane manufacturing that are made by phase inversion techniques, such as PP, PES, and nylon, whose topographical structures are modeled as closely packed spheres (Simioni et al., 2011).

$$\frac{\tau}{\varepsilon} = \frac{(1+V)^2}{(1-V)^2} = \frac{(2-\varepsilon)^2}{\varepsilon^2}$$

Equation 2-3

Where V, τ and ε are the polymer volume fraction, membrane tortuosity and porosity, respectively.

Materials such as PTFE membranes are typically stretched to form their porous structure and as a consequence have pores that are elongated. Equation 2-4 should be used instead to estimate the membrane tortuosity from porosity because it is better modeled as loosely packed spheres (Simioni et al., 2011).

$$\tau = \frac{1}{\varepsilon}$$

Equation 2-4

2.8. Mass Transfer Model

Mass transfer coefficient is an important coefficient used in predicting mass transfer flux. It is also important in evaluating and describing membrane contactor designs. The factors that affect mass transfer coefficient can be used to find the optimal operating configurations and conditions, especially for the design of industrial scale contactors. The overall mass transfer coefficient is a lumped parameter where the effects of the hydrodynamics of the gas and liquid phases, the chemical reaction and the presence of the membrane are combined (Hoff, 2003).

The mass transfer of CO_2 through this flat sheet membrane process can be described by the film model (Chen, Lin, Chien, & Hsu, 2010). The overall mass transfer resistance can be

divided into three parts: the liquid film resistance, the membrane resistance and the gas film resistance in series. It is also known as the resistance in series model.

The overall resistance and three resistance parts can be expressed as Equation 2-5 (Chen et al., 2010; Hoff, 2003; Khaisri et al., 2011):

$$\frac{1}{K_{OL}} = \frac{H}{Ek_L} + \frac{1}{k_M} + \frac{1}{k_G}$$

Equation 2-5

Where K_{OL} is the overall mass transfer coefficient, k_L, k_M, and k_G are the liquid, membrane, and gas mass transfer coefficients. H is dimensionless Henry's constant. E is the dimensionless enhancement factor which is included to account for the effect of the reaction.

The individual mass transfer coefficients can be described using the correlation of a form as:

$$\text{Sh} \propto Re^{\alpha} Sc^{\beta} f(geometry)$$

Equation 2-6

Where Sh, Re and Sc are the Sherwood number, the Reynolds number and the Schmidt number, respectively, and f is a function of geometry. The exponents α, β, and the function f must be determined from mass transfer experiments or models. A review (Stanojevi, Lazarevi, & Radi, 2003) was given on the correlations developed for different membrane module configurations and modes of operation.

The liquid mass transfer coefficient takes the correlation form as the following equation known as Leveque's correlation (Chen et al., 2010):

$$Sh = \frac{k_L d_h}{D_L} = 1.62\left(\frac{d_h^2 v_L}{L D_L}\right)^{1/3}$$

Equation 2-7

where d_h is the hydraulic diameter of the module (cm) or the thickness of the liquid film formed in the module in this study, v_L is the velocity of liquid phase ($cm \cdot s^{-1}$), and L (cm) is the membrane length which is equal to d_h for round membrane, and D_L is the diffusivity of CO_2 in liquid phase ($cm^2 \cdot s^{-1}$)

The gas mass transfer coefficients can be described as following equation (Chen et al., 2010):

$$Sh = \frac{k_G d_h}{D_G} = 0.023\left(\frac{d_h \rho v_G}{\mu_G}\right)^{0.8}\left(\frac{\mu_G}{D_G \rho}\right)^{0.33}$$

Equation 2-8

where D_G is the diffusivity of CO_2 in the gas phase ($cm^2 \cdot s^{-1}$), v_G is the velocity of gas phase ($cm \cdot s^{-1}$), μ_G is the viscosity of gas (Pa·s), ρ is the density of gas phase ($g \cdot cm^{-3}$)

The membrane mass transfer coefficient is predicted by equation as shown below (Khaisri et al., 2011):

$$k_M = \frac{D_e \varepsilon}{\tau \delta}$$

Equation 2-9

where ε is the porosity of the membrane, τ is the fiber tortuosity, and δ is the thickness of the membrane. D_e is the effective of diffusivity ($cm^2 \cdot s^{-1}$), which can be defined by equation as

shown below:

$$\frac{1}{D_e} = \frac{1}{D_k} + \frac{1}{D_G}$$

Equation 2-10

where D_G is the diffusivity of CO_2 in the gas phase, D_k is the Knudsen diffusivity of CO_2 (cm^2s^{-1}).

The calculation equations and steps of membrane mass transfer coefficient (k_M), gas phase mass transfer coefficient (k_G), and liquid phase mass transfer coefficient (k_L) followed the calculation methods developed by Khaisri et al. (Khaisri et al., 2011).

The enhancement factor characterizes the relation between the chemical and the physical absorption flux at the same driving force (Hoff, 2003) . It may be considered as a correction to the liquid side mass transfer coefficient due to the chemical reaction occurring in the concentration boundary layer (Hoff, 2003). The enhancement factor can be calculated by Equation 2-11 (Chen et al., 2010):

$$E = \frac{\sqrt{k_r C_b D_L}}{k_L}$$

Equation 2-11

where k_r is the second-order reaction constant, C_b is the bulk concentration of active components, D_L is the CO_2 diffusivity coefficient in liquid phase, and k_L is the liquid mass transfer coefficient. Different calculation approach of E is also provided (Khaisri et al., 2011). Detailed calculation of k_M, k_G, k_L, H and E are shown in Appendix C.

3. EXPERIMENTAL SYSTEM DESIGN, CONSTRUCTION, AND VALIDATION

This chapter introduces the experimental system for CO_2 absorption and solvent stripping by membrane contactors. Detailed design and construction concerns about the system were presented, including all the meticulous considerations, such as material compatibility, heating and cooling configuration selection and the design rules we used. Analytical methods of CO_2 in both gas and liquid phases were discussed. System validation results were shown. Experiment results were presented to verify whether the system was capable of absorbing and stripping CO_2.

3.1. System Overview

Typical CO_2 absorption/stripping system involves these major parts: A CO_2 absorption column to absorb CO_2 from flue gas; a circulating pump between the absorber and stripper; a stripper column, usually packed or trayed column, to provide contact interface for gas liquid separation; a reboiler to provide heat duty to evaporate the solvent; and finally an heat exchanger between absorber (at around 40ºC) and stripper (at around 120ºC) so that the temperature swing of the lean and rich CO_2 solvent can actually happen. Our lab-scale system (Figure 3-1) has the similar function parts as mentioned above, with the stripping column replaced by a membrane contactor.

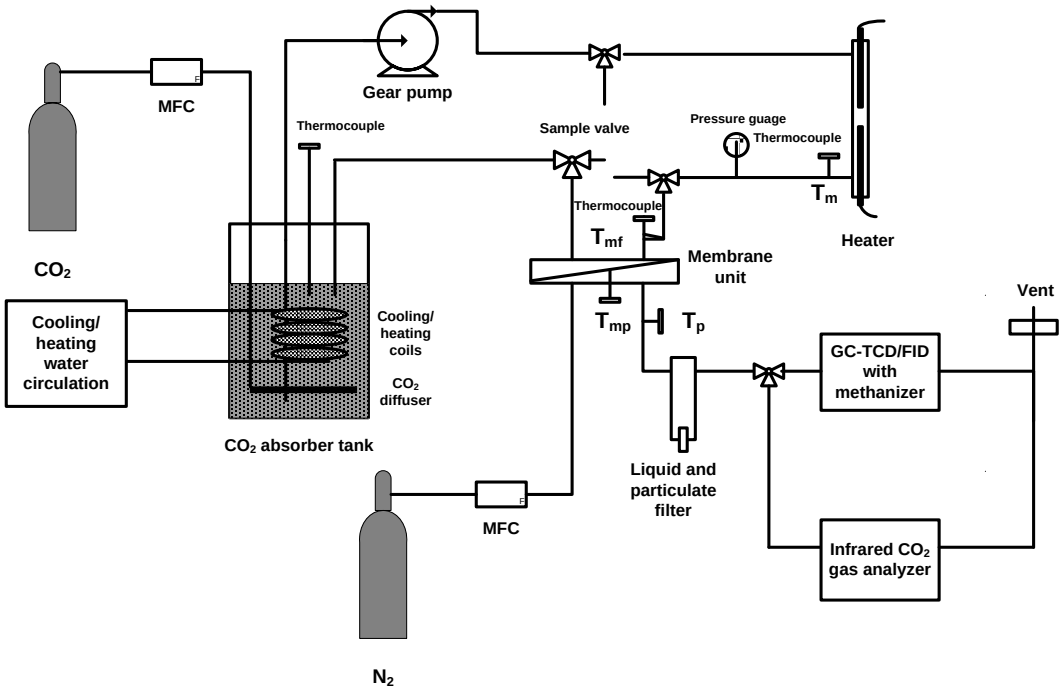

Figure 3-1 Schematic of the membrane evaluation system

This CO_2 evaluation system consists of a CO_2 absorption tank, a feed delivery pump, an inline heating system and a membrane separation unit that houses a polymeric membrane. N_2 sweep gas is used for permeate removal. CO_2 is pre-loaded to the solvent by mass flow controlled (Brooks 9400) flow from gas cylinder (Praxiar) till saturated. In stripping process, CO_2 saturated solution is pumped from the solvent tank to a heater to achieve a desired temperature and then delivered to the membrane cell for separation and the stripped retentate solutions flows back to the tank. This small amount of retentate lean solution is diluted by the large volume solution in the tank in terms of both temperature and CO_2 saturation level. Meanwhile, cooling water circulating through cooling coils in the tank takes away accumulated heat and maintained low temperature in the absorption tank constantly. A schematic of the system is shown in Figure 3-1 and a picture of the actual system is shown in Figure 3-2.Detailed equipment list is in Appendix A.

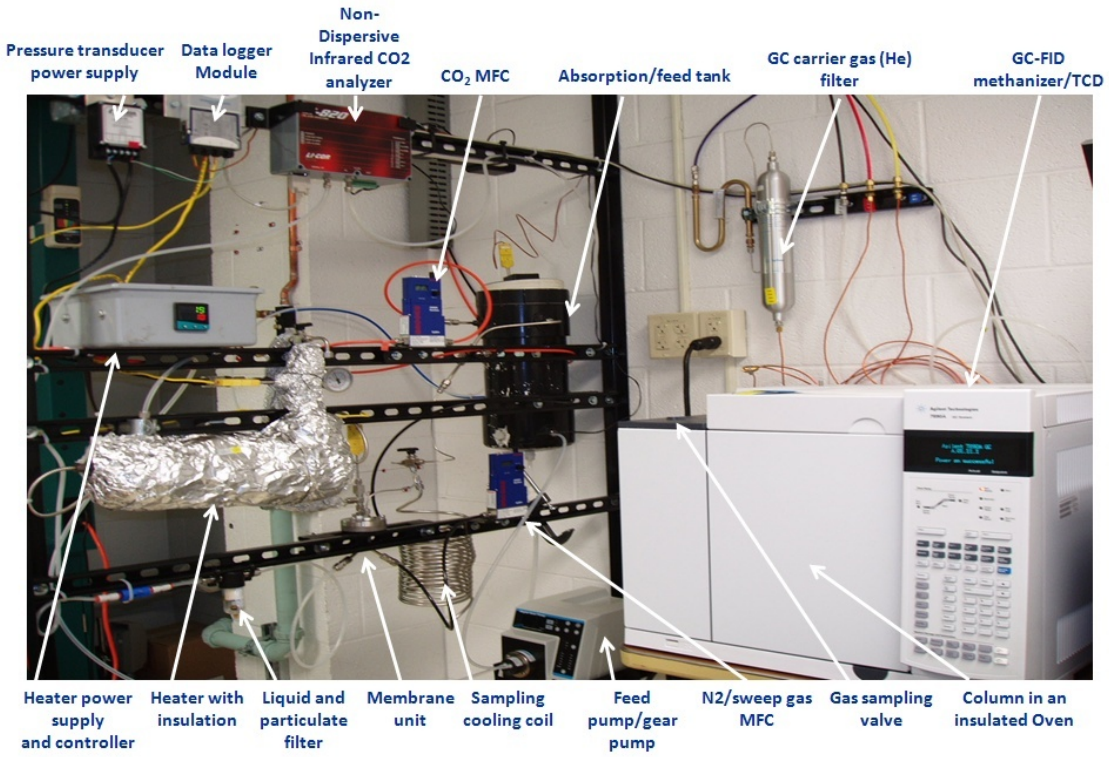

Figure 3-2 Actual view of the membrane evaluation system

3.1.1. Absorption/Feed Tank

CO_2 absorption takes place in a 6-liter solvent tank that was custom-made at the University of North Dakota Chemical Engineering Department workshop using a 6-inch inner diameter PVC pipe. This tank is equipped with in-house made heat exchange coils to maintain constant absorption solution temperature and a gas spurge to diffuse and saturate CO_2 into the absorption solution. A pressure relief valve and a thermocouple are mounted on the lid, which prevents pressure buildup and reduces solvent evaporation.

The material selection for solvent tank requires additional consideration. Chemical solvent, such as MEA, has high alkalinity, and increasingly becomes corrosive at high temperatures, can potentially cause failure through corrosion and degradation of the tank materials. Common materials such as stainless steel, cast iron and PTFE, have good long-term

compatibility with MEA performance included (Wallace, 2006), but generally are more expensive or/and harder to be processed. So PVC pipe is chosen as tank building materials because it is a common building material with easy availability and inexpensive cost. Although PVC becomes brittle with MEA at elevated temperatures, it is employed here because CO_2 absorption usually happens at relatively lower temperature ($\leqslant 40^{o}C$).

This absorption tank was equipped with an in-house made CO_2 gas disperser, a cooling/heating coil, and a K type thermocouple for monitoring temperature. Professional grade gas spurger or dispenser would be a better option on mass transfer performance, but probably would not make a significant improvement due to the fast reaction kinetics of CO_2 and MEA. The circulation pump may also generate some turbulence and enhance the contact area of CO_2 and solvent.

Tap water was circulated through the cooling coil to take away extra heat and maintain constant tank temperature. The flow in the tube was concluded to be laminar flow due to its low Reynolds number. The necessary length of the cooling coil was estimated by the heat transfer Equation 3-1 for a heat exchanger (Mccabe, Smith, & Harriott, 2005):

$$Q = h \cdot 2\pi \cdot r \cdot L \frac{(T_{surr} - T_{out}) - (T_{surr} - T_{in})}{\ln\left(\frac{T_{surr} - T_{out}}{T_{surr} - T_{in}}\right)}$$

Equation 3-1

Where Q = the amount of heat that is transferred; h = the average heat-transfer coefficient based on entire pipe surface; r = the outer radius of the tubing; L = the length of the tubing; T_{surr} = the

surrounding temperature; T_{out} = the temperature of the outgoing stream from the tubing; and T_{in} = the temperature of the ingoing stream.

The heat transfer amount Q that should be cooled is equal to the heat that the circulating hot MEA solution brings to the absorption tank. It can be calculated using Equation 3-2.

$$Q = \dot{m} \cdot c_{p,solution} \cdot (T_{out} - T_{in}) .$$

Equation 3-2

Nusselt number (Nu) is estimated using empirical Equation 3-3 because the heat transfer is similar with natural convection current surrounding a hot, horizontal pipe (Mccabe et al., 2005). The heat transfer coefficient can then be calculated by the correlation of Nusselt number, diameter and thermal conductivity. Dimensionless Grashof number (Gr) is calculated by Equation 3-4 and Prandtl number (Pr) is calculated by Equation 3-5. These equations show that h depends on pipe diameter, thermal conductivity, specific heat, and viscosity, coefficient of thermal expansion, density and temperature difference.

$$Nu = \frac{hD_o}{k_f} = 0.53(Gr \times \Pr)_f^{0.25}$$

Equation 3-3

$$Gr = \frac{D_o^3 \rho_f^2 \beta_g \Delta T_o}{\mu_f^2}$$

Equation 3-4

$$\mathrm{Pr} = \frac{c_p \mu}{k}$$

Equation 3-5

Where h = average heat-transfer coefficient based on entire pipe surface; D_o = the outside pipe diameter; k_f = the thermal conductivity of fluid; c_p = specific heat of fluid at constant pressure; ρ_f = density of fluid; β = coefficient of thermal expansion of fluid; g = acceleration of gravity; ΔT_o=average difference in temperature between outside of pipe and fluid distant from wall; and μ_f=viscosity of fluid..

Based on our lab experimental setup, the fluid properties μ_f, ρ_f and k_f were evaluated at mean film temperature. The coefficient of thermal expansion β was assumed constant over the temperature range and calculated by Equation 3-6:

$$\beta = \frac{(\partial v / \partial T)_p}{v} = \frac{(\Delta v / \Delta T)}{v} = \frac{\rho_1 - \rho_2}{\frac{\rho_1 + \rho_2}{2} \cdot (T_2 - T_1)}$$

Equation 3-6

Where v = specific volume of fluid and $(\partial v / \partial T)_p$ = rate of change of specific volume with temperature at constant pressure.

The values of Table 3-1 were used to estimate the dimensionless numbers (Nu, Gr, Pr) and heat transfer coefficient h. The Nusselt number is the ratio of convective to conductive heat transfer across the thermal boundary. Its value was 4.5 for this experimental setup, which is typical for a system in laminar flow. The estimated heat transfer coefficient h was 427 W/m^2K. This value is in agreement with an example empirical h value of shell and tube exchanger which used an organic solvent as the hot fluid and water as the cold fluid (Mccabe et al., 2005).

Table 3-1 Values used to estimate the tubing length

Parameter	**Unit**	**Value**
T_{surr}	°C	40
$T_{out,water}$	°C	30
$T_{in,\ water}$	°C	20
$T_{out,\ MEA\ solution}$	°C	70
$T_{in,\ MEA\ solution}$	°C	40
k_f	W/m.K	0.598
$c_{p,\ water}$	J/kg.K	4180
$c_{p,\ MEA}$	J/kg.K	2780
$c_{p,\ solution}$	J/kg.K	3970*
ρ_f	kg/m^3	1000
$\mu_{water,\ 20^oC}$	μPa.S	1002
D_o	m	6.35×10^{-3}
$\dot{m}_{\ MEA\ solution}$	kg/s	3×10^{-3}
β	N/A	3×10^{-4}
Pr	N/A	7.0
Gr	N/A	769
Nu	N/A	4.54
h	$W/m^2.K$	427
*MEA solution was made with 15% of MEA and 85% of water, $C_{p,solution} = 0.15 \times 2780 + 0.85 \times 4180 = 3970$ J/kg.K.		

With the values provided in Table 3-1, assume pump circulating MEA solution at the flow rate of 180 mL/min, the total tubing length needed for the cooling helixes was calculated to be approximately 2.9 m.

3.1.2. Membrane Unit

Membrane contactor is the core component that provides surface area for separation. A membrane unit (Millipore XX4404700) that holds a 47 mm diameter circular membrane was selected to test the conceptual technical feasibility and screen membrane materials. This membrane unit was designed to filtrate gases or liquids at inlet pressures up to 275 psi. The inner membrane cell dimension is 7.6 cm in diameter and 2.7 cm in height. It is sealed by a silicone O-ring as shown in Figure 3-3.

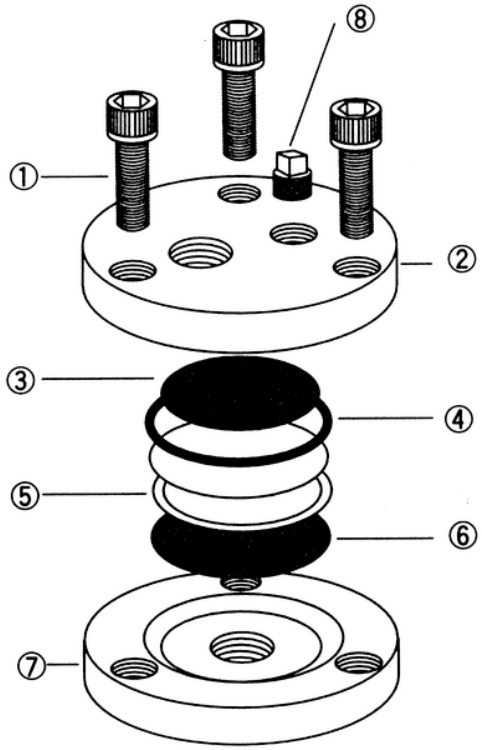

Figure 3-3 Original configuration of the membrane holder (bottom plated was modified with inlet and outlet) Hex-cap Screw; 2. Top Plate; 3. Back-pressure Screen; 4. O-ring; 5. Support Screen; 6. Under drain Screen; 7. Bottom Plate; 8. Pipe Plug.

The major advantage of this membrane unit is that it is a standardized lab scale unit and field tested by manufacturer. Many types of polymeric membranes with 47 mm diameter that fit this unit are commercially available. This membrane unit is well suited for the early stage

conceptual test trials, as well as for parametric study and membrane material candidates screening. The major drawback of this unit is that it provides limited surface area, thus resulted in limited stripping efficiency. If the research purpose is to strip large volume of CO_2 loaded solvent or to measure the stripping limit, a membrane module with much larger surface area, such as a hollow fiber membrane module, should be employed instead.

Since the original Millipore membrane unit was designed for microfiltration, some modifications were adopted to fulfill our membrane separation purpose and research needs. The original downstream portion was equipped with only one outlet to be connected with a vacuum pump. It was modified to two openings via 1/4-in. stainless steel Swagelok tubing; one for sweep gas inlet and one for sweep gas outlet. N_2 was used as sweep gas for permeate removal because it is chemically inert, easily accessible and inexpensive. N_2 as sweep gas may cause a little confusion here because actual flue gas is mainly composed of N_2 and CO_2. Technically, any other kind of gas other than CO_2 can be used as sweep gas for experimental studies. Therefore, N_2 was chosen over He and other gases due to its inexpensive cost and abundant availability.

3.1.3. Heating System

Special consideration and precautions should be drawn on the design of the heater. A temperature controller (Cal 9400) with PID control strategy was used to control the heaters. Proportional band/gain, integral time, proportional cycle-time, and derivative time/rate were tuned and optimized from factory setting to ensure the feed solutions being heated with appropriate ramp rate and provide steady temperature manners in continuous flow. Many heater configuration options can be considered in order to find a sustainable heater for performing the fast, stable and homogenous heating function. Most common configurations in the lab scale is to

use heating coil in a temperature controlled oven to heat the feed solutions gradually, or keep the permeation cell in the oven to ensure stable temperature. The drawback of this configuration is that extra length of coils in the circulation is needed and it is hard to maintain pressure on the retentate side. Another option is an in-line heating system that can provide fast heating along the line. This option would require better heating and control system. The drawback of this configuration is that it may experience small amount of heat loss between the heater and the membrane cell.

Two kinds of heaters were employed during our experimental runs. The first kind was in-house made two cartridge-heaters fitted into Swagelok tubing. It provided desired heating function. This kind of heaters failed in the long term course run because the heaters were heating two different media: one part of the heater was in contact with stainless steel fitting and tubing while the other part was in contact with flowing gas and vapor solvent. The heaters failed at this interface possibly due to different heating loads caused by different heating conductivities of these two media. A professional grade of low flow air process and liquid circulation heater (AHPF-121) was then employed and provided desired function with better reliability.

3.1.4. Analysis and Data Acquisition

Permeate molecules were volatilized from the downstream side of the membrane under N_2 sweep gas and transported to the CO_2 Infrared analyzer or the GC-FID methanizer/TCD. Data acquisition was carried out using NI Labview software. Temperature and pressure data in 10-second intervals were averaged and recorded in a text file during the run.

3.2. Analytical Methods

3.2.1. CO_2 Determination in Liquid Phase

The state of MEA solvent and the CO_2 loading in the MEA can be characterized by the solvent concentration and CO_2 loading, as well as pH value. Aqueous solution of 15 wt% MEA was used for these experiments because solutions at this concentration can absorb sufficient CO_2 that it can be quickly analyzed, yet is not too corrosive. 30 wt % MEA is the industrial standard but it is usually used in more diluted state or/and together with inhibitors for corrosion protection purpose. The CO_2 and MEA concentrations were determined using titration apparatus adapted from the Chittick CO_2 analyzer apparatus (Ji, Miksche, Rimpf, & Farthing, 2009). A schematic of the apparatus is shown in Figure 3-4.

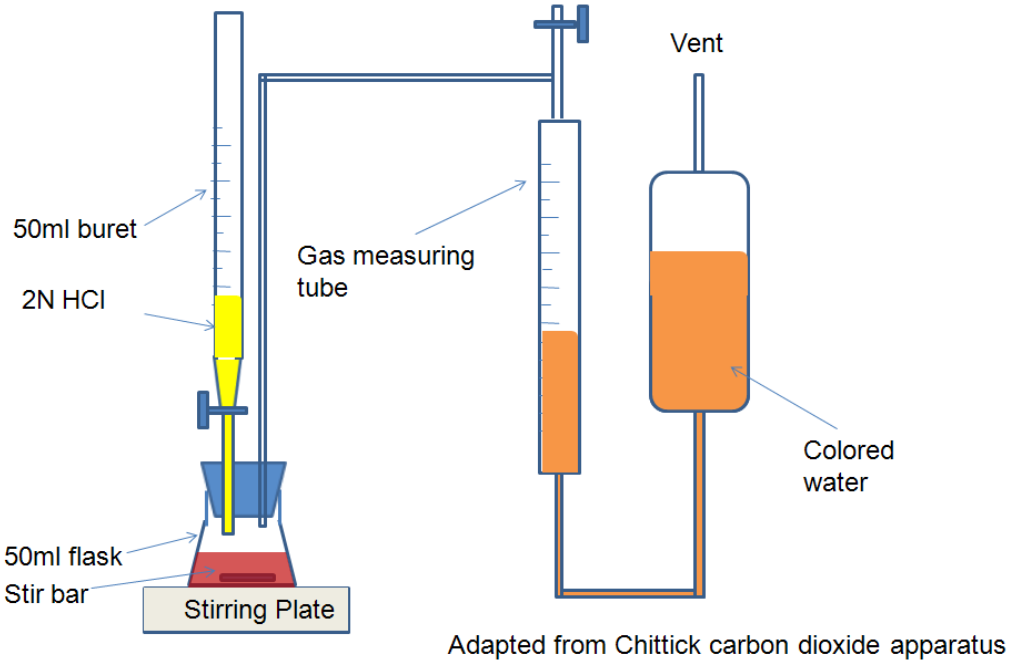

Figure 3-4 MEA and CO_2 titration apparatus

During the titration, a sample of known volume (0.5 mL, 1 mL, or 2 mL), titration indicator and a stir bar were placed in the reaction flask. The flask was then connected and sealed

to a graduated gas measuring tube and adjustable leveling bulb reservoir which contains colored water. Hydrochloric acid (2M HCl) was slowly added to the reaction flask using a 50mL titration burette until the titration indicator changed color. The solution was also stirred by a magnetic stir bar to homogenize and help liberate CO_2 from the solution. The consumed HCl was used to calculate the MEA weight fraction of the solution. Figure 3-5 shows a titration plot for a 15 wt% MEA solution containing small amount of CO_2 only due to ambient conditions.

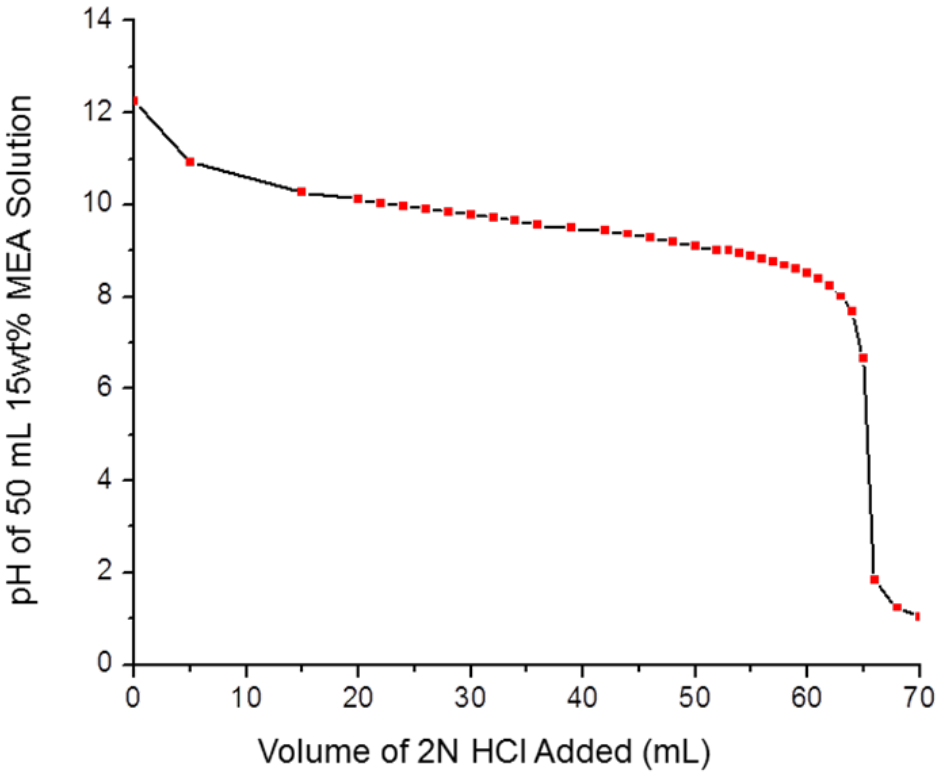

Figure 3-5 Titration plot of lean 15 wt% MEA solution

The titration showed a sharp pH change between 7 and 2. This was the endpoint where all the MEA had reacted with HCl and all the CO_2 had been released from the solution to the gas phase. Methyl orange, which is often used to titrate weak bases with strong acids, indicated this change by color change from orange-yellow (at pH 4.4) to red (at pH 3.1). CO_2 vapor evolved

from the reaction and displaced the fluid in the tube, which allowed for the evolved gas to be measured.

The MEA solution concentration was determined by Equation 3-7 (Ji et al., 2009):

$$C_1V_1 = C_2V_2 .$$

Equation 3-7

Where: C_1 = MEA solution concentration (mol/mL); V_1 = MEA solution sample volume (mL); C_2 = HCl concentration (mol/mL); and V_2 = Acid volume consumed for titration (mL).

The amount of CO_2 absorbed by the amine solution (defined as moles of CO_2 per mole of amine group) was obtained by Equation 3-8 (Ji et al., 2009):

$$\alpha = \frac{moles(CO_2)}{moles(MEA)} = \frac{[\frac{(V_{gas} - V_{HCl})(P)(273K)}{(101325Pa)(T)(22.4L/mol)}]}{C_1V_1}$$

Equation 3-8

Where: α = solution CO_2 loading (mol CO_2/mol MEA); C_1= MEA solution concentration (mol/mL); P = pressure (Pa); T = room temperature (K); V_1 = MEA solution sample volume (mL); V_{CO2} = volume of CO_2 collected (mL); V_{gas} = volume of displaced solution in the gas measuring tube (mL); and V_{HCl} = volume of HCl titrant (mL)

It should be noted that the pressure created by liberating CO_2 from MEA in the flask is higher than atmospheric pressure. This pressure difference drives the colored water displacement in the gas measuring tube. However, this pressure difference is relatively very small (less than 2% according to different measured displacements) compared to atmospheric pressure. The pressure

difference is neglected to simplify the calculation and the pressure of the system is approximated as atmospheric pressure.

Titration is the best available technology to study the MEA conditions and CO_2 loading; but it is subject to human operational discrepancy and error. In order to compensate for operator error, an UV-vis spectroscopy method was developed to show CO_2 loading and solution changes. Original lean aqueous MEA solution was used as a reference. The fully CO_2 loaded solution or stripped solution samples were analyzed by subtraction of the reference scan, thus only the CO_2 absorption peak (around 270 nm) and/or solution compositional changes were prominently shown in the spectra. The drawback of this analytical method is that it can only show the differences of CO_2 absorption peak and/or solution. Detailed analysis, especially quantitatively analysis of the CO_2 loading, is challenging to achieve.

3.2.2. CO_2 Measurement in Gas Phase

Gas Chromatography (GC) and a non-dispersive infrared (NDIR) CO_2 analyzer were coupled in parallel to provide complete range of gas phase CO_2 analysis. Low concentration CO_2 ($\leqslant$ 2%) in the reference N_2 was continuously monitored and recorded in-situ by the NDIR CO_2 analyzer (Li-COR 820). Relatively high CO_2 concentration in the N_2 gas ($\geq$2%) was determined by an Agilent 7850A GC-TCD.

The photograph of the NDIR CO_2 analyzer, software program on computer and the inside schematic are shown in Figure 3-6. With fixed optical bench length and other parameters, the concentration of absorbing species should have a linear relationship with absorbance according to Beer-Lambert law. More specifically for CO_2, chemical bonds of CO_2 molecules have

vibrational frequencies that are excited by photon energy of IR light. By setting frequencies to target CO_2 molecule bonding energy, the amount of radiation absorbed by CO_2 bonds is measured, which can be equated to the quantity of CO_2 in the flow by comparing to the source radiation. Commercially available low concentration CO_2 in balance N_2 gas cylinders for calibration purposes (Praxair) were used for concentration verification.

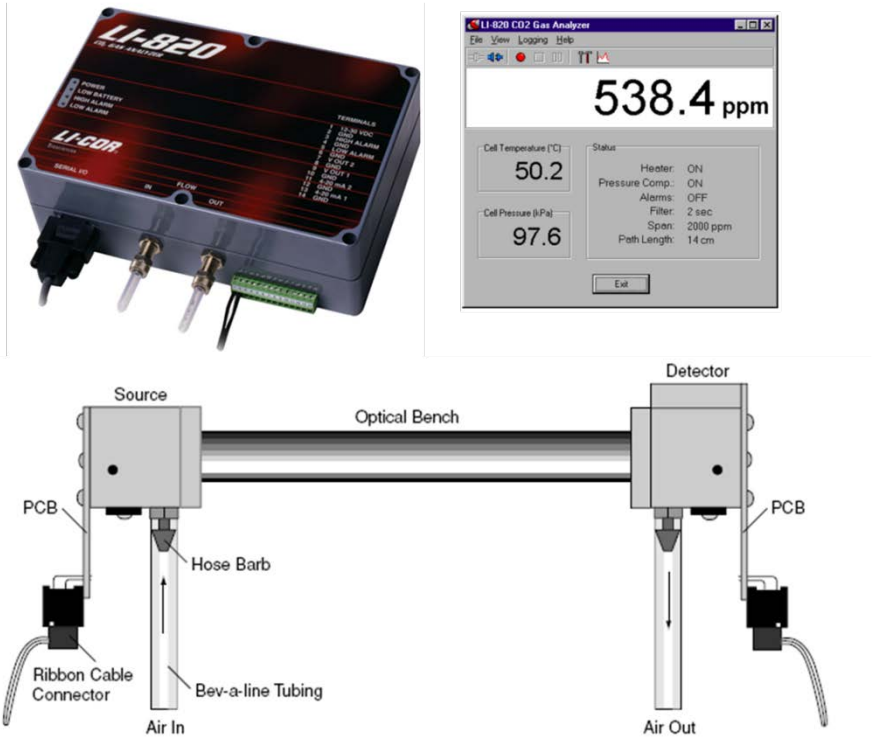

Figure 3-6 Non-dispersive infrared (NDIR) CO_2 analyzer

Detailed GC settings and analysis parameters for CO_2 detection are listed in Table 3-2. Bake out parameters shown in Table 3-3 are employed during cleaning and maintenance to remove potential residuals in the column.

Table 3-2 GC setting and analysis parameters

GC components	Parameters	Specification
Front inlet	Temperature	240°C
	Pressure	5 psi
	Operation mode	Splitless
	Purge time	0.4 min
	Purge flow	15 mL/min
	Septum purge flow	1 mL/min
	Total flow	60 mL/min
Column	Carrier gas	Helium (≥99.99% purity)
	Flow rate	40 mL/min
	Separation column	Porapak Q 80/100 mesh (1.83m ×3.18mm in×2.1mm SS)
	Column pressure	5 psi
	Oven/column temperature	45°C
TCD	Heater	200°C
	Reference flow	40 mL/min
	Makeup flow	5 mL/min
Methanizer	Temperature	375°C
FID	Heater	315°C
	H_2 flow	45 mL/min
	Air flow	400 mL/min
	Makeup flow	5 mL/min
	Flame current	0.2 pA

Table 3-3 GC column and TCD bake out parameters

GC components	Parameters	Specification
Front inlet	Temperature	240°C
	Pressure	18 psi
	Operation mode	Splitless
	Purge time	0.4 min
	Purge flow	15 mL/min
	Septum purge flow	1 mL/min
	Total flow	30 mL/min
Column	Carrier gas	Helium (≥99.99% purity)
	Flow rate	30 mL/min
	Separation column	Porapak Q 80/100 mesh (1.83m ×3.18mm in×2.1mm SS)
	Column pressure	18 psi
	Oven/column temperature	200°C
	Ramp rate	25°C/min
TCD	Heater	220°C
	Reference flow	40 mL/min
	Makeup flow	5 mL/min
Methanizer	Temperature	375°C
FID	Heater	350°C
	H_2 flow	45 mL/min
	Air flow	500 mL/min
	Makeup flow	25 mL/min

Injection method

Injection method was developed to allow for an automatic injection using auto-sampler valves. The Agilent GC was equipped with an automatic injection system which consists of 6-

port rotary style gas sampling valves. Gas sample was collected at the load position, and introduced to the GC at the injection position. Upon command, an electric motor actuates the valve from the flushing to the sampling position. The valve channels allow introduction of sample gas using sample loop of 0.25 mL volume. The most important aspects of the process are that the injection volume is precise and the injection dynamics are highly repeatable.

Column selection

Porapak Q packed column was selected for separation of CO_2 and N_2 in this study. GC column is the most important part that performs the function of separating analytes. This separation process segregates the gas mixture into components for the purpose of identifying and quantifying specific compounds. Under desirable conditions, only one component carried by the carrier gas passes over the detector at a retention time.

A packed column is commonly preferred for gas sample over a capillary column as larger volume is preferred for gas analysis. Packed columns are metal tubes, filled with fine particles or packing. Packing properties are chosen specifically for the application to cause separation of the sample components by chemical interaction, physical impediment, or polarity interaction. A packed column exhibits a characteristic retention time for different compounds – small molecules relative to the packing porosity may pass through almost unhindered, while larger molecules usually require much longer to work through the column. Similarly some molecules may interact more with the packing due to polarity or reactive groups and take different time to elute (Wallace, 2006).

Several columns were reported to be suitable for the analysis of CO_2. HP-PLOT Q capillary column was used to analysis natural gas sample on the Agilent GC catalog and gained good separation of different gases. This column is a bonded polystyrene-divinylbenzene (DVB) based column that has been specially developed for the separation of targeted apolar and polar compounds including: hydrocarbon (natural gas, refinery gas, ethylene, propylene, all C_1-C_3 isomers); CO_2, methane, air/CO, and water. 3" or 6" Silica Gel column was used to analysis room air and showed good performance as reported in the SRI GC manual. Porapak Q is also reported that it is mainly used for hydrocarbon separation but also is able to separate CO_2 from air and water (Wallace, 2006). Stainless steel HayeSep D packed column with 6' length, 1/8" outer diameter, and 80/100mesh was proven usable in our lab as HayeSep D polymers offer superior separation characteristics for light gases. It is a high-purity divinylbenzene polymer with 80% highly-crosslinked DVB and combines high surface area with a high operating temperature.

Lowering column temperature and carrier gas flow rate enhances the performance of a column. Sample molecules in the column move and vibrate faster in a more random manner at higher temperatures, thus the separation function is weakened. Lower carrier gas flow rate provides samples more adequate contact time with the column for separation. Helium carrier gas flow rate is preset for GC at about 40 ml/min. An isothermal temperature program set to 45°C was employed because although this is a relatively low temperature for separation it is high enough to be less affected by ambient temperature changes.

GC detector selection

In this study, a thermal conductivity detector (TCD) detector and a flame ionization detector (FID) detector with a methanizer were coupled in sequence for the detection and

determination of CO_2. The FID has quick response and good sensitivity; however, CO_2 is one of the very few gases to which almost no response can be acquired. The TCD is the most universal detector, as it can detect a wide variety of compounds due to their own different thermal conductivities, and is relatively simple, inexpensive, robust and easy to use.

The methanizer is usually packed with a nickel catalyst powder. During analysis, the methanizer is heated to 375°C (for Agilent). When the column effluent mixes with the FID hydrogen supply and passes through the methanizer, CO and CO_2 are converted to methane without changing their retention times. The methane can then be detected by FID, thus enabling the detection of low ppm and ppb levels of these gases. The detection limit for CO_2 with helium as the carrier gas with a TCD can reach about 100 ppm with appropriate GC conditions. The methanizer and FID can do a far better job for low-level detection and should only be used for measuring less than 100 ppm of CO or CO_2. Higher concentrations of CO or CO_2 cannot be accurately measured by the FID and methanizer as it may exceed the maximum reducing capability of methanizer.

The TCD consisted of four current carrying tungsten-rhenium filaments connected in a Wheatstone bridge circuit, encased in an isothermal aluminum box with thermal insulation. Each filament has the carrier gas passing over it at precisely controlled temperature, pressure and flow rate. The TCD operates on the principle that each gas has a unique thermal conductivity; a gas with a high thermal conductivity is capable of conducting more heat away from the filament than that with low thermal conductivity.

The operation parameters of TCD tested included TCD detector temperature, TCD cell temperature. The relatively optimized parameters employed are listed in Table 3-2. To gain

maximum sensitivity to CO_2, it was recommended to run the TCD at maximum allowable current for the detector temperature. But the increased the load on the filaments also increased background noise, instability and the heat up period of the detector. This was significant for trace analyses if the background noise due to operating parameters was large and comparable to the analyte response. On the other hand, condensation of high boiling point components on the filaments is possible when operating at low temperatures. With the detector at just 100°C, it is possible for water and traces of MEA vapor to condense. Detector temperature was set at 200°C to exceed boiling point of MEA (171°C). Prominent signals and relatively low noise was achieved. and this point is also well below the maximum operating temperature so that it ensured the filament should not be oxidized fast and can be operated in long term. TCD Cell temperature should be set about 20°C higher than column temperature to avoid condensation in the TCD cell and maintain stable atmosphere for the TCD filaments.

Calibration Method

Three calibration methods can be used for quantitative chromatographic analysis. These methods include (1) external standard calibration, (2) internal standard calibration, and (3) method of standard addition. External standard calibration method is the most commonly used method. This technique compares the detector response (peak height or peak area) between known concentrations of analyte with samples containing unknown concentrations. External standard calibration is best suited for conditions in which sample preparation steps are simple and injection volume precision is well controlled. Thus this method is appropriate for the present application.

Gas mixture sample composition can be determined by the response of each gas component. By taking into account the different thermal conductivities of the different gases, component percentage can be calculated. The GC manual provides relative thermal conductivity factors of common gases. Calibration is performed and results from the GC-TCD analyses rely on the external calibration standard. This means that the accuracy of the GC-TCD is a function of the calibration standards. If the standards are not accurate, all measurements derived from the GC will be offset from the true CO_2 concentration.

A series of standards of different CO_2 concentrations in N_2 were used to generate a calibration curve. Table 3-4 and Table 3-5show typical calibration standards data (2%, 5%, 10%) from May 2011 and 2012, respectively. Relatively high concentration standards ($\geq$ 2%) were prepared by different flow rates of CO_2 in N_2 gas (purchased from Praxair) mixed via mass flow controllers. Low concentration standards were purchased from Praxair. The response (the ratio of $CO_2/(N_2+CO_2)$ peak area) should be linear as a function of CO_2 concentration. The CO_2 concentration of unknown sample was read directly from the developed calibration curves which are shown in Figure 3-7 and Figure 3-8 from May 2011 and May 2012, respectively. Results suggest that the TCD detector responses remained stable over time.

Table 3-4 Calibration standards and GC response performed in May, 2011

External Standards			**Retention Time**		**Peak Area**		**Peak Ratio**
Actual CO_2 conc. (%)	CO_2 flow (sccm)	N_2 flow (sccm)	CO_2 (min)	N_2 (min)	CO_2 (a.u.)	N_2 (a.u.)	$CO_2/(N_2+CO_2)$ (%)
0	0	1000	N/A	2.144	N/A	9818	N/A
2	20	980	5.467	2.139	188	14190	2.24
5	50	950	5.444	2.141	829	13780	5.67
10	100	900	5.433	2.142	64	1293	11.36
25	250	750	5.411	2.145	4252	11060	27.77
50	500	500	5.396	2.155	5709	4058	58.45
100	1000	0	5.339	2.163	12850	138	98.90

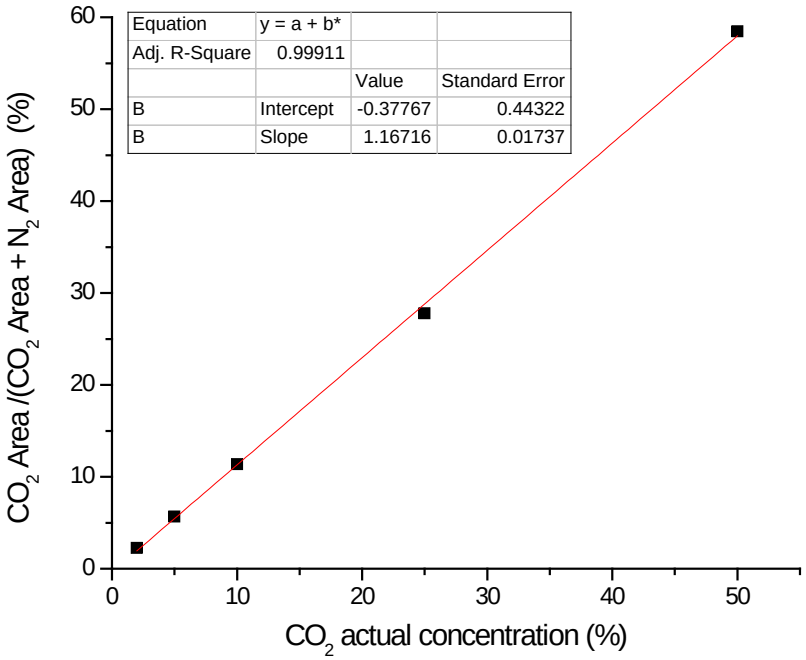

Figure 3-7 Calibration curve obtained in May, 2011

Table 3-5 Calibration standards and GC response performed in May, 2012

External Standards			Retention Time		Peak Area		Peak Ratio
Actual CO_2 conc. (%)	CO_2 flow (sccm)	N_2 flow (sccm)	CO_2 (min)	N_2 (min)	CO_2 (a.u.)	N_2 (a.u.)	$CO_2/(N_2+CO_2)$ (%)
23.1	150	500	5.460	2.153	2984	8388	26.2
15	150	850	5.465	2.149	2536	12630	16.7
10	100	900	5.472	2.147	1687	13300	11.3
5	50	950	5.477	2.145	831	13900	5.6
2	20	980	5.481	2.144	323	14300	2.2
1	10	990	5.478	2.143	5.6	1423	1.0

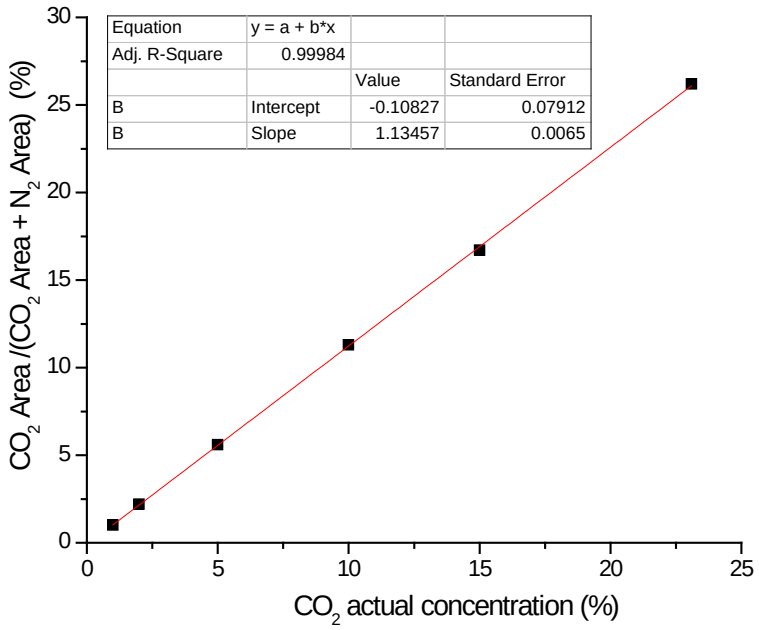

Figure 3-8 Calibration curve obtained in May, 2012.

3.3. System Verification

Before the membrane study began, it was necessary to determine that the system was capable of performing as expected. Several sets of experiments were conducted to verify that the

system was capable of absorbing and stripping CO_2. This subsection outlines (1) validation of pump and pressure control, (2) validation of the temperature control, (3) verification of absorber performance, and (4) verification of Membrane stripping performance. Details of the verification and validation process are discussed as are relevant insights taken from the validation of the data obtained.

3.3.1. Validation of Pump and Pressure Control

A Cole-Parmer digital gear pump equipped with a GA-T23 micro-pump head was employed to circulate the feed solution at the retentate side. The preset pumping speed range for the pump is 0 to 330 ml/min. The pumping speed was manually calibrated using a timer (Fisher Scientific) and a graduated cylinder (250mL, ±2mL) using tap water. The measured actual flow rates were slightly higher than the settings. Discrepancies were more apparent at higher pumping rates as is shown in Figure 3-9.

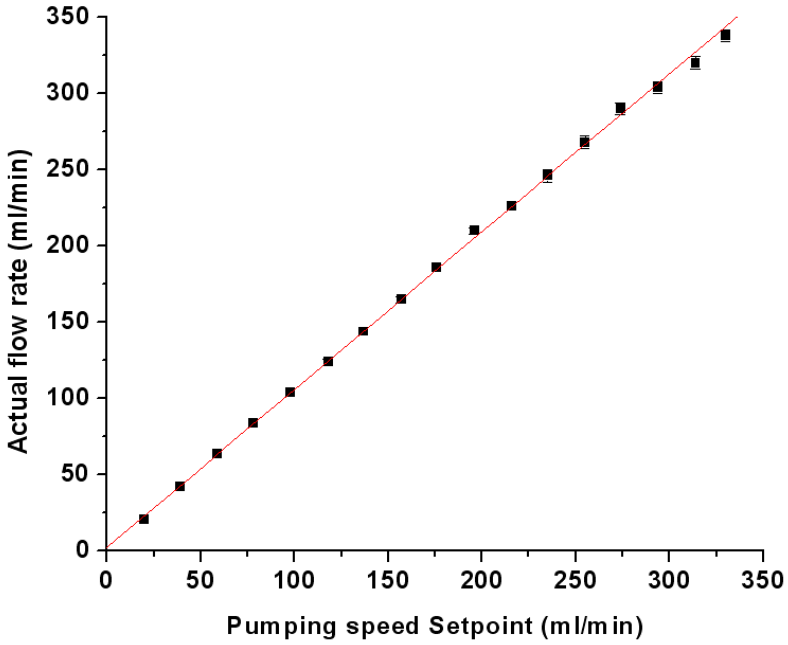

Figure 3-9 Pumping speed calibration curve.

Higher pumping speeds were also found to cause higher pressures in the tubing leading to the membrane and in the membrane unit itself. Therefore, the relationship between the pumping speed and pressure was studied. Pressure readings were monitored by the pressure transducer and record by NI data logger and Labview program in 10 second intervals. Pressure gauge showed that it takes about 30 seconds for the system to reach steady state when pumping speed changed. A needle valve on the tubing back to the absorption tank can be partially closed in order to get higher pressure in the system. Pressure profile as function of both pumping speed and needle valve opening was plotted in Figure 3-10.

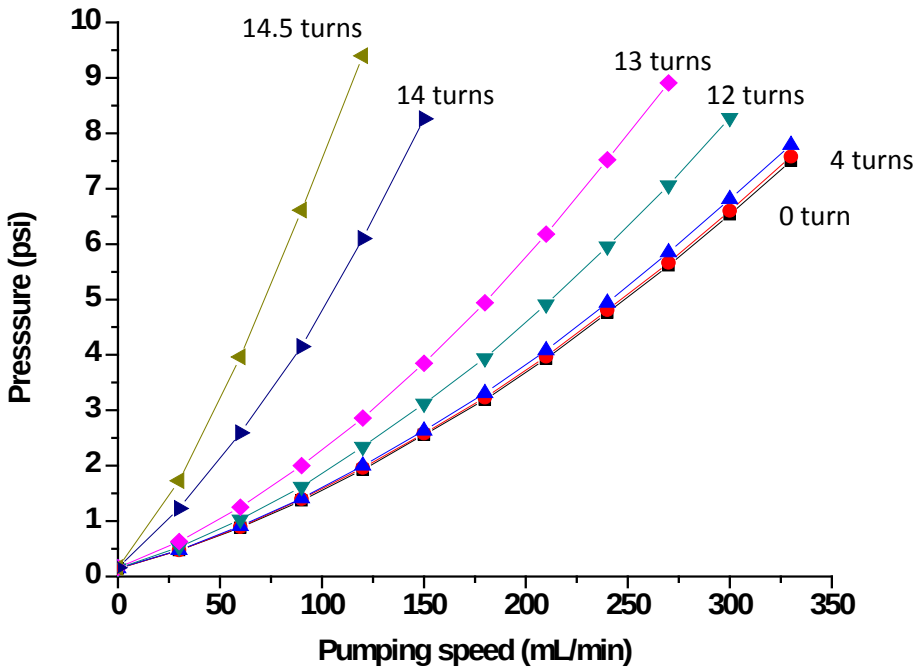

Figure 3-10 Pressure change in the tube caused by varying pumping speed and needle valve opening.

3.3.2. Validation of Temperature Control

Temperature profiles were measured using tap water as the heating solution while it was circulating at the speed of 100 mL/min. Aluminum foil was used as a barrier in the membrane holder during these measurements. Temperatures near the outlet of the heater and at the membrane were measured by the thermocouples and recorded by the data logger when the controller was set at 50°C and then 70°C, as shown in Figure 3-11. Temperatures at the heater were higher than the set points because there was a gap between the heater and the thermocouple of the controller, thus causing a temperature response delay and resulting in slight overheating. The temperature at the membrane was slightly lower than the temperature at the heater because

of the heat loss along the tube. The temperatures at steady state were quite stable with the temperature variance less than 1°C.

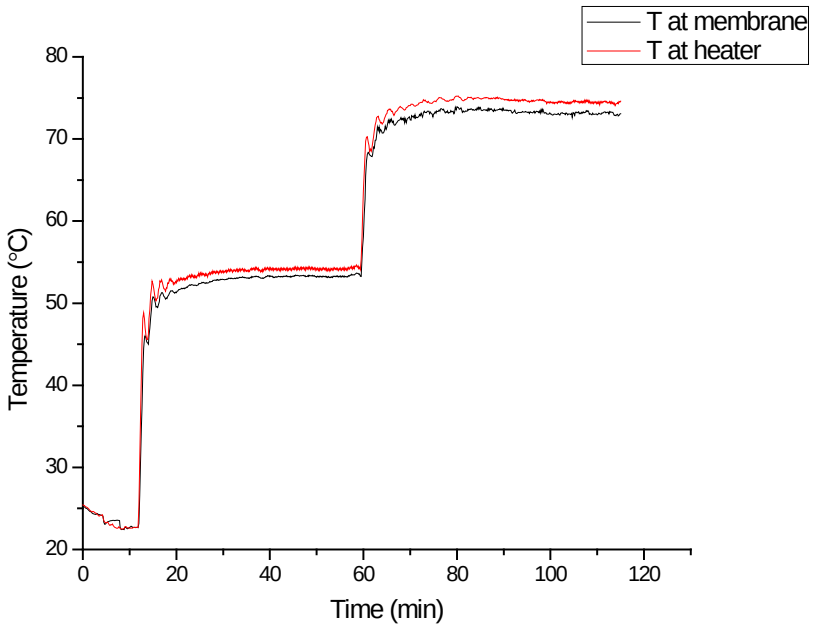

Figure 3-11 Temperature profile near the outlet of heater and at the membrane when the controller was set at 50°C and then 70°C

The temperature in the absorption tank was also monitored and recorded. With the large volume solution in the tank and with the cooling water running in the heat exchange coils, temperature at the tank was maintained at a steady point of 20°C. Figure 3-12 showed temperature profiles when the controller was set at 40°C, 60°C, 80°C, 90°C in sequence. It should be mentioned here that the temperature variance at the membrane became larger at 90°C while the temperature variance at the heater was still pretty small. This very likely indicated that water leakage or breakthrough happened at the membrane unit as the heating performance still behaved well and stable regardless what happened at the membrane.

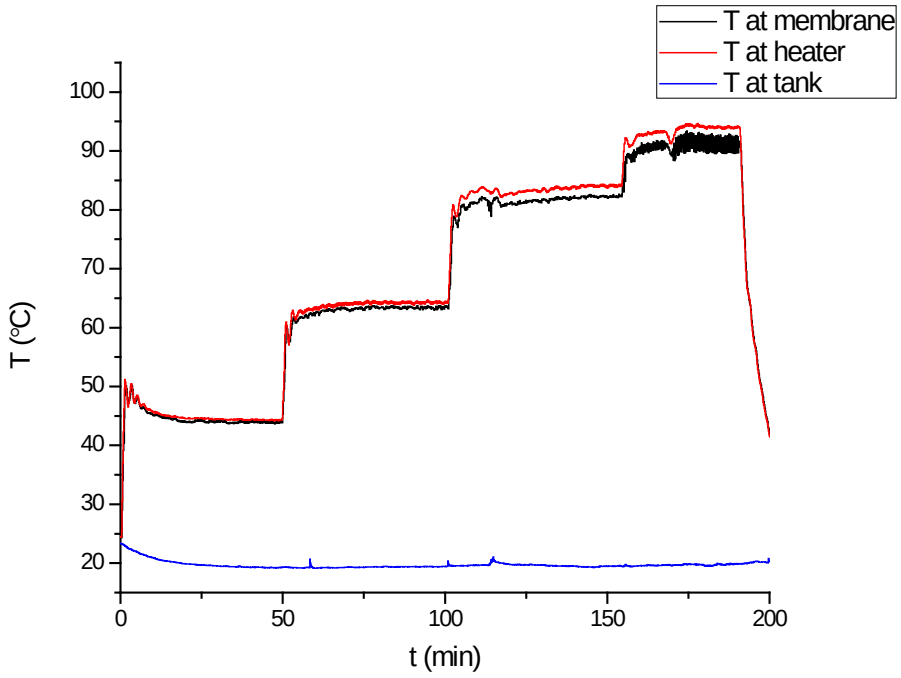

Figure 3-12 Temperature profiles when the controller was set at 40°C, 60°C, 80°C, 90°C in sequence.

3.3.3. Verification of Absorber Performance

CO_2 absorption was carried out by delivering CO_2 at 500sccm flow rate to 5L 15% wt lean aqueous MEA solution. Twenty-two solution samples were collected over a 12 hours span. Titration analysis and pH value of these samples were measured. CO_2 loading as a function of absorption time was shown in Figure 3-13.

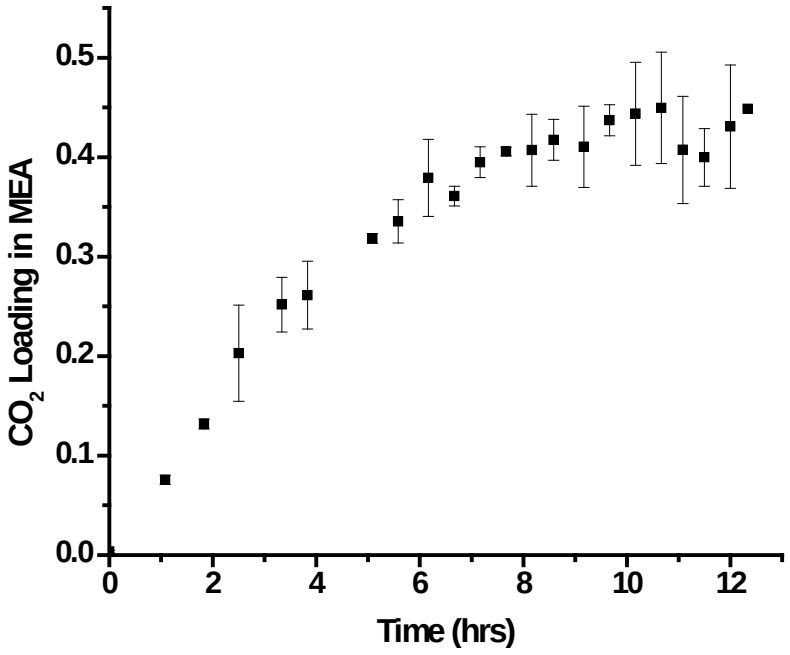

Figure 3-13 CO_2 loading versus absorption time.

Figure 3-13 showed that CO_2 loading gradually increased over time. A mass balance analysis showed that almost all CO_2 was absorbed by MEA solution due to the fast reaction kinetics before saturation. The CO_2 loading became saturated at about 0.45 (mol CO_2 per mol MEA), which was close to reaction stoichiometric point of 0.5. The large error bars arise from solvent and gas evaporation during sampling as well as from the inherent measurement error in this method. Despite the error, these measurements verified the capability of the absorber. The pH values of these samples were also measured over time (Figure 3-14). CO_2 loading and pH were found to have a fairly linear relationship $Y= 12.4 – 10.0X$ ($R^2= 0.98$) in Figure 3-15. The pH value of 15 wt% of lean aquerous MEA was in agreement with the reported pH value (Veldman Ray, 1989).

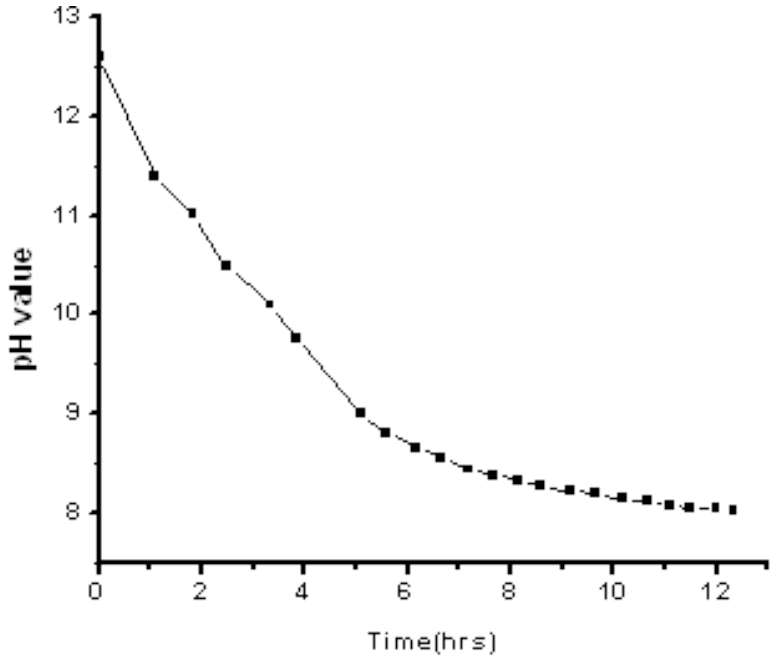

Figure 3-14 15 wt % aqueous MEA pH value vs. CO_2 absorption time

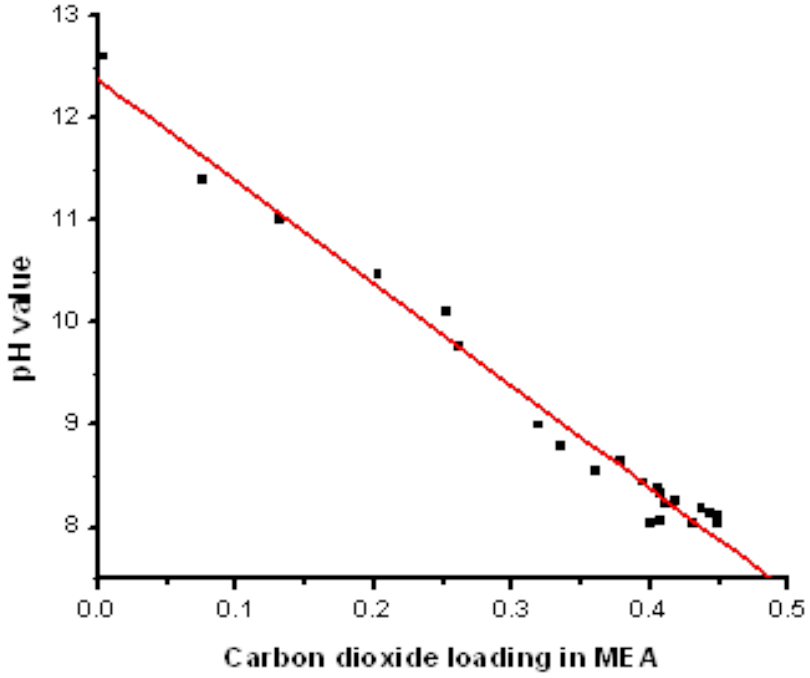

Figure 3-15 15 wt % aqueous MEA pH value vs. CO_2 loading

3.3.4. Verification of Membrane Stripping Performance

Stripping experiments were performed using a 0.45 micron porous Polypropylene membrane (GE Water & Process Technologies) to strip CO_2 from 6L of 15 wt% aqueous MEA solution. CO_2 concentration in the 1000 sccm N_2 sweep gas was monitored at pumping speed of 120 mL/min and membrane unit temperature of 80ºC. Temperature and pressure were recorded every 10 seconds by LabView during 10 hours of running.

The CO_2 flux through the membrane was calculated by Equation 3-9 and plotted in Figure 3-16.

$$Flux\ (CO_2) = (CO_2\ ppm\ value)(10^{-4})(Retentate\ flow\ rate\ in\ sccm)\left(\frac{1min}{60sec}\right)\left(\frac{1}{7.6cm^2}\right)$$

Equation 3-9

Nine samples were collected in this experiment from the absorption tank and the pH value was measured (Figure 3-17). The pH value increases over time as the CO_2 is stripped out of the solution. A mass balance calculation showed that it would take about 60 hours to strip all CO_2 out of 6L 15 wt% MEA under the average flux of 0.3 cm^3 (STP)/(cm^2.s) due to the small membrane surface area in this experiment. While this experiment was run for only 10 hours, it nonetheless verifies the ability of the system to strip CO_2 from the MEA solution.

Substantial average CO_2 flux of 0.3 cm^3 (STP)/(cm^2.s) (1.3×10^{-1} mol.m^{-2}.s^{-1}) was detected for 10 hours run courses after steady state was reached. Naim et al. (Naim et al., 2012) reported CO_2 stripping flux from DEA solvent achieved by PVDF hollow fiber modules with 5 wt% LiCl was 1.6×10^{-2} mol.m^{-2}.s^{-1}. Khaisri et al. (Khaisri, deMontigny, Tontiwachwuthikul, & Jiraratananon, 2011)used PTFE hollow fiber membrane module stripped 3-7 kmol/m^3 CO_2

loaded MEA at 90-100ºC, CO_2 desorption flux measured ranged from 2×10^{-5} $mol.m^{-2}.s^{-1}$ to 6×10^{-3} $mol.m^{-2}.s^{-1}$ at various process parameters. The CO_2 stripping flux we achieved was much higher than both reported values. This could be attributed to many factors, including the very small surface area with abundant CO_2 and CO_2 loaded solvent; much fast inline heating kinetics in our system, the subsequent turbulence created by it, and membrane differences itself such as pore size and composition. The exciting part about all three results is that they all showed promises of using membrane contactors for stripping CO_2 loaded solvents.

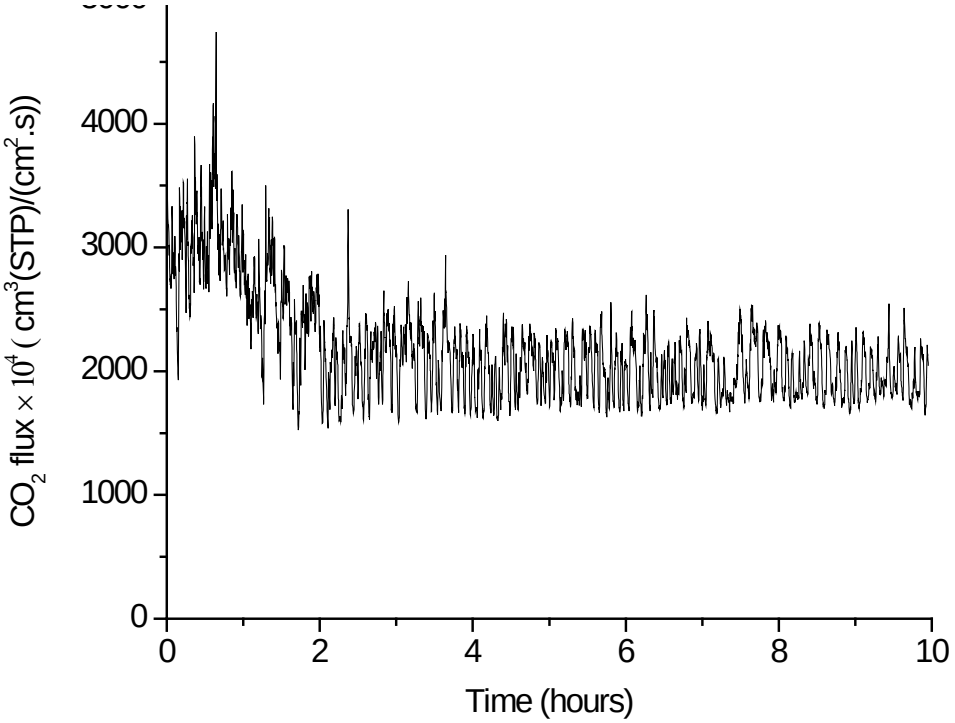

Figure 3-16 CO_2 flux versus stripping time.

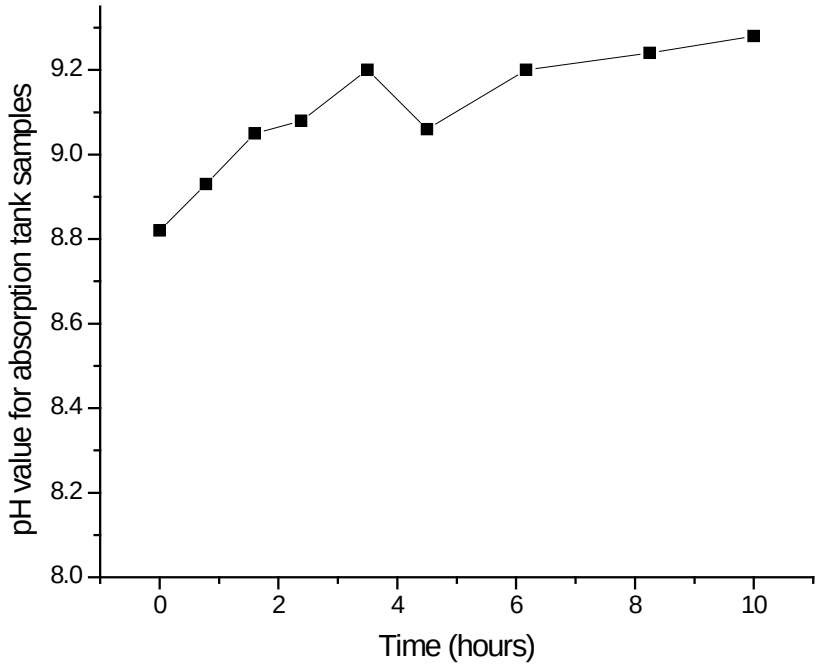

Figure 3-17 pH of the solution in the absorber over time.

The permeated liquid was collected at the coalescing filter and analyzed. UV-vis spectra (Figure 3-18) confirmed the stripping performance. CO_2 absorption peak (at around 270 nm) intensities decreased prominently after 4 hours stripping. The permeated liquid through membrane was collected at coalescing filter and showed very different composition than the solutions at retentate side. The differences could be explained from two aspects: one could be due to majority of CO_2 was stripped off the permeated liquid; and the other reason could be more water vapor permeated than MEA vapors due to its higher concentration and lower boiling point.

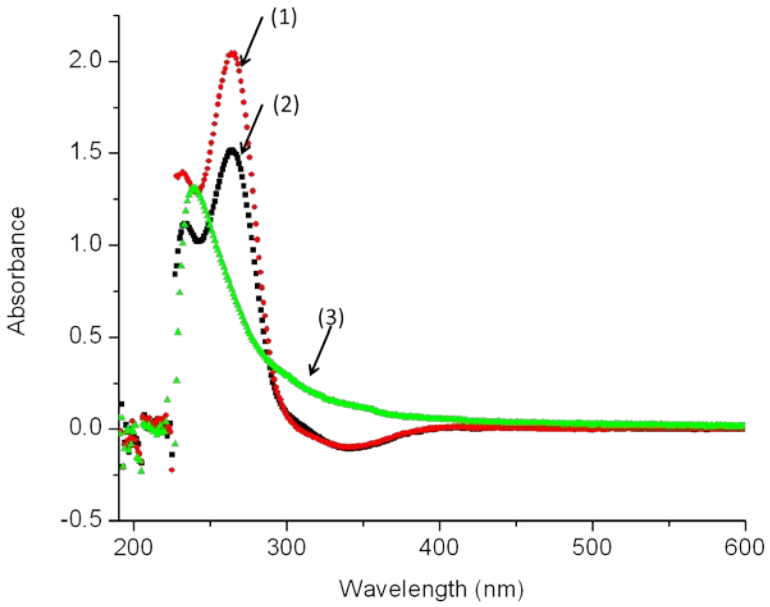

Figure 3-18 UV-vis spectra of (1) full CO_2 loaded aqueous 15 wt% MEA solution; (2) solution after 4 hours of stripping; (3) liquid collected at the coalescing filter during course run. (All with lean aqueous 15 wt% MEA solutions as a reference)

4. POROUS MEMBRANE MATERIALS SCREENING STUDY

Membrane process efficiency relies on the membrane material performance and reliability. During the first stage of this study, various materials were screened to assess their potential for this process. These membranes are listed in Table 4-1. The candidates were chosen from relatively inexpensive and commercially available microfiltration membranes. PTFE membranes from two different sources with different pore size were included. For membrane performance, both high CO_2 flux and high selectivity towards CO_2 are favorable. Other operational aspects considered included mechanical strength, chemical and thermal stability of the membranes, and hydrophobicity.

Table 4-1 List of membrane candidates

Membrane materials	**Abbreviation**	**Pore size (μm)**	**Thickness (mm)**	**Sources**
Polyethersulfone	PES	0.22	0.16	Millipore
Polyvinylidene Fluoride	PVDF	0.45	0.12	Millipore
Mixed Cellulose Ester	CE	5.0	0.12	Advantec
Polytetrafluoroethylene	PTFE-1	1.2	0.07	Sartorius Stedim
Polyester	PETE	0.4	0.01	GE Water & Process
Laminated Teflon	PTFE-2	0.45	0.12	GE Water & Process
Polypropylene	PP	0.45	0.16	GE Water & Process
Polyamide	PA	0.45	0.12	Sartorius Stedim
Cellulose Acetate	CA	5.0	0.12	Advantec

4.1. Porous Membrane Screening

Porous membrane candidates (Table 4-1) were tested under the same conditions of pumping speed at 120 mL/min, the heater temperature at 80ºC, and the N_2 sweep gas rate at 1000 sccm. The CO_2 concentration in sweep gas was measured every 10 seconds by NDIR. The measurements for 6 hours after steady state reached were used and averaged to calculate the CO_2 permeation flux. Permeated liquid collected by the coalescing filter was also measured to calculate the liquid flux. Selectivity was obtained as the ratio of permeated CO_2 flux and permeated liquid flux.

Table 4-2 Porous membranes flux and selectivity

Materials	**CO_2 flux ($cm^3/(cm^2.s)$)**	**Liquid flux ($cm^3/(cm^2.s)$)**	**Selectivity**
PTFE-1	0.80±0.36	7.45×10^{-4}	1074
PTFE-2	0.23±0.02	2.41×10^{-4}	954
PP	0.32±0.03	3.51×10^{-4}	930
PETE	1.56±0.13	2.33×10^{-3}	672

The performance of membrane candidates is shown in Table 4-2. PTFE and PP showed similar performance on both permeation flux and high selectivity. Polyester had a significantly higher flux of both CO_2 and liquid but the selectivity toward CO_2 is much lower, which could be due, in part, to its thinner membrane thickness. Mixed cellulose ester membranes, PVDF, polyamide, and cellulose acetate were tested but suffered from excessive liquid leaks, which is likely due to the hydrophilic nature of these materials. It was concluded that these membranes are too easily wetted by the aqueous solvent and are likely too hydrophilic for this application. For PES, it was found that the CO_2 flux decreased dramatically over time (Figure 4-1). After

taking the membrane out from the system, it was observed that this membrane had become fouled by a yellowish cake-like deposit. The decrease of CO_2 flux is likely due to the severity of the fouling effect and the accumulation of the thickness of this layer.

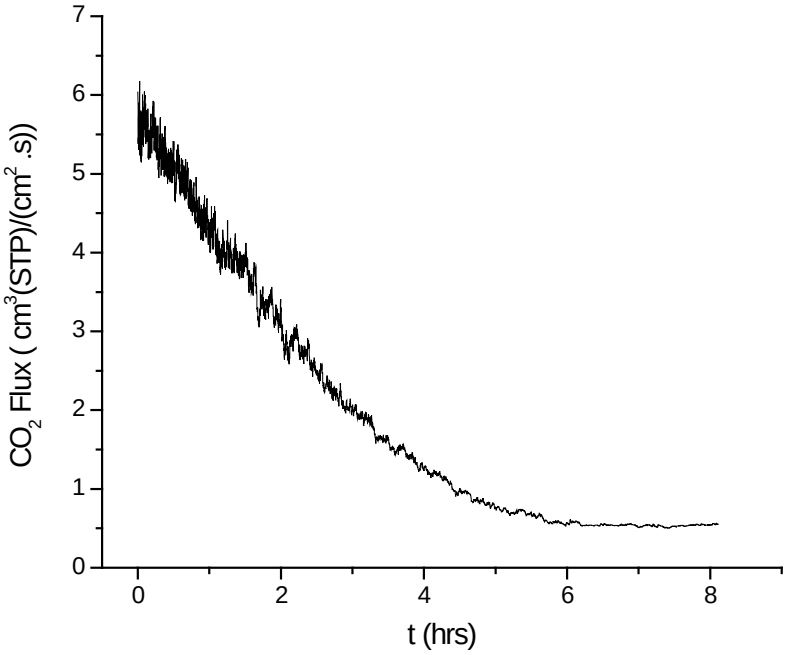

Figure 4-1 CO_2 flux for PES membrane versus stripping time

4.2. Porous Membrane Surface Morphology

Membrane surface morphology was observed using an optical microscope for changes. No significant surface changes were observed for PP and PTFE using optical microscopy (Figure 4-2), but some yellowish deposits were found on the PETE membrane surface (Figure 4-3). This could possibly be the precipitated MEA or the by-product of MEA degradation which could not adhere to PP and PTFE surface due to their hydrophobicity or low surface energy.

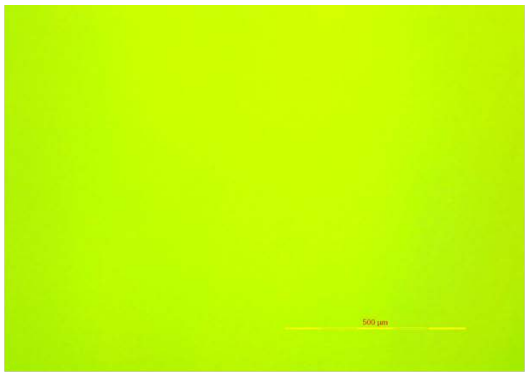

PP membrane before run

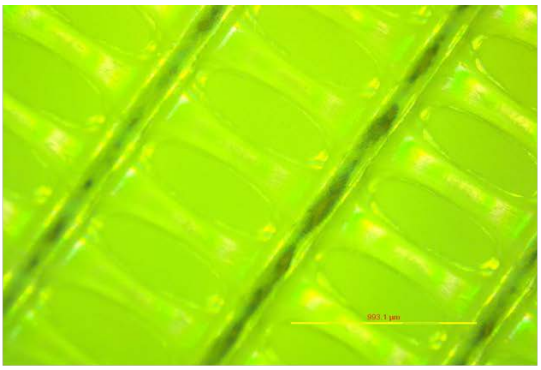

PTFE membrane before run

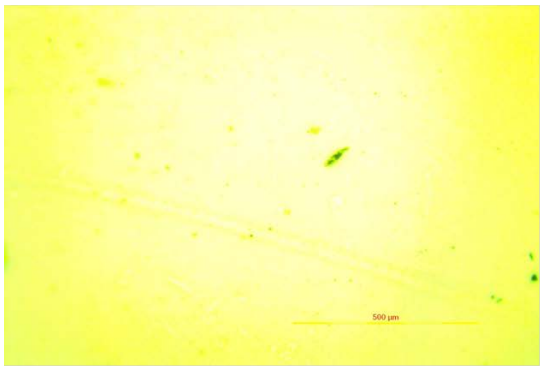

PP membrane after run

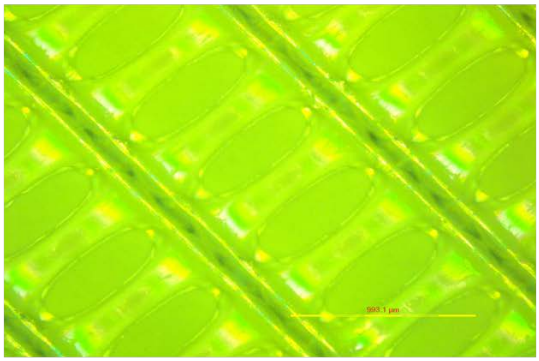

PTFE membrane after run

Figure 4-2 PP and PTFE membrane surface before and after run

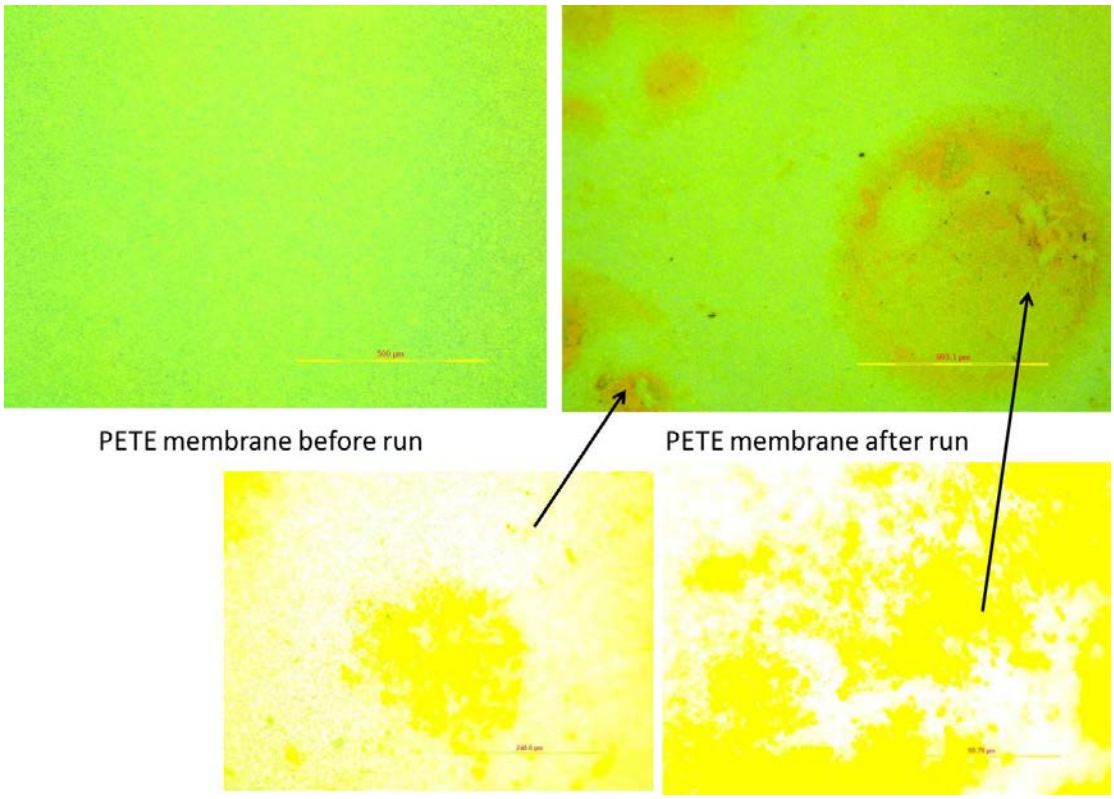

Figure 4-3 PETE membrane surface change before and after run

4.3. Compositional and Structural Characterization

DSC was used to measure the glass transition temperature and melting point of the membranes and characterize the potential structural changes (Figure 4-4). In the cases of PP and PTFE, crystalline peaks were observed, and little change was seen after the permeation experiments. A significant change was observed for PETE. It appears that the material becomes more crystalline during the course of the run, as seen by the sharp peak in the DSC curve, due to this semi-crystalline polymer being raised above its glass transition temperature.

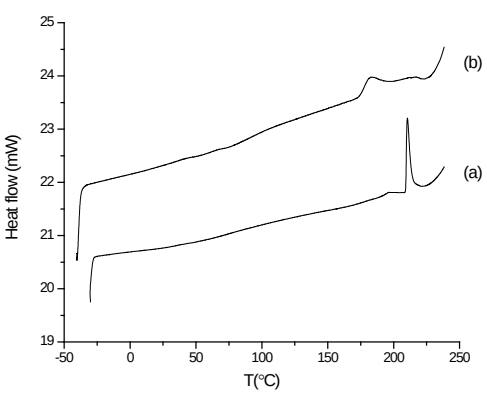

(1)

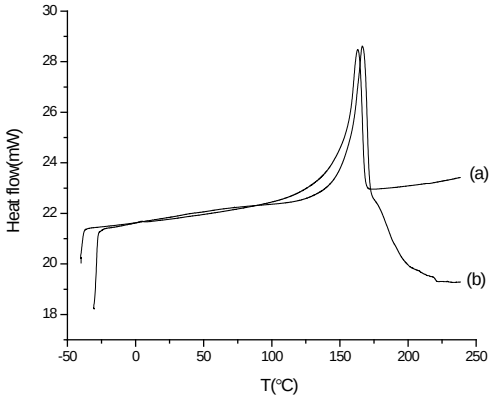

(2)

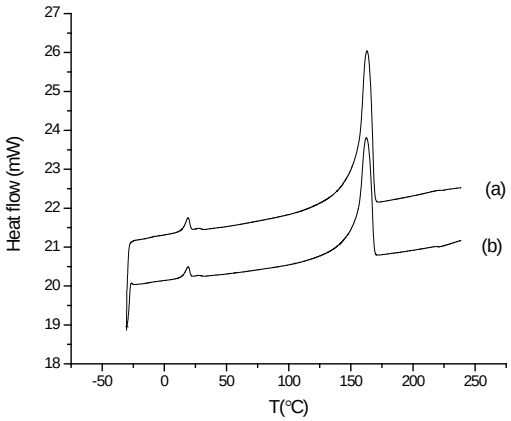

(3)

Figure 4-4 (a) Membrane after experiment; (b) Membrane before experiment (1) DSC results of PETE, (2) DSC results of PP, (3) DSC results of PTFE

FTIR (Thermo Scientific, Nicolet IR 200) was used to characterize the compositional change between the fresh membrane and membrane that was exposed to MEA/CO_2 solution at elevated temperature for stripping runs (Figure 4-5 and Figure 4-6). Dried membranes were mounted on ATR (attenuated total reflectance) accessory which contains a ZnSe crystal to cause internal reflections at the membrane surface, 16 scans were performed for each membrane at 2 cm^{-1} resolution and the background spectrum was recorded in the air and subtracted.

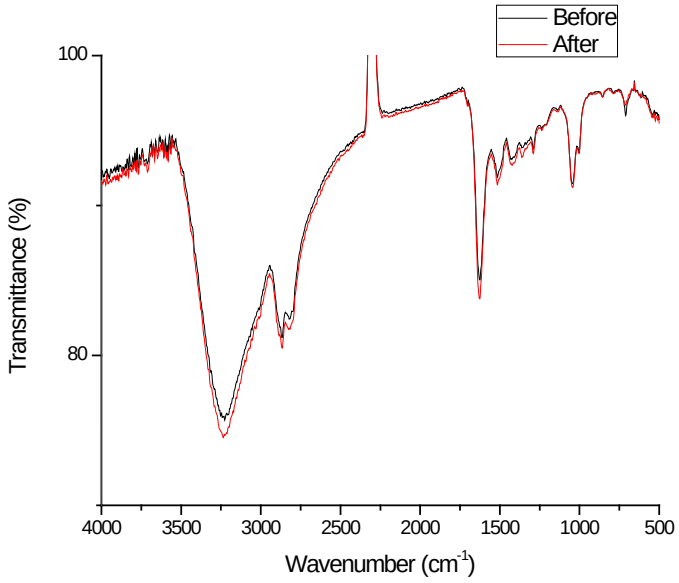

Figure 4-5 FTIR spectrum for PETE membrane before and after run

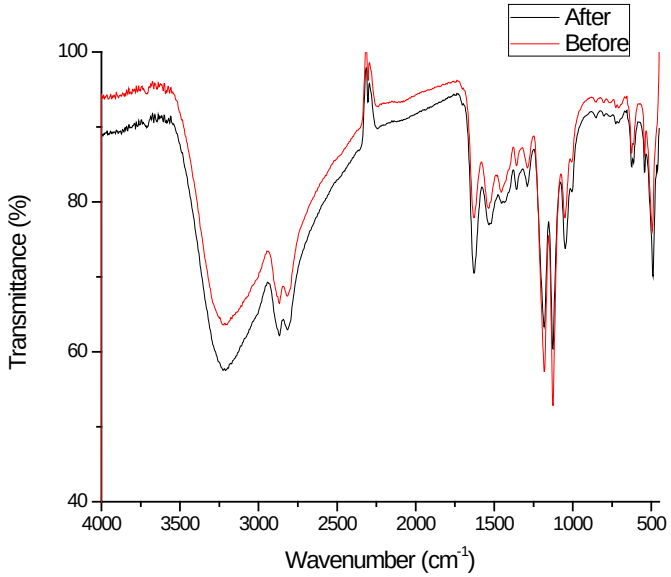

Figure 4-6 FTIR spectrum for PTFE membrane before and after run

The spectra consist of a lot peaks from many sources. The broad peak at 3300 cm^{-1} may come from the OH contribution of water indicating residual water signals (Rabiller-Baudry, Le

Maux, Chaufer, & Begoin, 2002). CO_2 absorption peaks appear near 2350 cm^{-1} and 670 cm^{-1}. The spectra showed no significant changes. This again might suggest that the MEA solvent could be adsorbing onto the membrane surface but no chemical reaction happened between the membrane and the solvent.

4.4. Membrane Sorption Study

As previously reported, significant differences were observed in the performance of various membrane materials during porous membrane screening measurements. It was assumed that the hydrophilicity of the material was primarily responsible for these differences, but that chemical incompatibility of some materials to the MEA solution may also play a role. To understand these effects further, Sorption experiments were performed to study the absorption of MEA solution into each material, as well as membrane solvent interaction and compatibility. Aqueous solution of 15 wt. % lean MEA was used as solvent. The membrane thickness was measured using a digital micrometer (Fowler IP54, ±0.00001in) and weighed on a microbalance (Fisher Scientific, ±0.00001g). Duplicate fresh samples were measured (Table 4-3), then immersed in 2L of solvent and heated in a vented water bath (Precision microprocessor controlled 280 series) at 83°C for 20 hours. Samples were removed from the solvent using tweezers, and then excess solvent was removed by clean dry filter paper (Scientific Products). The membranes were weighed and recorded every 30 minutes until no more weight loss.

Table 4-3 Physical properties of membranes before sorption test

Membrane Type	Mass (g)	Thickness (cm)	Volume (cm^3)	Density (g/cm^3)
PES-1	0.0857	0.0164	0.2853	0.3003
PES-2	0.0860	0.0167	0.2901	0.2964
PVDF-1	0.1235	0.0110	0.1917	0.6443
PVDF-2	0.1246	0.0110	0.1917	0.6500
PTFE-1-1	0.0780	0.0072	0.1249	0.6247
PTFE-1-2	0.0793	0.0072	0.1263	0.6277
PETE-1	0.0174	0.0012	0.0205	0.8461
PETE-2	0.0179	0.0011	0.0191	0.9374
PTFE-2-1	0.0767	0.0106	0.1836	0.4177
PTFE-2-2	0.0754	0.0110	0.1902	0.3963
PP-1	0.0433	0.0167	0.2901	0.1493
PP-2	0.0430	0.0171	0.2967	0.1449
PA-1	0.0638	0.0116	0.2012	0.3170
PA-1	0.0617	0.0114	0.1976	0.3123
CA-1	0.0779	0.0120	0.2079	0.3748
CA-2	0.0771	0.0120	0.2049	0.3763

It was found that roughly 2/3 aqueous MEA solution was evaporated by the end of the experiment. The solution was more like a yellowish emulsion dispersed in the solution. Some yellow residuals deposited on the membrane surfaces as well.

Membrane appearance changed significantly (Figure 4-7). The change was likely attributed to a combination effect of the strong alkalinity of the MEA, the high temperature and the MEA concentration increase caused by relatively faster water evaporation rate over time. The sorption conditions in this experiment are probably pretty extreme and a lot more harsh than the conditions of the actual process, especially after significant solvent evaporation.

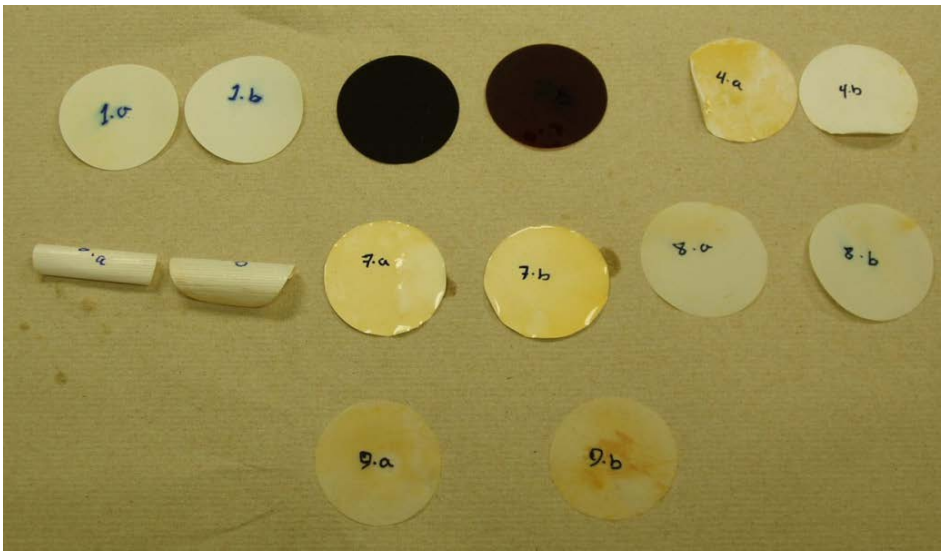

Figure 4-7 Membrane appearance after sorption for 20 hours.

The mass gain of each membrane for approximately 30 hours was shown (Figure 4-8). This slow liquid evaporation rate might suggest that the liquid absorbed by the membranes was probably not water alone. The final mass of PVDF, PP, CA and PTFE are close to the original mass. PES and PA had significantly mass gain after sorption, which possibly came from the yellowish deposits from the solution.

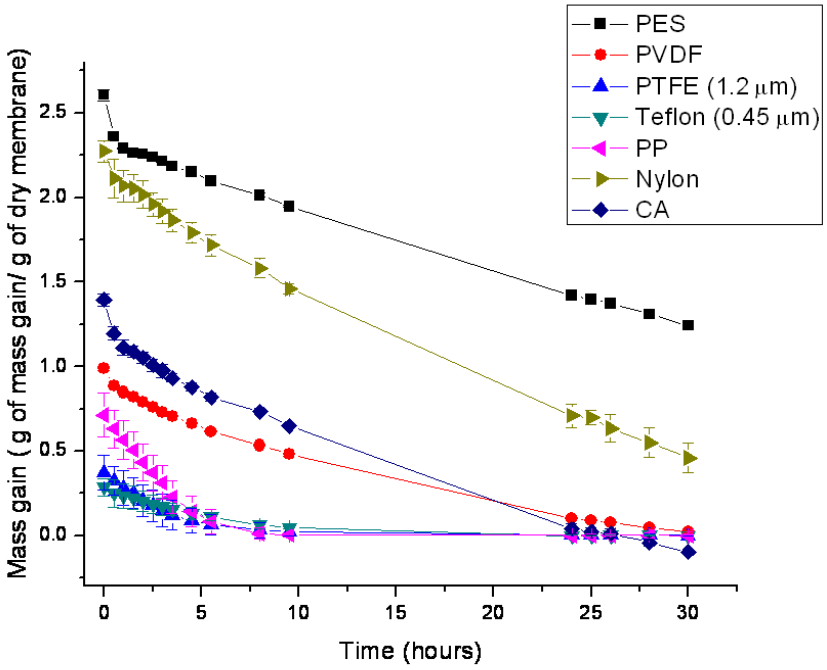

Figure 4-8 Mass change of different membranes after sorption vs. drying time

The mass gain for the membranes is composed of two parts: the non-evaporative deposits on the membrane surface; and solvent swelling which is evaporative (Figure 4-9). Both two types of mass gain will deteriorate the membrane performance and permeation flux. PP and PTFE showed outstanding performance to be almost free of deposits and have relatively low swelling effect, possibly attributed to their low surface energy and high hydrophobicity. PES and PA have relatively high percentage of non-evaporative mass gain and showed high probability of deposit formation and fouling. PA, PVDF, PES and CA showed much higher hydrophilicity than PP and PTFE. For CA, non-evaporative mass gain is negative which may imply cellulose deacetylation in the MEA aqueous solution.

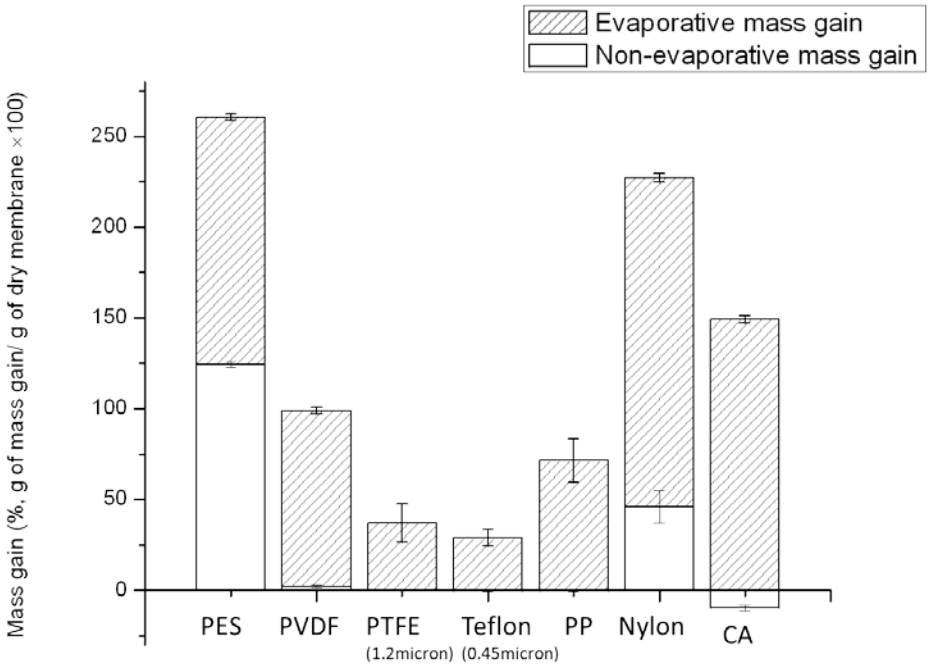

Figure 4-9 Percentage of evaporative and non-evaporative mass gain

Using the criteria developed by Yamaguchi et al (Yamaguchi, Nakao, & Kimura, 1993), the solubility coefficient was calculated using equation:

$$s = \frac{\frac{\Delta W}{\rho_1}}{\frac{\Delta W}{\rho_1} + \frac{1}{\rho_2}}$$

Equation 4-1

Where ΔW is weight of liquid dissolved in the membrane (g of solvent/g of dry membrane) and ρ1 and ρ2 is density of liquid and dry membrane respectively. The calculated values of solubility coefficient for different membranes are shown in Figure 4-10.

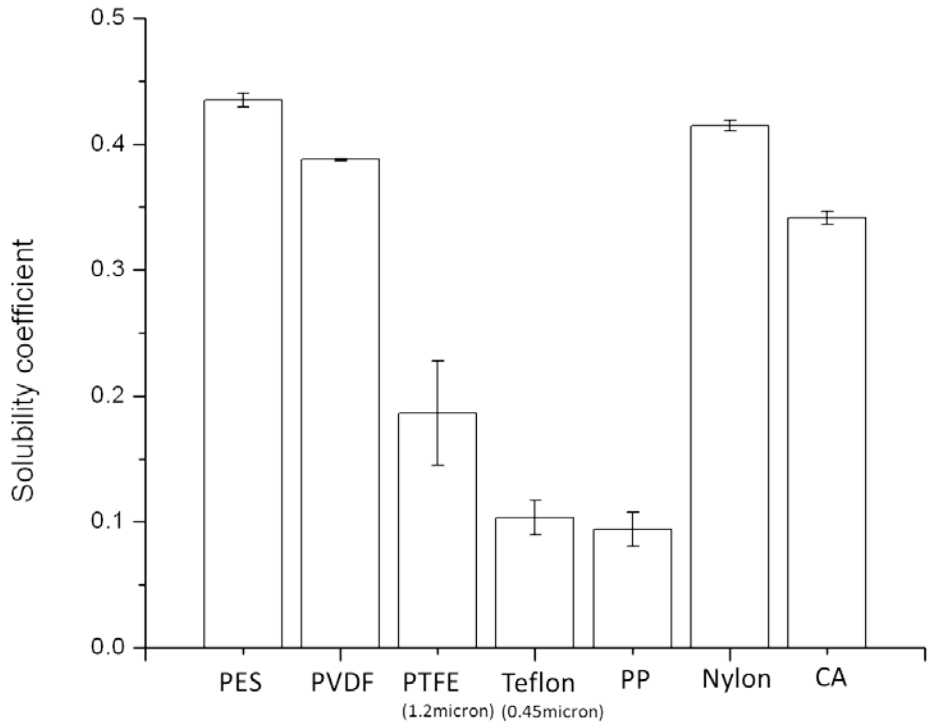

Figure 4-10 Solubility coefficient for different types of membranes

Additional sorption experiments were performed to study the solvent alkalinity effect on membranes. Because the CO_2 loading of aqueous MEA can significantly affect the pH of the solution, measurements were taken in both lean and loaded solutions. Experiments were performed using a lean 15% aqueous MEA solution (pH=12.5) and a CO_2 loaded 15% aqueous MEA solutions (pH=9.2). Lid was used to prevent significant solvent evaporation.

Samples of each material were first weighed and then placed in the respective solutions at a temperature of 82^{o}C. After 20 hrs, the membranes were taken out of solution and weighed. Using a moisture analyzer (OHAUS), the samples were dried by gradually heating to 105^{o}C and holding it at this temperature until the mass no longer changed. The final weight of each sample was then recorded.

Figure 4-11 is a plot of the mass of each membrane before and after absorption, as well as after drying, for those measurements with a lean MEA solution. Figure 4-12 presents this data as a percentage of the original mass of the membrane. What these data show is that PES, Nylon, PVDF and CA are very hydrophilic, absorbing in some cases 100% or more of their mass in MEA solution. Each of these materials had slight changes in mass after drying, but this was attributed to variability in the mass measurements. Interestingly, PETE completely dissolved in the MEA solution, likely due to hydrolysis of the ester bonds. CA was found to lose considerable mass during the measurement, which could also be due to hydrolysis of the acetate groups in the strong basic solution. As expected, PTFE and PP showed hydrophobic behavior, with only slight mass changes observed after absorption and after drying.

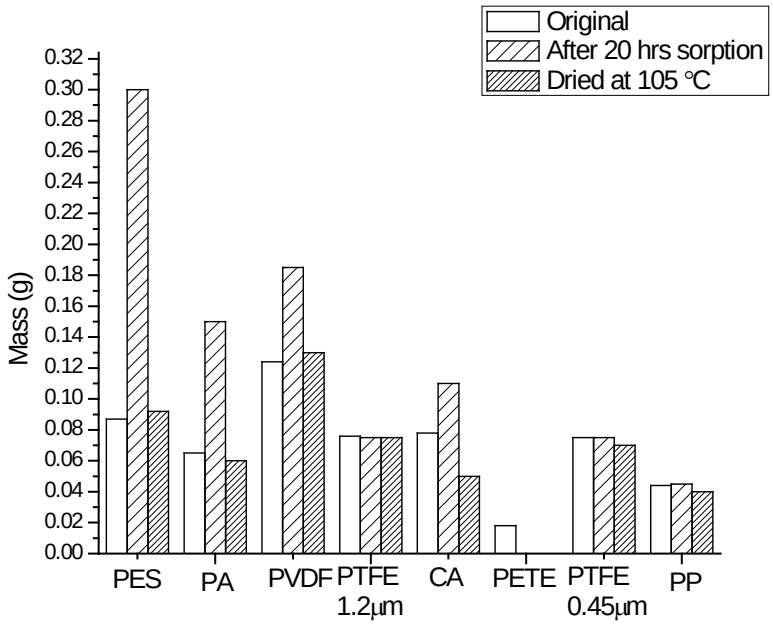

Figure 4-11 Mass comparison for the original membranes, the membranes after absorption in a lean 15% aqueous MEA solution (pH=12.5) at 82^{o}C for 20 hrs, and after drying at 105^{o}C.

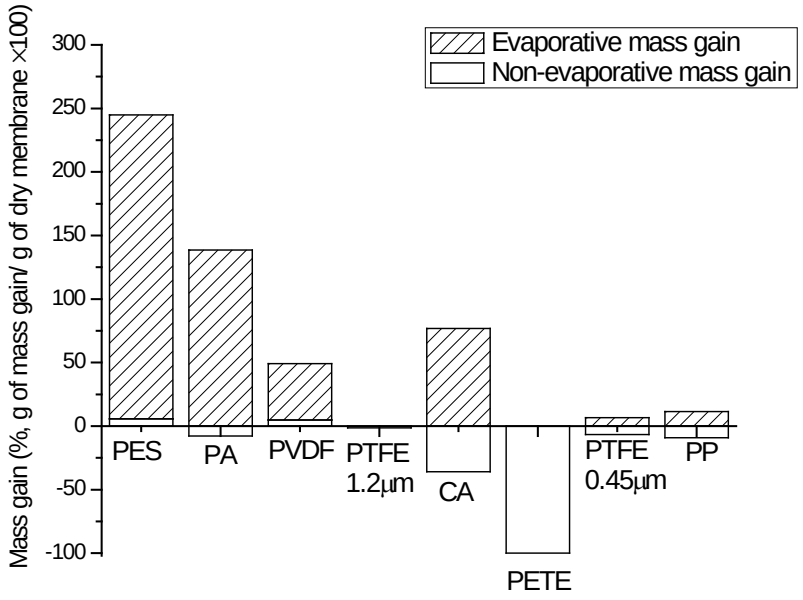

Figure 4-12 Mass change as a function of the original membrane mass, after absorption in lean solution and after drying.

For those measurements in MEA solution loaded with CO_2 (Figure 4-13 and Figure 4-14), the results differed in several ways. First, the amount of solution absorbed by the hydrophilic samples was higher in all cases. For CA, the amount of mass lost was significantly lower. The biggest difference was observed with PETE, which did not dissolve in the solution as it had with lean MEA. The findings for CA and PETE are consistent with the slower rate of hydrolysis at a lower pH. The hydrophobic samples showed essentially the same behavior as with the lean solution.

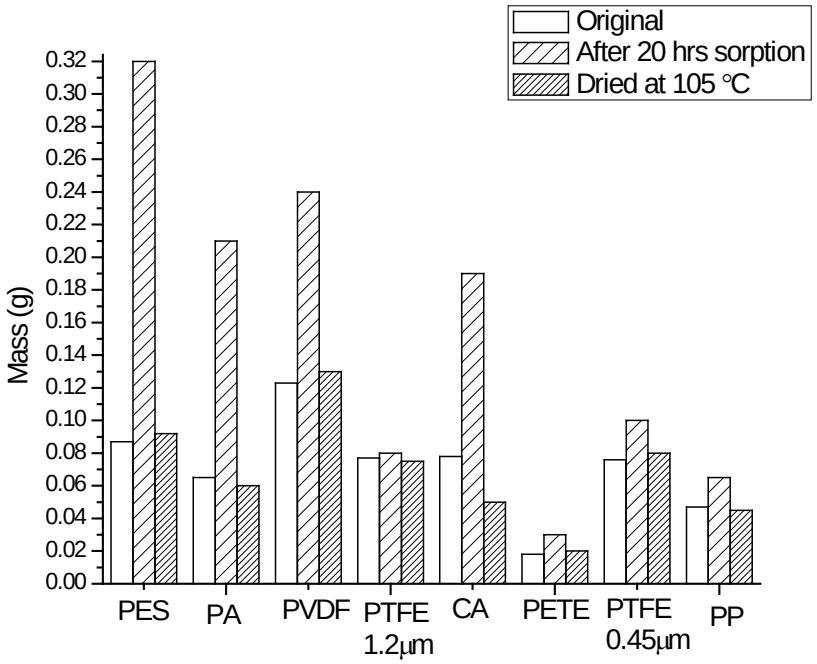

Figure 4-13 Mass comparison for the original membranes, the membranes after absorption in a loaded 15% aqueous MEA solution (pH=9.2) at 82^{o}C for 20 hrs, and after drying at 105^{o}C.

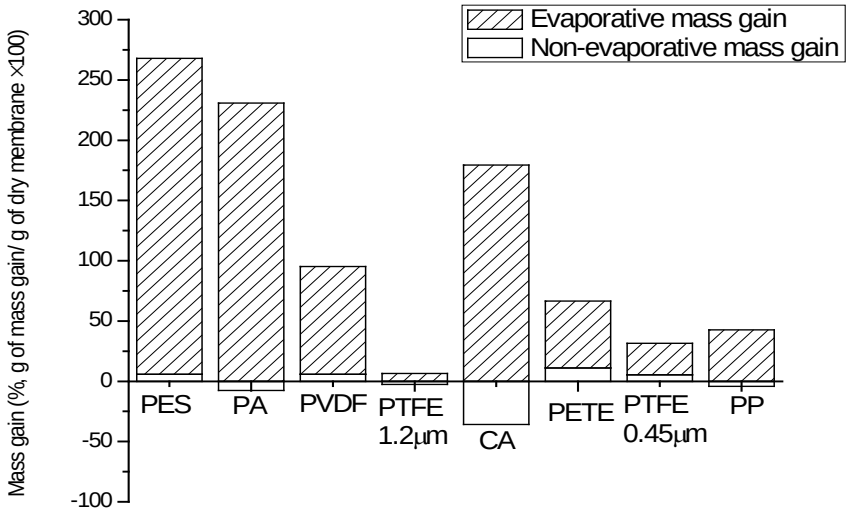

Figure 4-14 Mass change as a function of the original membrane mass, after absorption in loaded solution and after drying.

These findings are generally consistent with the membrane screening trials. Hydrophobic materials, in which the solution does not wet the pores of the membrane, perform best. Hydrophilic membranes resulted in excessive wetting and, eventually, an unacceptable rate of leaks. Despite being dissolved in the lean MEA solution, PETE was able to perform well in our membrane screening trials. Since these trials used a fully-saturated MEA solution, hydrolysis was not an issue. However, it could become an issue if CO_2 in the solvent is totally stripped off together with large amount of solvent evaporation , thereby raising the solution pH and the MEA concentration.

4.5. Chapter Conclusion

Eight commercially available microfiltration membranes were evaluated for the application of CO_2 regeneration from 15 wt% aqueous MEA solutions. PTFE and PP membranes outperformed PVDF, PES, PETE, PA, CA and CE membranes showed promises. PTFE and PP exhibited excellent hydrophobicity while allowing substantial fluxes of CO_2 permeation. Their composition and structure remained stable and no significant change was found during the course of run. The sorption study showed the membranes' ability of staying free from fouling and wetting from the MEA. Again, PTFE and PP showed better performance than the other candidates.

5. PARAMETRIC STUDY FOR CO_2 REGENERATION

For the promising membranes found in the screening study to be suitable for this application, a more detailed parametric study was conducted in order to determine the effect of temperature, liquid flow rate, sweep gas flow rate, and liquid pressure. The effect of individual parameters was studied. Two-level, three-factor full factorial experiment runs were also performed to identity significant factors and seek parametric optimization. Based the experiment results and observations, the mass transfer mechanism was discussed. The goal of this work is to understand the parameters affecting the mass transfer rate in this system in order to scale up our results so that they can be compared to a conventional CO_2 absorber-stripper system.

5.1. Data Analysis Method

Other than CO_2 recovery flux and permeated CO_2/liquid selectivity, data obtained from the parametric study were also used to calculate the % CO_2 recovered from the MEA solution. This was determined from the measured CO_2 flow rate in the sweep N_2 gas at the permeate side and the measured saturated CO_2 content in the MEA solution at the retentate side using Equation 5-1.

$$\%\ regeneration(t) = \frac{CO_2 \text{ content in the sweep gas flow at time t}}{CO_2 \text{ content in the feed solution at a fixed flow rate}}$$

Equation 5-1

For example, for 15 wt% aqueous MEA, the molar concentration of MEA is:

$$\frac{\frac{15\ \text{g}}{61.08\ \text{g/mol}}}{\frac{15\ \text{g}}{997\text{g/L}} + \frac{85\ \text{g}}{1012\ \text{g/L}}} = 2.46\text{mol/L}$$

Equation 5-2

Here, the MEA molar mass is 61.08 g/mol, the H_2O molar mass is 18.02 g/mol, the density of DI water is 1012 g/L, and the density of MEA 997g/L. The CO_2 loading of the MEA solution is typically 0.4, as measured by titration analysis. At fixed flow rate of 120 mL/min , the CO_2 flow rate on the feed side is

$$120\frac{\text{mL}}{\text{min}} \times 2.46\frac{\text{mol}}{\text{L}} \times 10^{-3}\frac{\text{L}}{\text{mL}} \times 0.4 \times 22.4\frac{\text{L(STP)}}{\text{mol}} \times 10^{3}\frac{\text{cm}^3}{\text{L}}$$

$$= 2645\ \text{cm}^3\text{(STP)/min}$$

Equation 5-3

On the permeate side, if the CO_2 concentration in the 1000 sccm sweep N_2 gas flow was measured at 5000 ppm, the CO_2 flow rate is

$$1000\frac{\text{cm}^3\text{(STP)}}{\text{min}} \times 5000\ \text{ppm} \times \frac{10^{-6}}{\text{ppm}} = 5\ \text{cm}^3\text{(STP)/min}$$

Equation 5-4

Therefore, the % CO_2 regeneration in this example is 0.19%. In these experiments, the CO_2 regeneration rate is generally low due to the small lab scale membrane surface area of 7.6

cm^2 (manufacturer specification) provided by a 47 mm diameter circular membrane holder. However, for a typical commercial membrane module, the surface area is several orders of magnitude larger.

5.2. Effect of Temperature

Temperature is expected to have a significant effect on the flux of CO_2 since the maximum loading of CO_2 in MEA decreases with temperature. Also, for membranes in general, an increase in temperature normally leads to increased permeability, though there is normally a decrease in selectivity as well.

A series of experiments was run using porous PTFE membranes to determine the effect of process temperature on the separation of CO_2 and aqueous MEA solution. Two pieces of porous PFTE membranes (Sartorius Stedim, 1.2 micron pore size, 47 mm diameter, 0.166±0.020 mm thickness for two) were mounted in the membrane holder. Aqueous MEA solution (15% wt) was pre-loaded and saturated with CO_2. This solution was circulated at a maximum speed of 330 mL/min at the retentate side under room temperature to make sure no liquid leaking was observed. Permeation measurements were performed for 8 hours of continuous running at each temperature of room temperature (no heat), 40ºC, 50ºC, 60ºC, 70ºC, and 80ºC. Other than the varying temperature setting, the feed side pumping speed was kept at 120mL/min and N_2 sweep gas deliver rate at 500 sccm, 300 sccm CO_2 was delivered to the absorption tank in the whole process to keep the same CO_2 saturation level.

The CO_2 flux through the membrane (Figure 5-1) showed no significant change up to around 60ºC. A significant flux increase was seen above 70ºC. These results matched with

previous reported MEA properties by other researchers, who found that aqueous MEA absorption of CO_2 occurs at temperatures up to approximately 60°C (Wallace, 2005). Yeh et al. (2001) reported no significant difference in absorption ability in the range 38-50°C for a 20 weight percent (wt%) aqueous MEA solution. The MEA–CO_2 reaction is exothermic and reversible by supplying heat to the system. The temperature swing absorption/evolution process reverses at approximately 70°C (Wallace, 2005).

The temperature, pressure and flux averages and standard deviations were calculated over the time period of the steady state. It was noticed that the CO_2 flux and pressure variation was much larger than the temperature variation and they both increased significantly as the temperature increased. The variance in both CO_2 flux value and pressure seem to increase with temperature. The pressure increase suggested that the feed solution flow became more turbulent with the temperature rise and the large variability of pressure measurements at high temperature suggested that gas and liquid may be co-exist in the system and this situation would likely facilitate this mass transfer process.

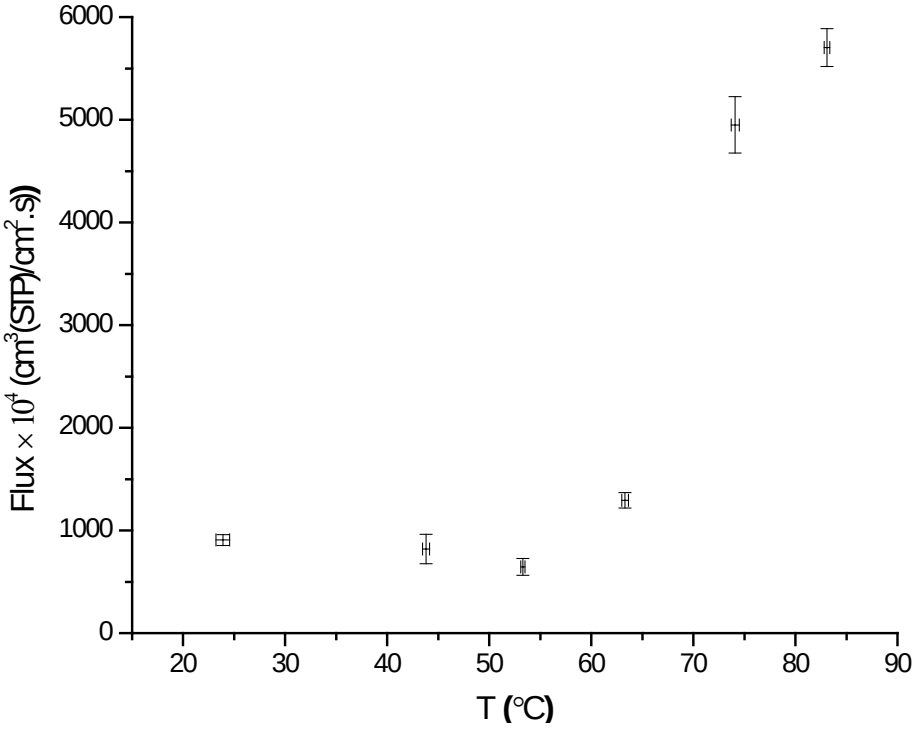

Figure 5-1 CO_2 average flux through the porous PTFE membrane at various temperatures.

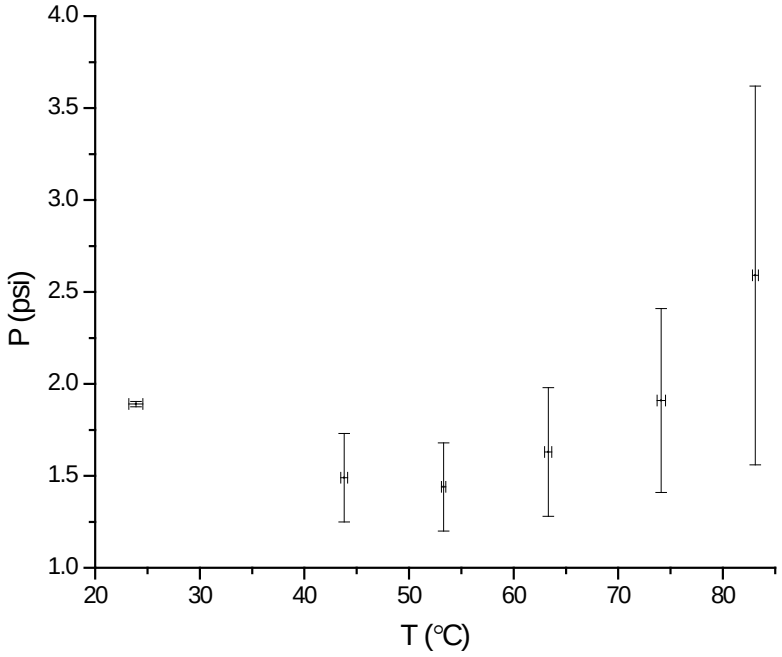

Figure 5-2 Pressure profile at the feed side at various temperatures

More experiments were performed in the promising process temperature range of higher than 70°and lower 100°C based on previous results. A trend of improved regeneration was shown (Figure 5-3) as temperature is increased. This result is expected based on previous results. Further runs at higher temperatures are planned in order to determine the maximum amount of CO_2 that can be recovered.

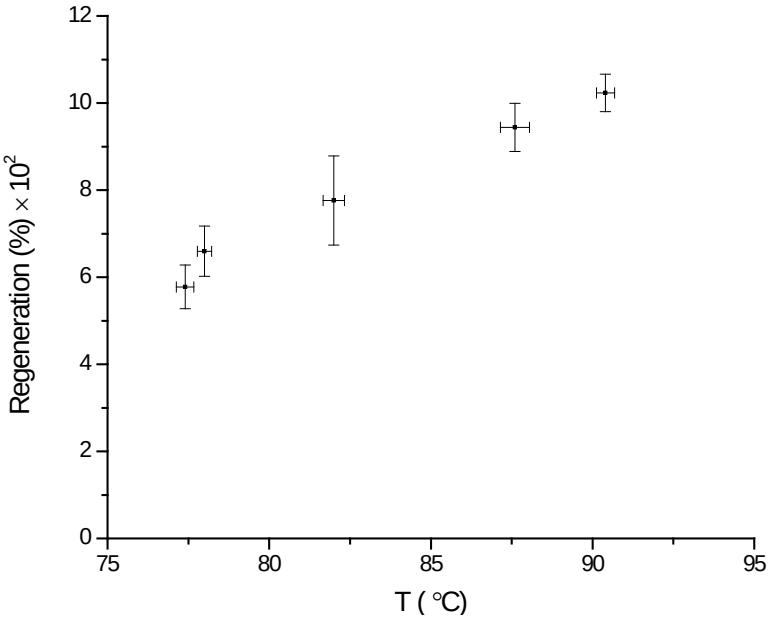

Figure 5-3 CO_2 regeneration as a function of temperature

5.3. Effect of Retentate Flow Rate

A series of experiments was performed to find the appropriate surface to flow rate ratio to maximize CO_2 regeneration yield. The determination of the membrane surface area is essential in membrane module design in order to achieve the best separation performance and reducing the capital size and energy consumption. The results showed that the increase in flow rate on the retentate side (shortened residence time) improved CO_2 flux until a flow rate of around 300mL/min, corresponding to a residence time of close to 0.12 min (Figure 5-4, Figure 5-5). The possible reasons caused CO_2 flux increase could be due to the thinner liquid boundary layer on

the membrane surface caused by higher flow rate. This result corresponded to the other studies results that an increase in the liquid velocity leads to a decrease in the liquid film mas transfer resistance, which is the controlling resistance and accounted for roughly 90% of the total mass transfer resistance of the system (Khaisri et al., 2011; Naim et al., 2012). The CO_2 flux sharp decrease at 330mL/min flow rate may be related to the membrane wetting caused by the high liquid partial pressure at high retentate flow rate. In terms of the regeneration efficiency, the increase of flow rate decreased it but not at a linear rate. This can be explained as a combined effect of the shortened residence time and improved mass transfer process. Our membrane surface area was a too small recovery surface area with respect to the flow rate, so faster retentate solution flow rate shortened the contact time, which is the dominant factor, and decreased the regeneration efficiency.

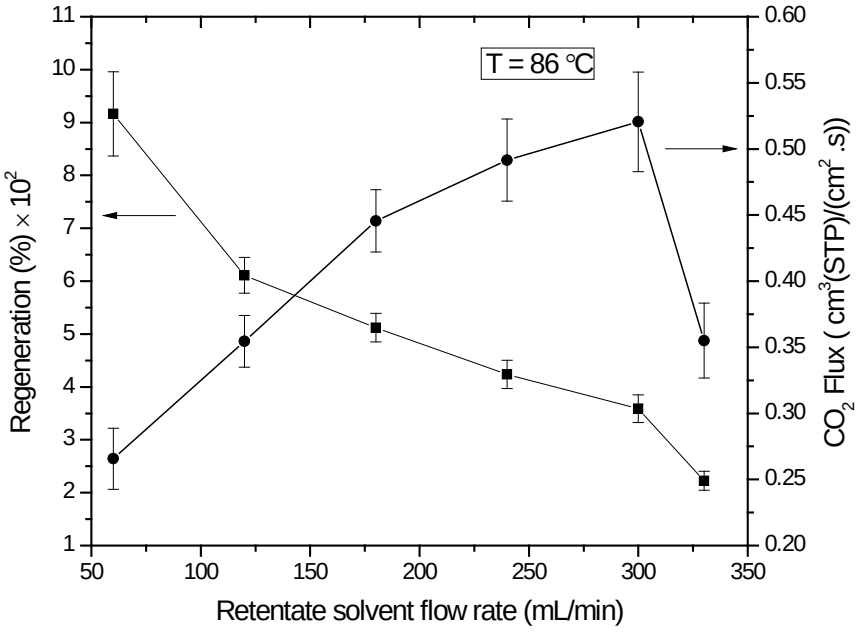

Figure 5-4 CO_2 regeneration as a function of retentate solution flow rate at constant temperature of 86ºC.

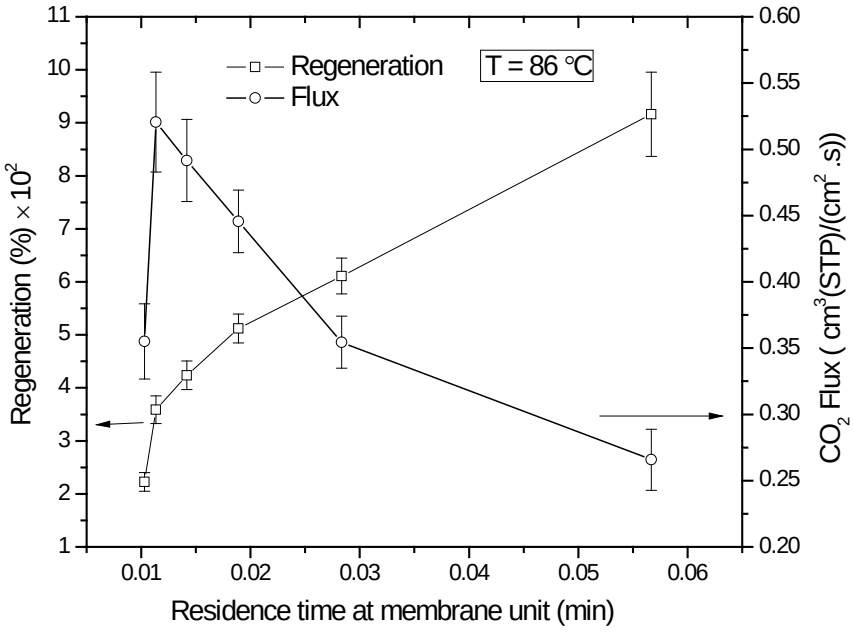

Figure 5-5 CO_2 regeneration as a function of residence time at constant temperature of 86ºC.

5.4. Effect of Pressure

The pressure on the retentate side of the membrane was controlled by manually closing a needle valve downstream of the membrane module. This valve was adjusted to four different positions: wide open (0 turns), 12 turns, 13 turns, and 14 turns. For reference, the valve can be closed all the way with 14.5 turns. The CO_2 recovery was measured as a function of the pressure at different temperatures (78ºC, 82ºC, 88ºC, 91ºC).

The results (Figure 5-6) show some interesting points. As can be seen in these graphs, there is considerable fluctuation in the pressure readings. For temperatures above 82°C, the CO_2 recovery generally decreases with increasing pressure and the effect is more pronounced at higher temperatures. This is unexpected for most membrane processes in which the rate of permeation increases with the pressure drop across the membrane. In this system however, the

reaction kinetics seem to be the dominant factor and so the same pressure effect is not seen. Another factor that needs to be considered is the multiple phase behavior of the feed solution. These results can be interpreted this way: The increase of the pressure compressed the gas phase more, made the liquid layer thicker, and caused more mass transfer resistance and lower mobility for this process.

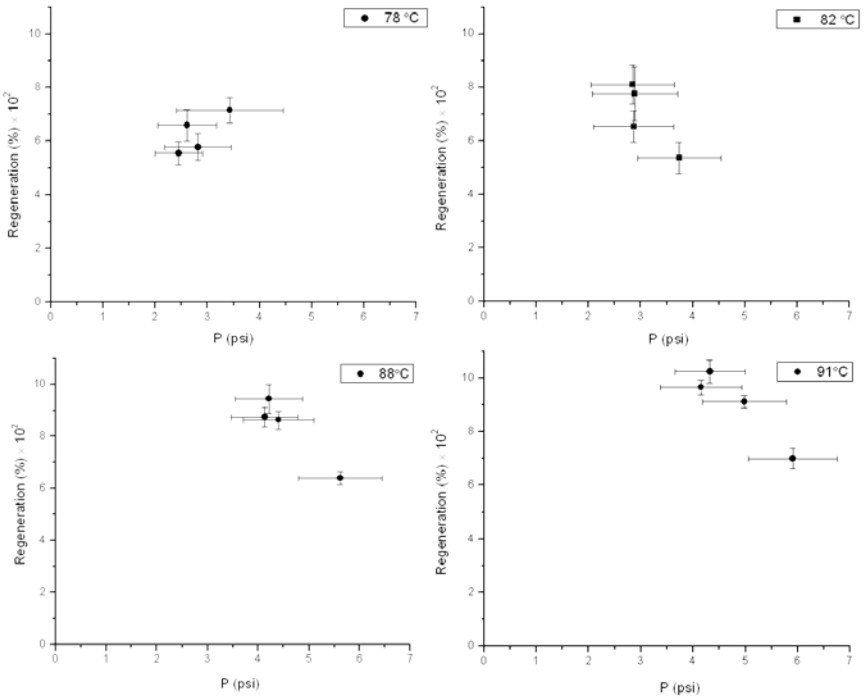

Figure 5-6 CO_2 regeneration as a function of pressure and temperature

5.5. Effect of Sweep Gas Rate

Figure 5-7 is a plot of CO_2 recovery vs. the flow rate of the N_2 sweep gas. The function of the sweep gas is to remove permeated CO_2 and maintain a low partial pressure of CO_2 on the permeate side of the membrane. The effect of the sweep gas flow rate on the CO_2 regeneration was investigated at a temperature of 77ºC and the feed solution flow rate of 180 mL/min. The N_2 sweep gas flow rate was set at 250, 500, 750, and 1000 sccm. The results showed no clear trend

as the sweep gas rate is increased. Similar results were obtained at different temperature and flow rate. We can conclude that the sweep gas flow rate does not have a significant effect at these conditions. In other words, the lowest sweep gas rate is sufficient to maintain a low CO_2 partial pressure.

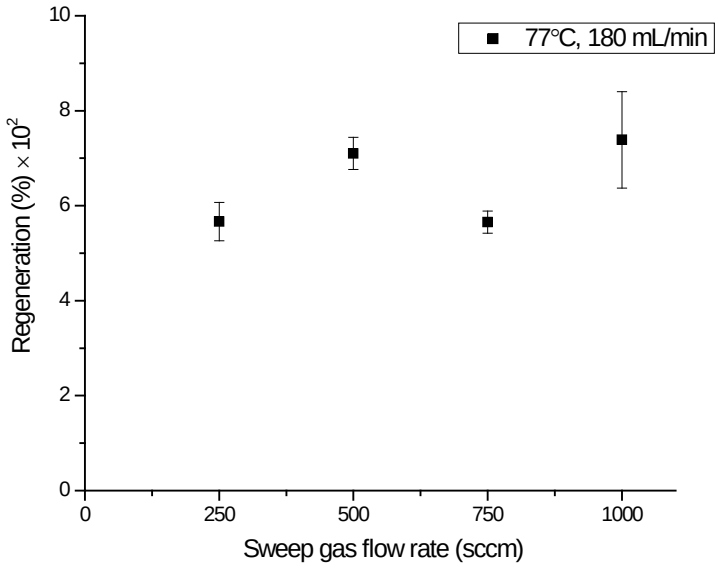

Figure 5-7 Regeneration (%) as a function of N_2 sweep gas flow rate.

5.6. Screening Design of Experiment Study

Two-level, three-factor full factorial experiment runs were performed to study significant factors and seek optimization of this process. Run order was randomized by Minitab to eliminate bias. CO_2 flux concentration in the sweep gas stream was recorded for each run after steady state was achieved.

Three factors studied were process temperature at the membrane unit; the retentate solution flow rate; and the permeate side sweep gas rate. Low value of process temperature has

to be higher than 70°C to reverse MEA-CO_2 reaction and release CO_2 gas from solvent. High value of process temperature should be lower than boiling point of water, otherwise large amount of solvent will be evaporated and make membrane process lose its attractiveness. For retentate solution flow rate, it should be high enough to maintain a positive trans-membrane pressure; but excessive high flow rate will shorten process resident time and lower CO_2 stripping efficiency. For sweep gas rate, it should be sufficient to sweep permeated CO_2 and maintain a low CO_2 partial pressure and concentration gradient cross the membrane; but too high sweep rate will increase the permeate side pressure, thus lower or offset the trans-membrane pressure, or even cause reverse permeation. The operation factor values were determined accordingly from these rules together with preliminary experiment results (Table 5-1). The responses of CO_2 permeation flux and selectivity over permeated liquid were analyzed by Minitab. A Pareto chart and main effects plot for CO_2 permeation flux are shown in Figure 5.8. There was no surprise to see that temperature to be the only significant factor, as the CO_2-MEA reaction is a temperature dominant reaction.

Table 5-1 Experiment factors and their low and high value

Factors	**(-) Low values**	**(+) High values**
Process temperature(°C)	73	92
Solution feed rate (mL/min)	120	180
N_2 sweep gas rate (sccm)	500	1000

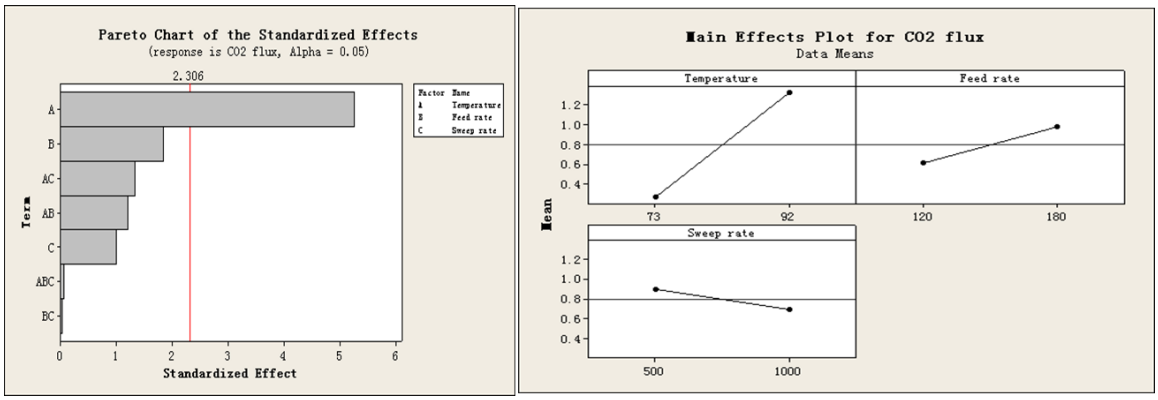

Figure 5-8 Pareto chart and main effect plot for CO_2 permeation flux

Pareto chart and main effect plot for selectivity was shown in Figure 5-9. Again, only temperature turned out to be the significant factor. This can be explained in two aspects: first, as temperature rises, more CO_2 gas and solvent vapor phases liberated at the retentate side, and more turbulence created by the gas and liquid mixture. These factors all facilitated the mass transfer process and caused selectivity change. On the other hand, for the membrane material side, selectivity is more like an intrinsic property for materials composition and structure, which has not much to do with the process parameters. Only process temperature could possibly change the selectivity by changing the material properties and structure.

The main effect plot for CO_2 permeation flux and selectivity also showed some interesting features. With temperature increasing, CO_2 permeation flux was improved but selectivity experienced some sacrifice. When operating at higher feed rate, higher pressure was created at the feed side, CO_2 permeation was enhanced but selectivity was weakened. Those results also suggested that for this specific membrane, both flux and selectivity probably cannot be improved at the same time unless modifying the membrane properties.

Screening design of experiments results were consistent with the individual parametric study. Temperature is a significant parameter to yield higher CO_2 flux and probably with some selectivity sacrifice.

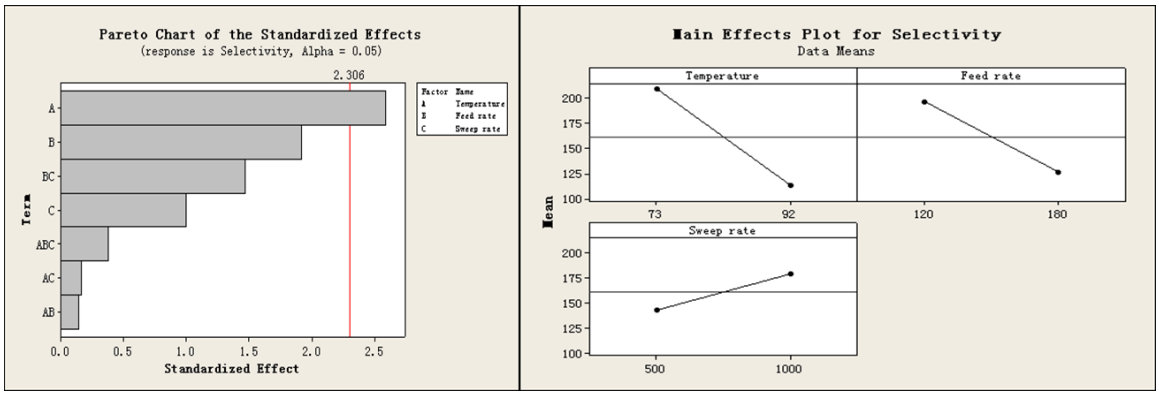

Figure 5-9 Pareto chart and main effect plot for selectivity

5.7. Membrane Mass Transfer Mechanism Study

Mass transfer study was carried out to understand the mechanism of how CO_2 and solvent vapors permeate through the membrane, what the major resistances for this process are and what determined the selectivity. The mass transfer mechanism study can help understand and improve the CO_2 recovery efficiency from lab scale experiments to potential industrial scale design and operation.

The principle of this process is a process similar to but more complex than a membrane distillation process. This separation process combines simultaneous mass transfer and heat transfer of the feed liquid and gas species through a hydrophobic microporous membrane. In the membrane contactor, a feed solution and possibly dissolved components at elevated temperature is in contact with one side of the membrane and colder sweep gas is in contact with the other side of the membrane. The CO_2 mass transfer process consists of three consecutive steps: 1) CO_2 and

solvent gas desorption (physical desorption/chemical reaction) from liquid phase and diffusive transport to the membrane interface; 2) Combined diffusive and convective transport of the gas and vapors through the membrane pores; 3) Gas and the vapor condensation dissociate the membrane on the permeate side of the membrane.

Consequently, the overall mass transfer rates can be expressed in a resistance-in-series model, which are the sum of the mass transfer resistances in the gas and liquid phase and the additional resistances caused by the membrane layer.

In the ideal situation, the micro-porous hydrophobic surface of the membranes only allow the CO_2 gas and the vapor state phases, but not the liquid phases ,to pass through the membrane pores. The surface tension of liquid solvent help liquids retain in the feed side. And the driving force comes from the effective gas/solvent vapor pressure difference produced by the trans-membrane temperature difference and/or concentration difference. What happens in the pores is likely to be explained by the pore-flow model (Wijmans & Baker, 1995): the liquid phase is restricted by the pores; and the gas and vapor phase evaporates from the interfaces of the liquid and pore openings and travel through the membrane pores. The phase transitions possibly happen in the pore channels as illustrated in the Figure 5-10.

There are some major problems that potentially hinder the mass transfer process and cause energy inefficiency.

1. The feed solution was heated at elevated temperature and flow through a membrane flat plate, there could be uneven temperature distribution and polarization across the membrane surface.

2. The feed side solution was maintained at elevated temperature and the permeate side sweep gas was at room temperature. There is conductive heat loss through the membrane.
3. If the feed solution is not well gas and liquid mixed turbulent flow, there is a laminar liquid layer in contact with membrane surface. Due to the positive trans-membrane pressure, this layer tends to stick close with the membrane and prevent lighter gas from diffusing into the membrane pores.
4. There is also resistance to the gas and vapor flow through the membrane due to the presence of trapped liquid or fouling deposits in the pores. This is more likely to happen when feed solution has turbulent flow which usually under the operation of higher pressure.

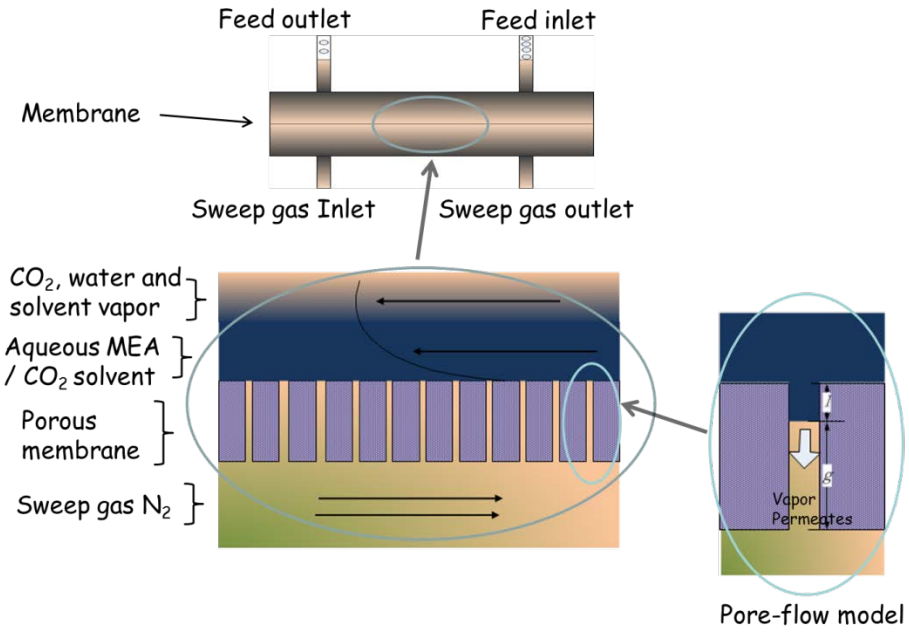

Figure 5-10 CO_2 mass transfer principle through membrane

Based on our proposed mass transfer mechanism, the lighter CO_2 gas phase took the least resistant route to exit the membrane unit. If we put our membrane unit upside down, in another words, switch the feed side and permeate side. Now the liquid phase under pressure would flow more towards the feed solution exit and thus caused more resistance for the lighter gas to exit. Consequently, more of the gas phase would flow towards the membrane and the gas concentration near membrane region should be much higher. As a result, the CO_2 flux through the membrane and regeneration rate should be greatly improved in this configuration. The experiment was carried out using same condition as previous test. The CO_2 regeneration results at steady state were measured at two different configurations and compared in Figure 5-11. As expected, CO_2 regeneration was significantly improved by changing to the configuration of putting feed solutions beneath the membrane. It agrees with our reasoning about the mass transfer mechanism in the membrane unit. On the other hand, it also can be concluded that the membrane module design is very important in terms of improving the regeneration performance.

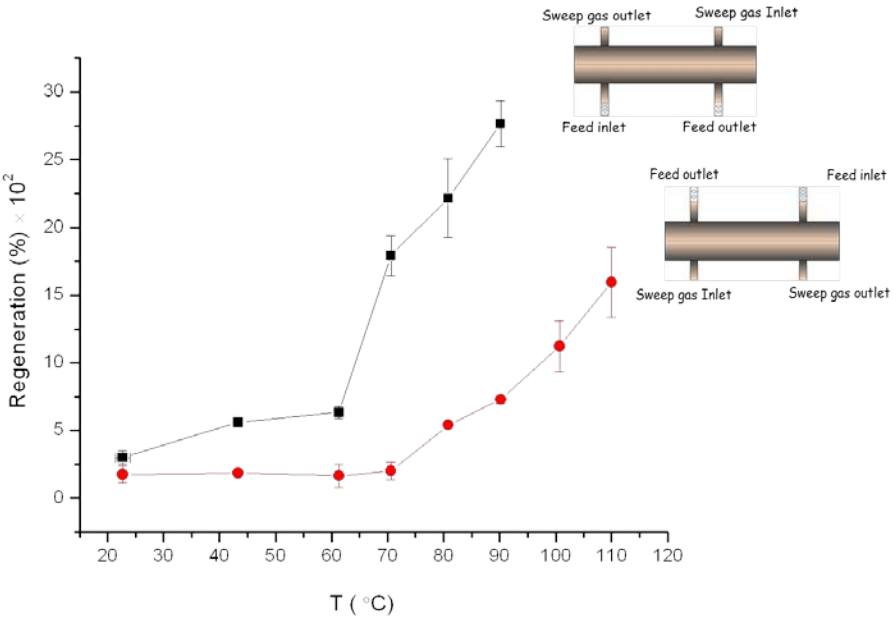

Figure 5-11 Significant CO_2 regeneration difference by simply changed configurations.

5.8. Flow Pattern in the Membrane Unit

According to the previous mass transfer mechanism, the feed solution flow pattern significantly affects the mass transfer process, thus is quite worth studying. In order to study and visualize the flow and gas/liquid phase conditions, part of the tubing before and after the membrane unit was replaced by transparent Teflon tubing. At low temperatures, the liquid entering and exiting the membranes showed no turbulent flow features. At temperature 70ºC and higher, continuous gas bubbles in liquid stream were seen to enter membrane unit. The gas bubbling rate increases with temperature rise. When the temperature is close to solvent boiling point, vapor phases were observed, and liquid bubble flow was also observed in the gas and vapor stream. The flow regimes showed the similar features like slug flow as visualized in the Figure 5-12. The liquid flows into the membrane unit at relatively faster flow rate, gas bubbles, possibly CO_2 generated by the heat-induced reverse reaction of CO_2/MEA, showed oval shape,

aligned up at in the middle, travel uniformly at relatively slow rate into the membrane unit. Bubbles were seen at the exit of the membrane unit as well, and the bubbles flow rate at the exit was not seen significantly slower than the inlet.

From those observations above, several points are noteworthy:

1. There are liquid and gas phases entering the membrane unit. And the ration and composition of the phases are changing corresponding to different temperatures. The gas phases are likely to be CO_2 or a mixture of CO_2 and liquid vapor. CO_2 is likely a product produced by the reverse reaction of CO_2/MEA.
2. Majority of the CO_2 entering the membrane unit took the membrane unit outlet pathway instead of diffusing towards and through the membrane to get recovered. The reason could be that the pressure drove heavier liquid phase towards the membrane and the lighter gas phase was driven against the membrane and took the membrane unit outlet as this is the least resistant pathway.
3. The CO_2 at the membrane permeate side was likely to be recovered from the CO_2 gas and liquid vapor evaporation at the interfaces of the liquid and pore openings.

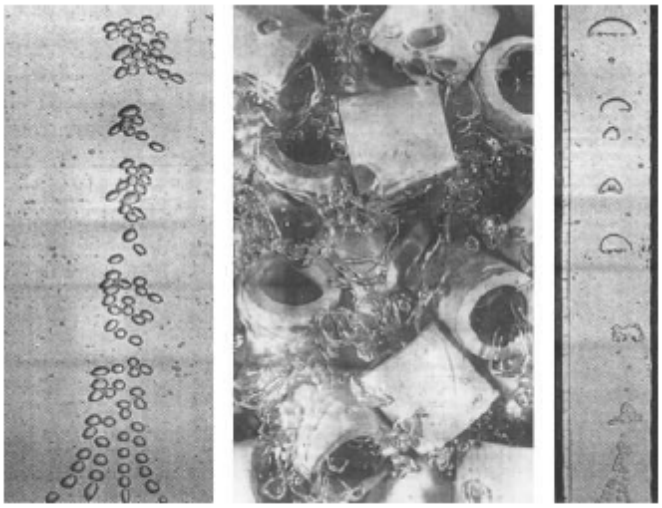

Figure 5-12 Visualization of flow regimes (Wallace, 2006) a) Homogenous; b) Churn turbulent; c) Slug flow.

Reynolds number was also calculated to measure the turbulence and characterize the flow in the membrane system. Vertically, Reynolds number in the tube and at the membrane inlet was calculated using the following equation (Buckley-Smith, 2006):

$$\mathrm{Re} = \frac{\rho V D}{\mu}$$

Equation 5-5

Where V is the average flow velocity in the tube (m/s), D is the diameter of the tube, ρ and μ are the density and viscosity of the feed solution. The density and viscosity were approximated to that of water ρ= 1000 kg/m^3 and μ= 0.000346 kg/(m.s) at 80ºC, and the tube diameter D = 0.00635 m. Linear flow rates were calculated from volumetric flow rate (m^3/sec) divided by the jet area = 4.03225 x10^{-5} m^2. Reynolds number as a function of feed solution flow rate was plotted in Figure 5-17.

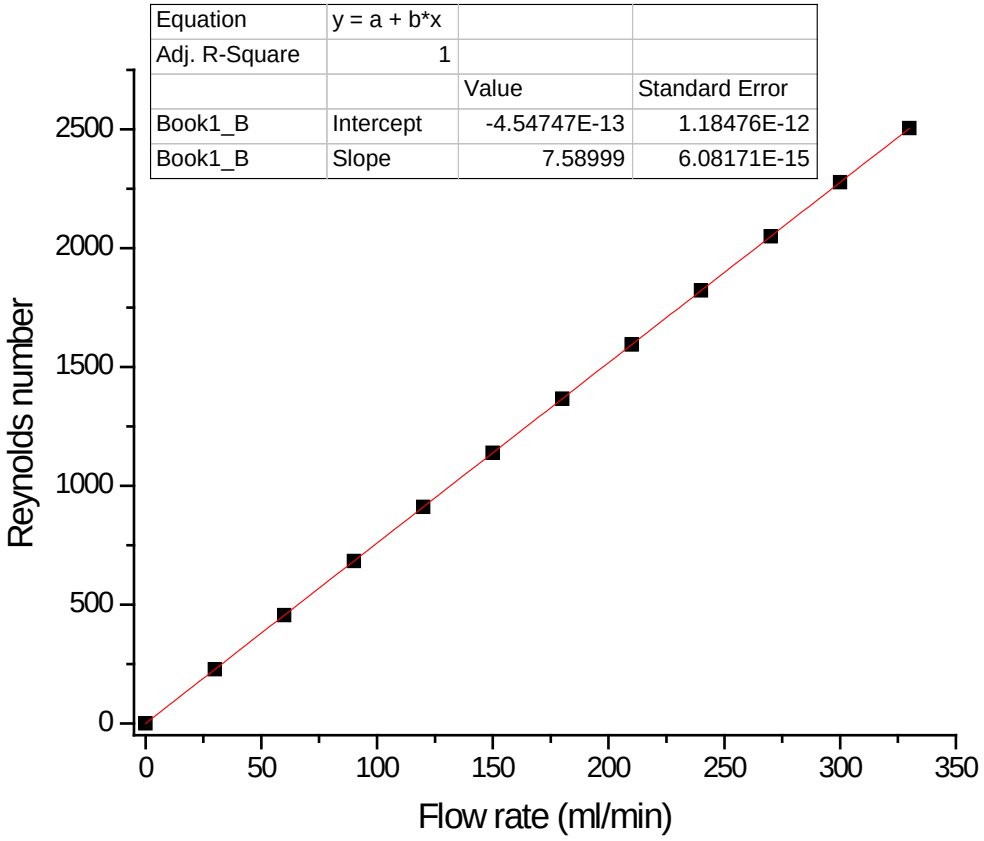

Figure 5-13 Reynolds number (vertical direction) at the membrane unit inlet as a function of feed solution flow rate

Horizontally, the Reynolds number for flow down a flat plate is defined by the equation (Mccabe et al., 2005):

$$\mathrm{Re} = \frac{4V\rho r_H}{\mu}$$

Equation 5-6

Where V is the average velocity in the tube (m/s); ρ and μ, the density and the viscosity of the feed solution. r_H = hydraulic radius.

For better understanding the flow pattern and flow velocity distribution across the membrane, 2-Dimensional membrane geometry was created using Gambit, and the flow path lines and velocity distribution was analyzed by Computational Fluid Dynamics software (Fluent). The results showed that the Reynolds number across membrane was in the laminar flow region. And it can also be seen from the flow pattern (Figure 5-14) that there exists dead flow region and the effective membrane surface area is smaller than the actual membrane surface area.

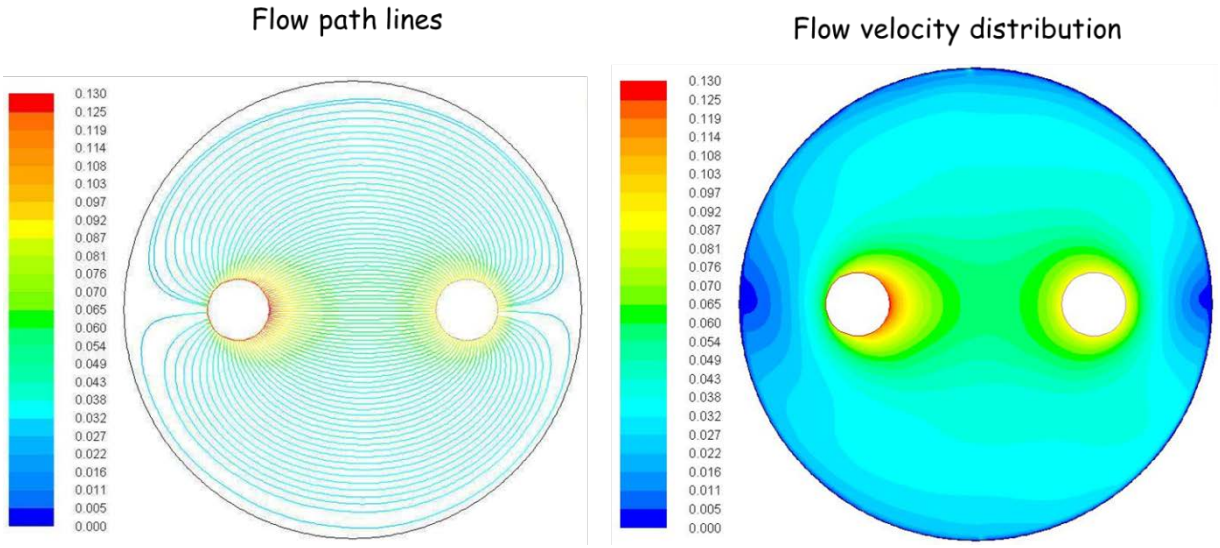

Figure 5-14 Flow path lines and flow velocity distribution across the membrane surface

Turbulence within a membrane unit is desirable for better mass transfer. And it also helps minimize the effects of fouling and concentration polarization in the boundary layer. Changes in the diameter of the pipe or tube, such as flow distributor for the membrane unit, can cause changes in the critical Reynolds number (usually Re = 2100). If a pipe converges, the critical Reynolds number required to achieve turbulence is higher. Whereas flow divergence as seen in our membrane unit, flow distributor produces a lower value for Newtonian fluids (Buckley-

Smith, 2006). The divergence occurring at the flow distributor increases the likelihood that feed flowing through the membrane unit will in fact be turbulent (Buckley-Smith, 2006).

Reynolds number is also a measure of mixing intensity of the phases in the flow. Better mixing can be achieved by operating at higher flow rates or by using mesh spacers or complex channels to induce turbulent flow (Cath, Adams, & Childress, 2004). For the similar application of direct contact membrane distillation, most studies showed positive dependence of flux on feed flow rate and the module operated at higher Reynolds numbers produced higher fluxes (Cath et al., 2004). But for our CO_2 recovery application, the impact of high Reynolds number is more complex. If high Reynolds number is achieved by higher flow rate, that gives lower surface to flow volume ratio and thus lower regeneration efficiency and more energy consumption. If high Reynolds number is achieved by mesh spacers or complex channels, the pressure and temperature would be hard to be maintained along the channels, which also causes additional mass transfer resistance and possibly reduces the effective surface area. In simple words, the improved mass transfer performance could be compromised by the reduced effective surface area and area-to-volume ratio. Therefore, an optimization study must be carried out in designing the membrane dimensions and configurations.

5.9. Temperature Polarization Effects

Heat in the membrane unit is transported and dissipated through several major routes. First route is the transport of the latent heat of evaporation across the membrane; second route is the reaction heat that strips the CO_2 by driving the CO_2/MEA reaction in the reverse way; third route can be the convective heat loss through the membrane together with other conductive heat

losses, which cause energy inefficiency. Table 5-2 listed the surface energy and thermal conductivity for some hydrophobic membranes.

Table 5-2 Reported surface energy and thermal conductivity of hydrophobic membrane materials (Zhang, 2011).

Membrane material	**Surface energy ($\times 10^{-3}$ N/m)**	**Thermal conductivity ($W.m^{-1}.K^{-1}$)**
PTFE	9.1	0.25
PP	30.0	0.17
PVDF	30.3	0.19

And the temperature polarization coefficient (TPC) used in membrane distillation, which is the ratio of useful energy for mass transfer of vapors to the total energy invested in the process, was employed in our study as an indicator to characterize the heat efficiency of our process. TPC is defined as (Lawson & Lloyd, 1997):

$$\mathrm{TPC} = \frac{T_{mf} - T_{mp}}{T_f - T_p}$$

Equation 5-7

Where T_{mf} is the interfacial feed temperature, T_{mp} is the interfacial permeate temperature, T_f is the bulk feed temperature, and T_p is the bulk permeate temperature. A schematic drawing of temperature polarization effect is shown in Figure 5-15.

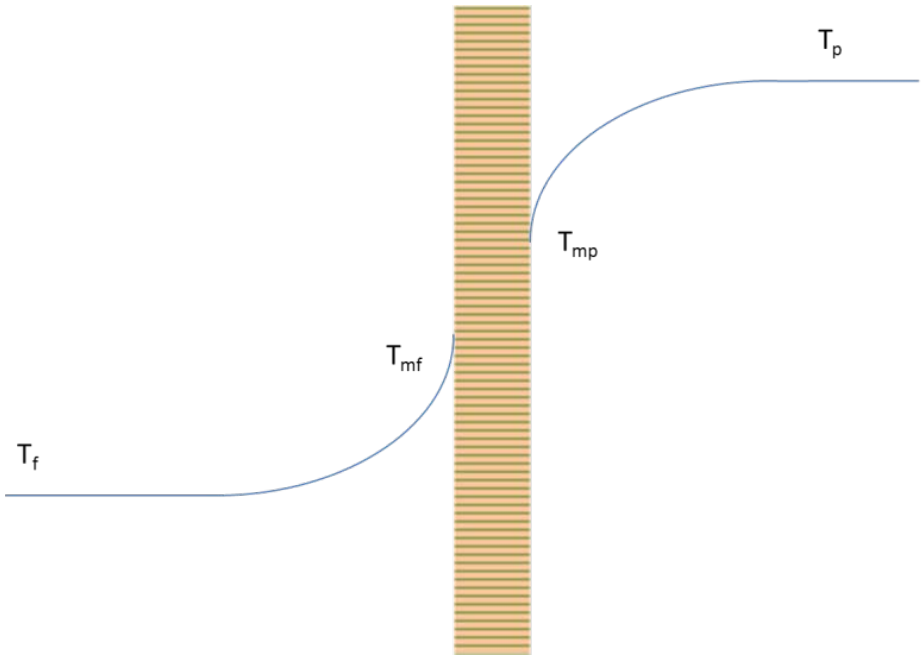

Figure 5-15 Temperature polarization effect

All these four temperature readings were monitored by thermocouples installed in the system (Figure 3-1) and recorded. Figure 5-15 and Figure 5-17 showed that TPC increases at higher temperatures, which agrees with our previous findings that the elevated temperature significantly improves gas and liquid vapor flux to permeate through the membrane pores, thus heat flux was also improved across the membrane. Higher retentate flow rate from 120 mL/min to 180 mL/min did not significantly change the TPC value.

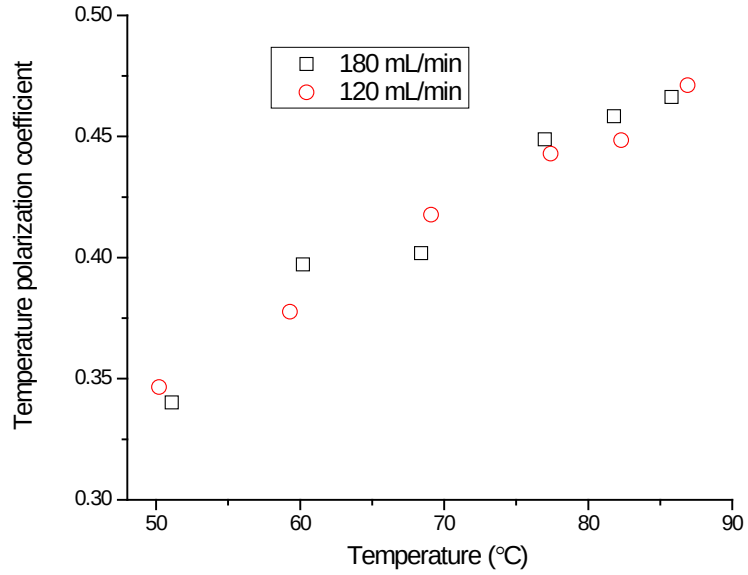

(a)

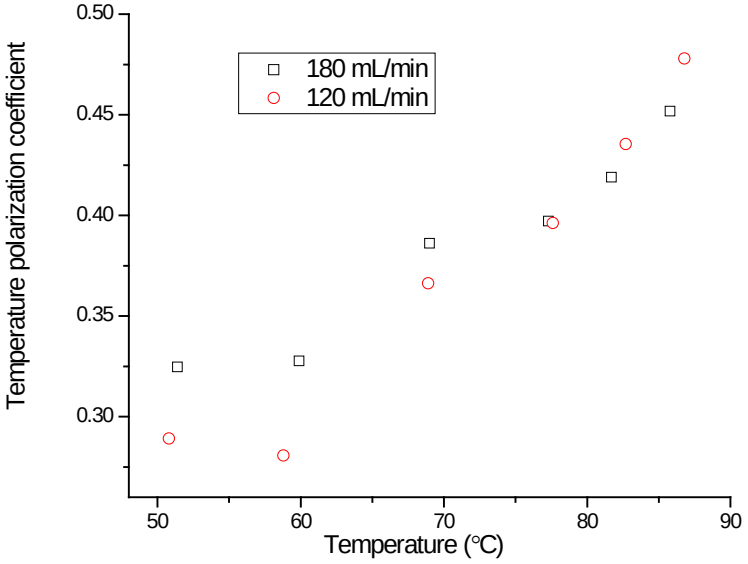

(b)

Figure 5-16 Temperature polarization coefficient vs. temperature for PP membrane at different retentate flow rates. (a) sweep gas rate at 1000 sccm; (b) sweep gas rate at 500 sccm

Figure 5-17 also showed the TPC value was slightly higher at higher sweep gas rate, possibly due to the faster sweep rate took away permeated mass and heat fluxes, and maintained greater temperature gradient. This suggested that the temperature gradient across the membrane could be a major driving force as well for the permeation fluxes, just like the membrane distillation process.

With the process temperature above 80ºC, The TPC measured for our experiment is approaching 0.5, which suggests that roughly half of the heat is used for the mass transfer of CO_2 gas and liquid vapors through the membrane pores. It should be noted here that the TPC value is used to characterize the energy performance of the membrane permeation including CO_2 and liquid vapor and any other permeation components as a whole. The TPC value cannot characterize the energy efficiency performance just for CO_2 alone.

Considering the CO_2 dissociation and liquid evaporation rate is primarily a function of temperature, it is reasonable to assume the CO_2 and vapor evaporation rates depend far more on the interfacial temperature than the bulk temperature. It is reported that most often the TPC varies between 0.2 to 0.9 depending on the membrane module configuration (Cath et al., 2004). TPC ranged from 0.4 to 0.53 at low crossflow velocity in laminar region to 0.87-0.92 at high crossflow velocity in turbulent region (Srisurichan, Jiraratananon, & Fane, 2006). This result also re-confirmed the flow through membrane surface is in the laminar regime.

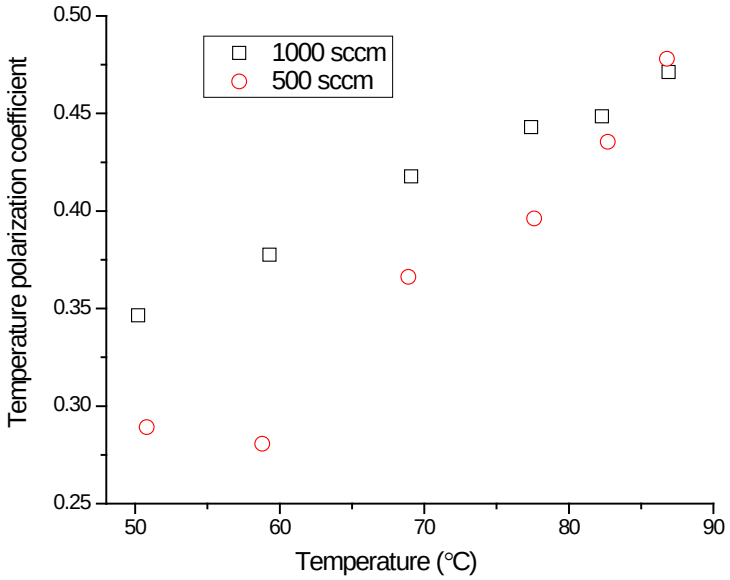

(a)

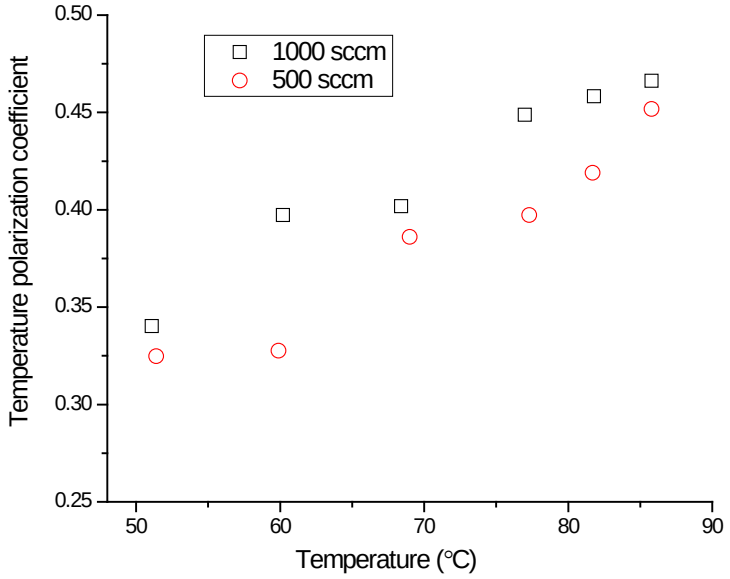

(b)

Figure 5-17 Temperature polarization coefficient vs. temperature for PP membrane at different sweep gas rates. (a) retentate flow rate at 180 mL/min; (b) retentate flow rate at 120 mL/min

5.10. Swelling and Fouling Effects on Mass Transfer

Swelling effect of membranes, also known as membrane wetting is an important factor on the operability of the membranes. If the liquid absorbent is water or aqueous solutions with inorganic solutes, the liquid has a high surface tension and usually cannot wet the common hydrophobic membranes such as PP and PTFE (Lawson & Lloyd, 1997). But the liquid surface tension drops rapidly when a low concentration of the organic compounds is added (Lawson & Lloyd, 1997). With the organic compound concentration exceed a critical point, the contact angle will decrease to less than 90 and the liquid will wet the membrane surface and the pores.

Breakthrough pressure, also known as Liquid Entry Pressure of Water (LEPW), is the minimum pressure for the water to overcome the hydrophobic force of the membrane and penetrate the pores. LEPW is a function of the membrane properties, the liquid, and the reaction between them, known as the Laplace (Cantor) equation (Alklaibi & Lior, 2005):

$$\Delta P = \frac{2B\gamma_L cos\theta}{r_{max}} < LEPW$$

Equation 5-8

Where B is a geometric factor determined by pore structure, γ_L is the liquid surface tension, r_{max} is the largest pore size, and θ is the liquid-solid contact angle. It was reported that the LEPW would be 200-400 kPa (29- 58 psi) for 0.2 μm pore size PTFE membranes and 100 kPa (14.5 psi) for 0.45 μm pore size PTFE membranes (Cath et al., 2004; Garcıa-Payo, Izquierdo-Gil, & Fernandez-Pineda, 2000). If feed solution is flowing at high Reynolds numbers, pressure can easily be over LEPW and results in solvent penetration into pores and slowing down the mass transfer process.

For the application in our system, a positive trans-membrane pressure, feed solution flow at a relatively high Reynolds number, and operation below LEPW are desired. And the most promising solution to meet this this desired requirements are probably to choose appropriate membrane materials with high hydrophobicity (low surface energy) and appropriate pore size. Bigger pore size facilitates the mass transfer and smaller pore size provides higher breakthrough pressure.

Based on the mass change measurement of membranes before and after an experimental run, it can be confirmed that all the membranes tested more or less experienced the membrane-wetting problem. Detailed data can be found from the mass change study of the membrane sorption study. Many researchers have reported that hydrophobic membranes such as PTFE, PP, and PVDF showed pretty good performance and were free of wetting (Li & Chen, 2005). At low temperatures this is probable. However at elevated temperatures, wherein the liquid approaches its boiling point, the liquid surface tension rapidly decreases (Garcıa-Payo et al., 2000), and membrane properties have the potential to change as well. The wetting of the membranes in the experimental study could be caused by liquid vapor penetration of the pores which could condense in the pores. It was observed by others that wetted membranes gave decreased permeate flux than the fresh membranes (Lawson & Lloyd, 1997).

Another possibility (Franco, deMontigny, Kentish, Perera, & Stevens, 2009) reported for the cause of membrane wetting is that the degradation product of MEA reduced the mass transfer rate of CO_2, and furthermore, these degradation acids are believed to adsorb into the PP, altering the surface properties and reducing the hydrophobicity of the membrane. This in turn increases the degree of wetting of the membrane pores. This suggests that membrane wetting and fouling

problem may affect each other and deteriorates the membrane performance and long-term stability. The same problem was also revealed on our membranes after stripping CO_2/MEA solvents (Figure 5-18). The MEA could be swelling or adsorbing into the PTFE as well. Figure 5-19 showed the SEM images of PP membranes suggested the similar features from Franco's study.

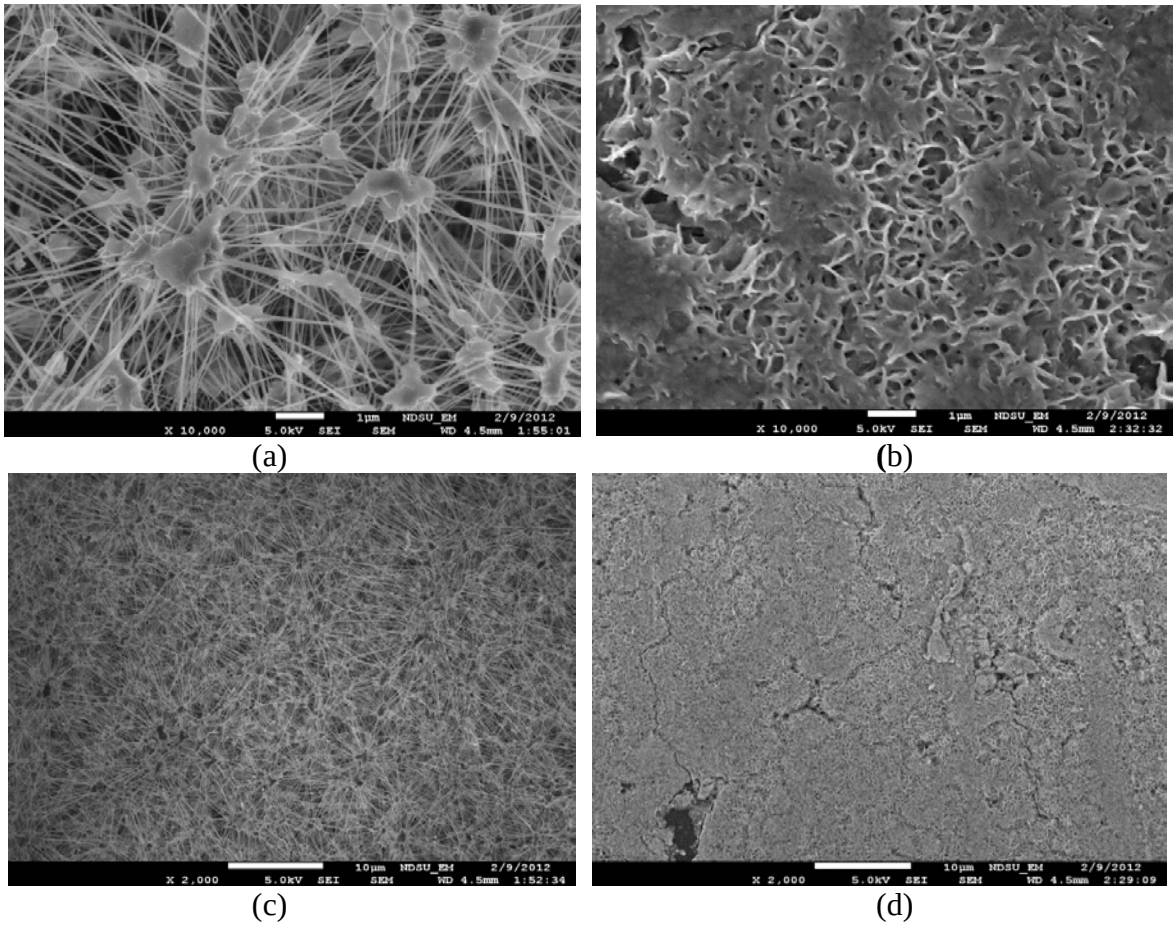

Figure 5-18 SEM images showing the change in surface morphology of PTFE membrane between fresh PTFE membrane and PTFE membrane that has been used to strip CO_2 from 15 wt% MEA at elevated temperature. (a) fresh membrane 10000x; (b) used membrane 10000x; (c) fresh membrane 2000x; (d) used membrane 2000x

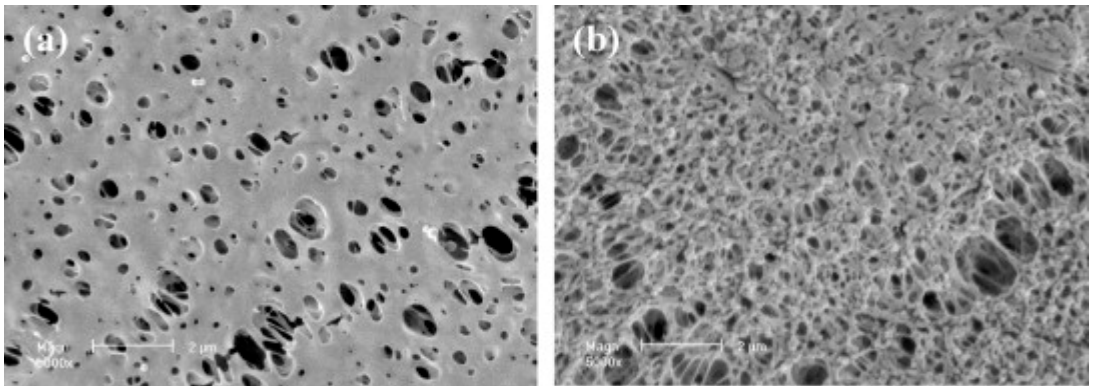

(a) (b)

Figure 5-19 SEM images depicting the change in surface morphology of PP membrane between (a) fresh PP membrane and (b) PP membrane exposed to 20 wt% MEA for 25 days 5000x (Franco et al., 2009)

5.11. Chapter Conclusion

Temperature was confirmed by both individual parametric study and design of experiment methodology to be a significant factor for this process, whereas the pressure, retentate flow rate and sweep gas flow rate were not significant factors of the process. There are multiple phases of gas, vapor and liquid co-exist in the membrane unit. Most CO_2 gas entered the membrane unit took the exit and didn't flow towards the membrane because of the mass resistance caused by the liquid film in contact with membranes, which was found to be the major resistance of this mass transfer process. The liquid flow pattern and Reynolds number estimation suggested liquids in the membrane unit take the form of laminar flow. The temperature polarization coefficient value also suggested laminar flow characteristics. At the process temperature at 80ºC and above, the temperature polarization coefficient measured was around 0.5, which suggested that roughly half of the heat energy was used for this separation process. MEA degradation residues were observed on the membrane surface after long term run, which could alter the surface properties, reduce the hydrophobicity of the membrane and slow down the mass transfer process.

6. MEMBRANE PORE SIZE SCREENING STUDY

In this CO_2 regeneration process, porous membrane contactor was chosen because it theoretically provides very little resistance for CO_2 gas transfer but the surface tension reduces the ability of the liquid to pass through the pores. A question regarding this assumption is that what pore size or what range of pore size of the porous membrane can achieve the best performance. However, there is little published literature comparing the performance and effects of membranes with different pore size, and little suggestions can be found about choosing the appropriate pore size for references. Moreover, using membrane contactors for CO_2 regeneration is a new application area that only very few researchers started to touch upon. Based on our knowledge, there is no similar work published in studying the effect of pore size on CO_2 regeneration process. Our experimental results will provide better understanding of CO_2 regeneration process by polymeric membrane contactors and lead to a wider and deeper range of research regarding better membrane materials, novel membrane design, process configuration, optimization and modeling about using membranes for CO_2 regeneration.

6.1. Theoretical Background

The transport phenomena of gases inside porous membranes can be described by three models: Knudsen diffusion, viscous flow, and molecular diffusion (Phattaranawik, Jiraratananon, & Fane, 2003). The applicability of the models is determined by the comparison of molecular

mean free path (λ) and the membrane pore size (d_p), as shown in Figure 6-1. For a single gas system if the mean free path of the gas is much larger than the pore size ($d_p < \lambda$), molecule–wall collisions occur much more often than the collisions between molecules and the gas transport is described by Knudsen diffusion. If the mean free path is much smaller than the membrane pore size ($d_p > 100\lambda$), molecule–molecule collisions become the dominant mass transport mechanism which can be described by viscous flow. When the membrane pore size falls in between ($\lambda < d_p < 100\lambda$), both diffusions happen in this region. For porous membrane, the gradients of total pressure, concentration, and partial pressure result in viscous flow, molecular diffusion, and Knudsen diffusion, respectively. In our experimental conditions, total pressure is close to atmospheric pressure. Consequently, viscous flow is theoretically omitted. Slip flow (viscous slip) and pressure diffusion can also be neglected. Surface diffusion can be ignored due to low molecule–membrane interaction. Therefore, only diffusion slip contributed from ordinary and Knudsen diffusion exists for the combined mode.

For the binary mixture of water vapor and air, the mean free path of water in CO_2 gas (λ_{w-CO2}) was evaluated at the average membrane temperature (T_{mb}) as shown in Equation 6-1:

$$\lambda_{w-co2} = \frac{k_B T_{mb}}{\pi((\sigma_w + \sigma_{co2})/2)^2 P_T} \frac{1}{\sqrt{1 + (\frac{m_w}{m_{co2}})}}$$

Equation 6-1

Where k_B is the Boltzman constant (1.381×10^{-23} J K^{-1}), P_T is the total pressure (1.013×10^5 Pa or 1 atm), σ_w and σ_{CO2} are the collision diameters for water vapor (2.641×10^{-10} m) and CO_2 (3.996×10^{-10} m)(Bird, Stewart, & Lightfoot, 2006), and m_w and m_{CO2} are the molecular weights

of water and CO_2. At the typical process temperature of 80ºC, the mean free path of water in CO_2 gas is 0.12 μm.

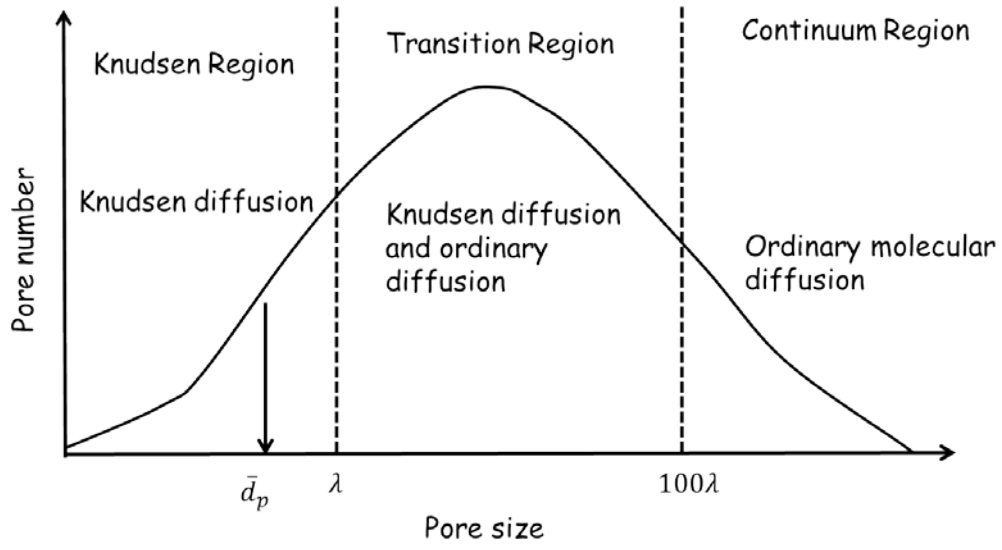

Figure 6-1 The applicability of three porous membrane transport models (Phattaranawik et al., 2003)

6.2. Membrane Selection and Characterization

Polypropylene (PP) membranes with different pore sizes ranging from 0.1 to 10.0μm were selected in this study (Table 6-1). Previously, it was roughly estimated that the mean free path of water in CO_2 gas is 0.12 μm. The smallest membrane pore size is close to this mean free path and the largest membrane pore size is close to 100 times of this mean free path. The membrane pore size roughly covered range of Knudsen region, transition region and continuum region. A total of eight membranes were acquired from two different sources: five membranes from Millipore were supported by a non-woven fabric layer and were designed for microfiltration; three membranes from GE were designed for membrane distillation application. Porosity of 0.35 was provided from manufacture specification by Millipore, from that, the volume faction and density of PP fibers can be calculated (0.976 g/cm^3) using Equation 2-3 (data

shown in Table 6-1). FTIR (Figure 6-2) and DSC (Figure 6-3) characterization showed that the composition and the structure of these PP membranes are similar. So the same density value was used for all the PP fibers of membranes to calculate membrane porosity and tortuosity using Equation 2-3 (Table 6-1).

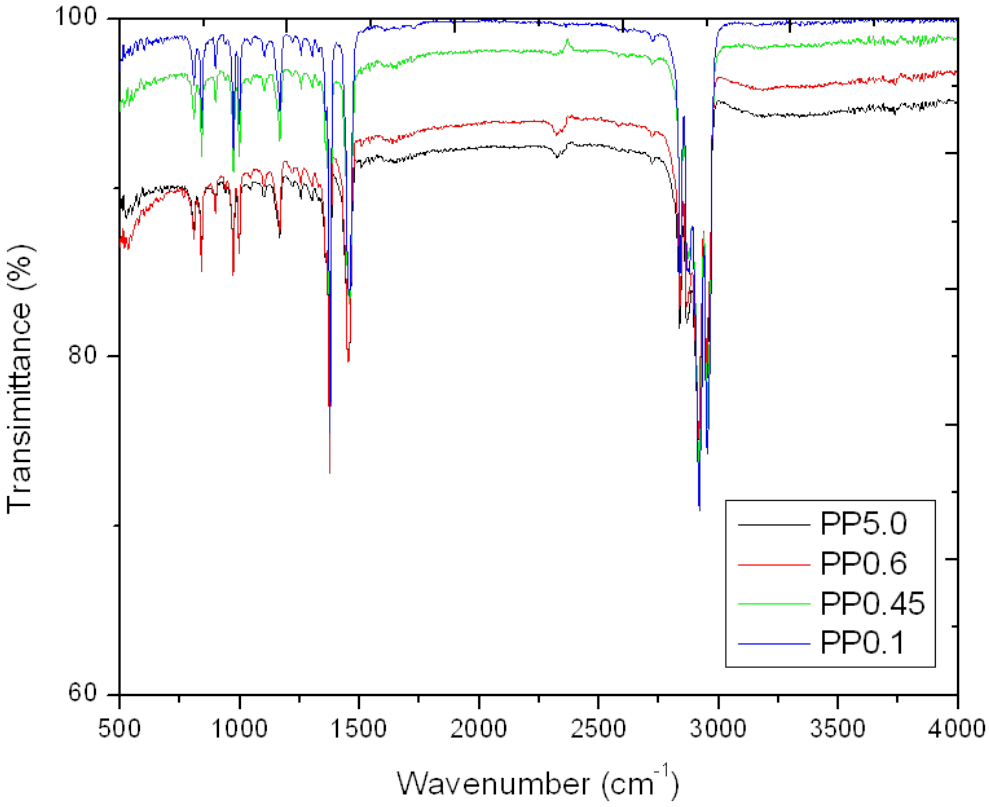

Figure 6-2 FTIR spectra of different membranes.

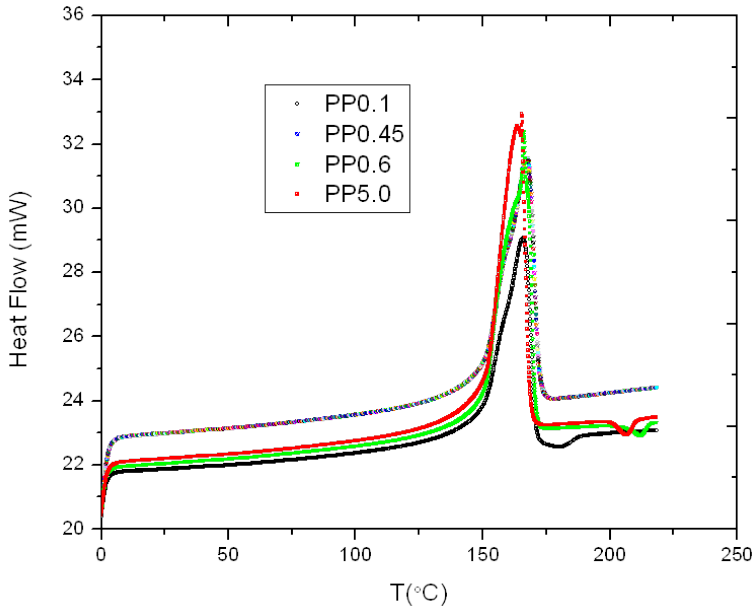

Figure 6-3 DSC spectra of different membranes.

Table 6-1 Membrane properties (* from manufacturer specification)

Membrane	**Nominal pore size (μm)**	**Thickness (mm)**	**Porosity**	**Tortuosity**	**Volume fraction**	**Provider**
$PP_{0.1}$	0.1	0.10	0.76	2.04	0.24	GE
$PP_{0.22}$	0.22	0.17	0.83	1.65	0.17	GE
$PP_{0.45}$	0.45	0.17	0.85	1.55	0.15	GE
$PP_{0.6}$	0.6	0.13	0.35*	7.78	0.65	Millipore
$PP_{1.2}$	1.2	0.13	0.35	7.78	0.65	Millipore
$PP_{2.5}$	2.5	0.13	0.34	8.07	0.66	Millipore
$PP_{5.0}$	5.0	0.10	0.40	6.19	0.59	Millipore
PP_{10}	10.0	0.13	0.59	3.36	0.40	Millipore

Figure 6-4 showed the SEM images of the membrane surfaces. It was clearly shown that the structures and shapes of GE PP membrane pores are different from the net-like knot non-woven fiber structures. GE membranes have more uniformly distributed pores on the surface

while the pores of Millipore membranes are relatively not uniformly distributed and have irregular pore shape. It seemed that the non-woven fibers of smaller Millipore pore size membranes were more compressed than the bigger pore ones. The observations were consistent with the porosity and tortuosity estimation, as GE membranes appeared to have more straight pores.

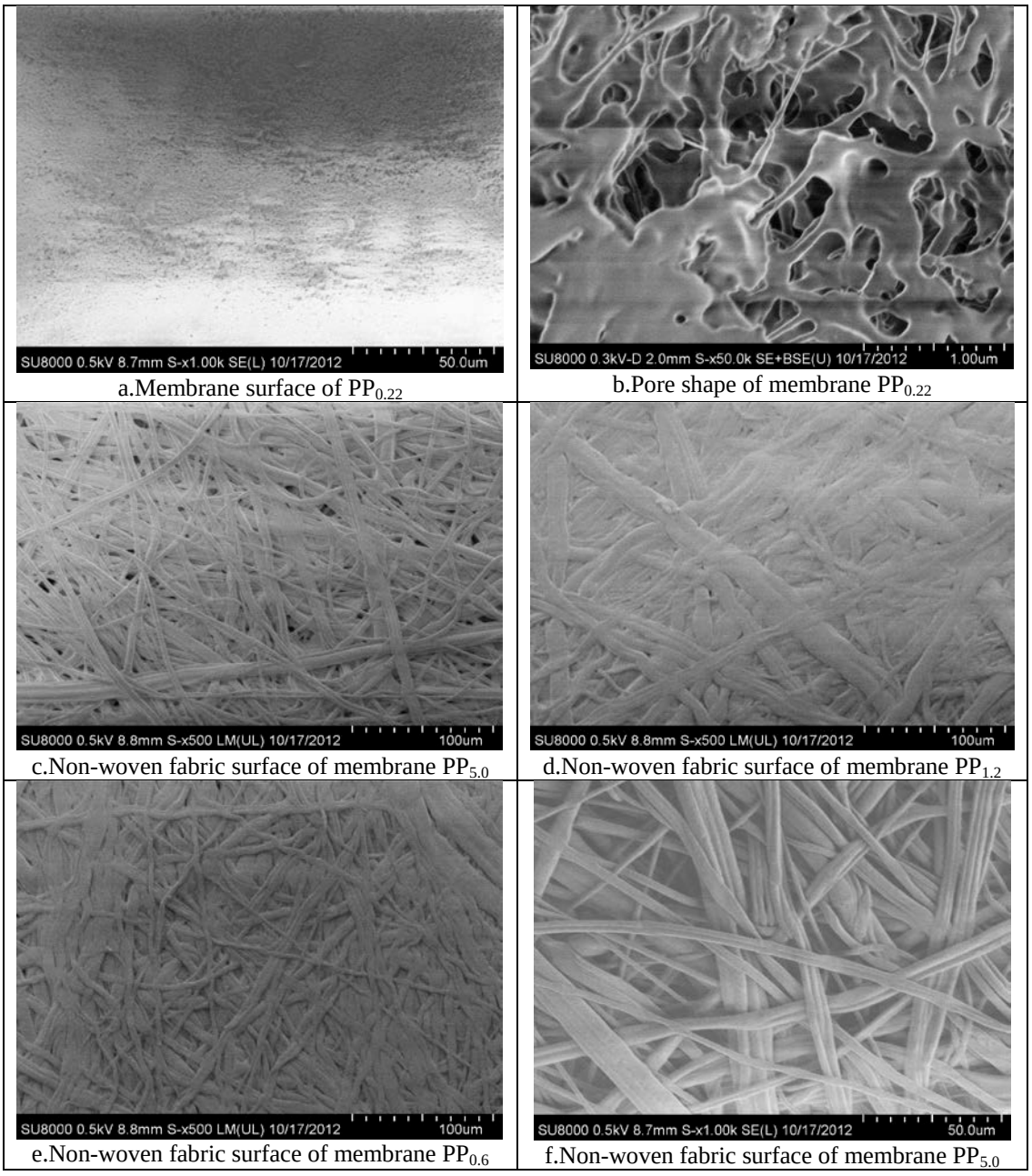

a.Membrane surface of $PP_{0.22}$ b.Pore shape of membrane $PP_{0.22}$

c.Non-woven fabric surface of membrane $PP_{5.0}$ d.Non-woven fabric surface of membrane $PP_{1.2}$

e.Non-woven fabric surface of membrane $PP_{0.6}$ f.Non-woven fabric surface of membrane $PP_{5.0}$

Figure 6-4 SEM images of different membrane surface.

6.3. Pore Size Screening

The 8 membranes with different nominal pore size were used for comparison in terms of CO_2 flux, CO_2 over liquid selectivity, TPC and membrane wetting and fouling conditions. All these experiments were carried out by carefully maintaining the process conditions the same as much as possible. Retentate flow rate was set at 120 mL/min and N_2 sweep gas rate was at 500 sccm. Temperatures at different locations in the system were monitored and recorded.

Results (Table 6-2) showed that CO_2 flux did not change significantly from 0.1 μm to 2.5 μm (Figure 6-5). For pore size of 5 μm and 10 μm, the CO_2 flux increased dramatically but the liquid flux increased even more, which caused significant loss of selectivity. Membranes $PP_{0.45}$ and $PP_{0.6}$ exhibited significantly better selectivity than the rest membranes (Figure 6-6). Especially, $PP_{0.6}$ membrane allowed substantial CO_2 flux and the volume of the permeated liquid and vapors condensate was one magnitude lower than other membranes.

Table 6-2 Flux and selectivity for membranes with different pore size

Nominal pore size (μm)	**CO_2 flux ($cm^3/(cm^2.s)$)**	**Liquid flux ($cm^3/(cm^2.s)$)**	**Selectivity**
0.1	0.47±0.06	2.19×10^{-4}	2152
0.22	0.94±0.17	4.25×10^{-4}	2207
0.45	1.02±0.21	2.30×10^{-4}	4420
0.6	0.94±0.18	4.61×10^{-5}	20431
1.2	0.59±0.04	7.30×10^{-4}	802
2.5	0.69±0.45	4.93×10^{-4}	1398
5.0	2.09±0.66	3.44×10^{-3}	608
10.0	6.04±1.43	1.04×10^{-2}	584

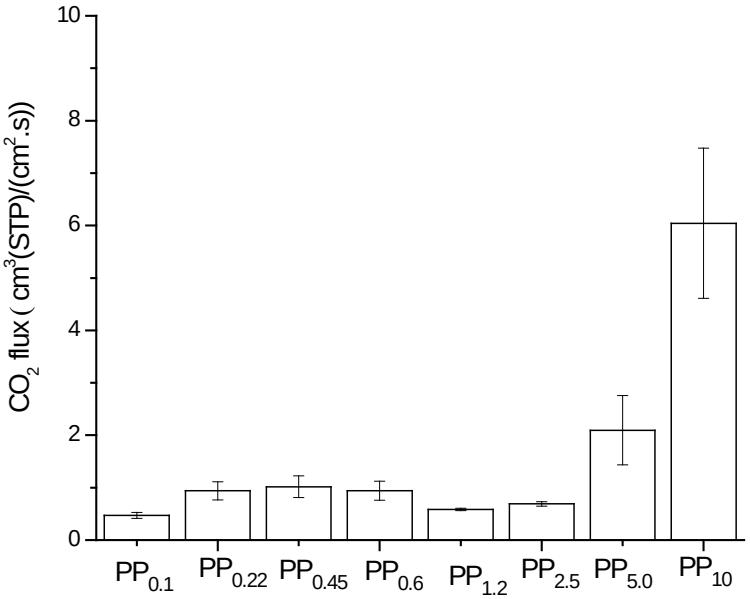

Figure 6-5 CO_2 flux of membranes with different pore size

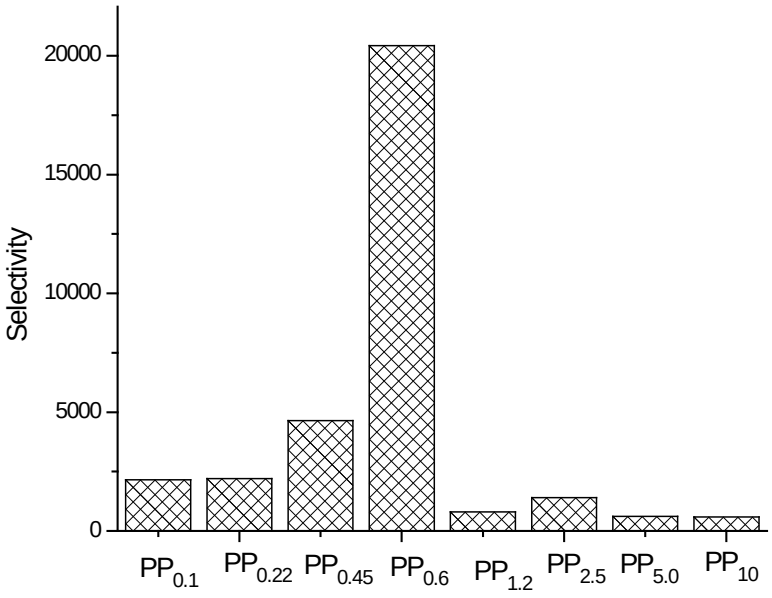

Figure 6-6 Selectivity of membranes with different pore size

Temperatures at the feed side membrane surface, at permeate side membrane surface, the bulk sweep gas and the TPC were listed in Table 6-3 and were plotted in Figure 6-7. There is no significant difference or apparent trend of TPC as a function of the pore size, suggesting that the membrane pore size does not significantly affect the energy utilization efficiencies. These results are reasonable because majority of both the mass transfer and heat transfer resistance is caused by the liquid layer on the membrane surface. The lower TPC of $PP_{0.6}$ was probably due to the excellent hydrophobicity of this membrane, allowing significantly lower liquid flux through the membrane, thus lowered the bulk permeate temperature and consequently lowered the TPC value.

Table 6-3 Temperature readings and TPC

Nominal pore size (μm)	**T_{mf} (°C)**	**T_f (°C)**	**T_p (°C)**	**T_{mp} (°C)**	**TPC**
0.1	77.7	81.1	52.5	64.9	0.448
0.22	77.6	81.0	52.9	65.6	0.427
0.45	77.4	81.0	52.3	65.1	0.429
0.6	76.8	80.3	41.8	62.8	0.364
1.2	77.5	81.2	50.6	64.0	0.441
2.5	77.8	81.4	48.7	62.9	0.456
5.0	76.9	79.6	56.9	66.1	0.476
10.0	76.9	80.5	55.0	64.4	0.490

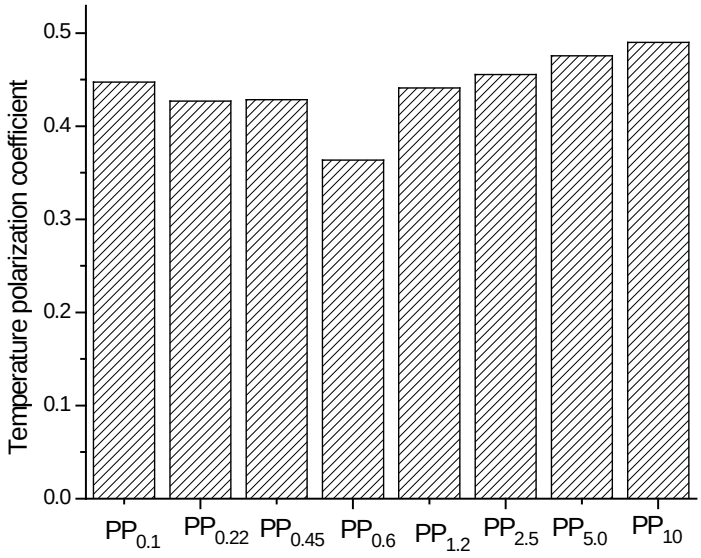

Figure 6-7 TPC comparison of membranes with different pore size

The membranes were weighed before the experiment and immediately after used. Then it was heated to 105 °C and weighed again by a moisture analyzer (Table 6-5). Mass comparison was plotted in Figure 6-8. $PP_{0.1}$, $PP_{0.22}$, $PP_{0.45}$, $PP_{0.6}$ showed excellent hydrophobicity and stayed almost non-wetted. $PP_{1.2}$ and $PP_{2.5}$ started getting wetted during the run. $PP_{5.0}$ and $PP_{10.0}$ were severely wetted, which most likely due to the liquid partial pressure exceeded the breakthrough pressure for the $PP_{5.0}$ and $PP_{10.0}$ membranes. With the same membrane material, liquid solvent, and the same operating parameters, the minimum pressure for the liquid to overcome the hydrophobic force of the membrane and penetrate the pores is proportional to the reverse of the largest membrane pore size as shown by Equation 5-8. Geometric factor B was assumed to be 1 for all membranes. The liquid-solid contact angle θ was estimated to be 105º, which is a typical value for polypropylene (Erbil, Demirel, Avcı, & Mert, 2003). The liquid surface tension γ_L value of 73 $mN.m^{-1}$ was found from literature (Fu, Xu, Wang, & Chen, 2012). Nominal pore size

was used as the r_{max} to estimate the breakthrough pressure. The breakthrough pressure values of membranes with different pore size were calculated using equation 5-8 and listed in Table 6-4. The calculated data were in good agreement with published results for porous membrane made of similar materials: e.g the breakthrough pressures were found to be 200-400 kPa (29- 58 psi) for 0.2 μm pore size PTFE membranes and 100 kPa (14.5 psi) for 0.45 μm pore size PTFE membranes (Cath et al., 2004; Garcıa-Payo et al., 2000).

Table 6-4 The breakthrough pressure versus membrane pore size

Nominal pore size (μm)	**ΔP (Pa)**	**ΔP (psig)**
0.1	35.2×10^4	51
0.22	16.0×10^4	23
0.45	7.8×10^4	11
0.6	5.9×10^4	9
1.2	2.9×10^4	4
2.5	1.4×10^4	2
5.0	0.7×10^4	1
10.0	0.35×10^4	0.5

Table 6-5 The original membrane mass, mass as used and after dried

Nominal pore size (μm)	**Original mass (g)**	**Mass as used (g)**	**Mass after dried (g)**	**Mass as used (%)**	**Mass after dried (%)**
0.1	0.041	0.040	0.040	97.561	97.561
0.22	0.049	0.050	0.045	102.669	92.402
0.45	0.043	0.045	0.045	104.651	104.651
0.6	0.143	0.150	0.145	104.895	101.399
1.2	0.143	0.155	0.135	108.392	94.406
2.5	0.145	0.160	0.140	110.345	96.552
5.0	0.100	0.140	0.095	140.000	95.000
10.0	0.090	0.180	0.085	200.000	94.444

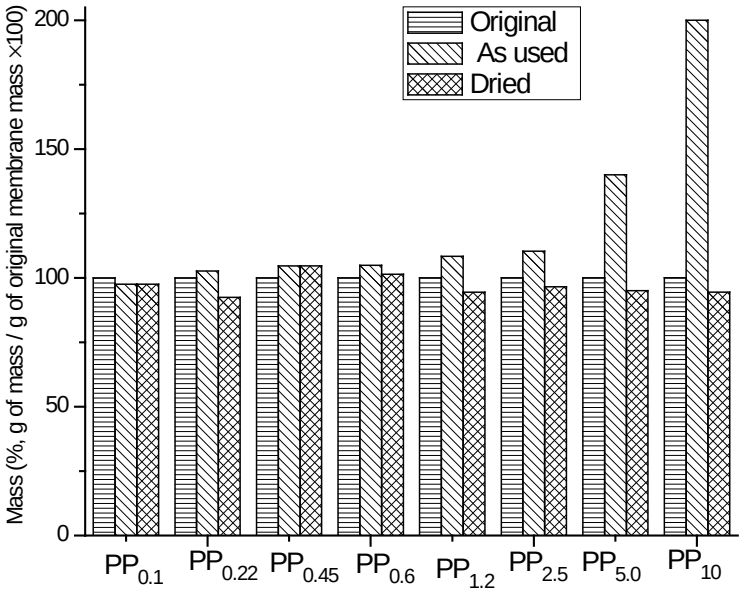

Figure 6-8 Mass comparison of membranes with different pore size

The mass transfer coefficients were calculated under the assumption that all the porous membranes are operated in non-wetted mode and the liquid side pressure is lower than the breakthrough pressure. The pores may be considered totally filled with gas. The gas/liquid interface is then located at the liquid side pore opening. The membrane mass transfer coefficient (k_M), gas phase mass transfer coefficient (k_G), and liquid phase mass transfer coefficient (k_L) and overall mass transfer coefficient (K_{OL}) were calculated using the mass transfer model discussed in section 2.5 of Chapter 2 and listed in Table 6-6.

Table 6-6 Summary of mass transfer coefficients for membranes with different pore size.

Membrane	k_L ($m \cdot s^{-1}$)	k_M ($m \cdot s^{-1}$)	k_G ($m \cdot s^{-1}$)	K_{OL} ($m \cdot s^{-1}$)
$PP_{0.1}$	1.04×10^{-4}	17.8×10^{-3}	2.70×10^{-3}	1.48×10^{-4}
$PP_{0.22}$	1.04×10^{-4}	23.1×10^{-3}	2.70×10^{-3}	1.48×10^{-4}
$PP_{0.45}$	1.04×10^{-4}	34.4×10^{-3}	2.70×10^{-3}	1.49×10^{-4}
$PP_{0.6}$	1.04×10^{-4}	4.04×10^{-3}	2.70×10^{-3}	1.44×10^{-4}
$PP_{1.2}$	1.04×10^{-4}	4.72×10^{-3}	2.70×10^{-3}	1.44×10^{-4}
$PP_{2.5}$	1.04×10^{-4}	4.85×10^{-3}	2.70×10^{-3}	1.45×10^{-4}
$PP_{5.0}$	1.04×10^{-4}	10.1×10^{-3}	2.70×10^{-3}	1.47×10^{-4}
$PP_{10.0}$	1.04×10^{-4}	21.6×10^{-3}	2.70×10^{-3}	1.48×10^{-4}

The data in Table 6-6 were within the range of published value found in the literature. For example, Hoff (Hoff, 2003) reported the membrane mass transfer coefficient (k_M) value of PTFE hollow fiber membrane module with pore size 1-10 μm used in his study for CO_2 capture at 40 °C is 0.03 m/s. Khaisri et al.(Khaisri et al., 2011) reported the mass transfer coefficient analysis results in desorption membrane contactors. The liquid layer mass transfer coefficient of 1.90×10^{-4} m/s; the membrane mass transfer coefficient of 4.97×10^{-4} m/s; the gas mass transfer coefficient 1.83×10^{-3} m/s to 3.21×10^{-3} m/s due to varying gas velocity; and the overall mass transfer coefficient of 1.84×10^{-4} m/s were reported. Simioni et al. reported overall mass transfer coefficient range of 1.0×10^{-4} m/s to 2.5×10^{-4} m/s from temperature 60 °C to 100°C using PTFE and PALL membranes stripping 30 wt% potassium carbonate. The value of 1.6×10^{-4} m/s was read from the plot for both membranes operating at 80 °C (Simioni et al., 2011), which was pretty close to our value regardless different solvent, membrane type, operating conditions and slightly different mass transfer calculation method.

Contribution of individual mass transfer resistance to overall resistance of membranes with different pore size was listed in Table 6-7 and plotted in Figure 6-9. Majority of mass transfer resistance is occurred in the liquid phase layer. It accounted for 90-93% of the overall resistance, which is consistent with our previous mass transfer mechanism study results. Similar results were found in many other literatures. Khaisri et al.(Khaisri et al., 2011) reported the liquid phase mass transfer resistance was roughly 90% of the overall resistance. This result also agreed with many membrane gas absorption studies for membrane contactors (deMontigny, Tontiwachwuthikul, & Chakma, 2006; Khaisri, deMontigny, Tontiwachwuthikul, & Jiraratananon, 2009). Hoff (Hoff, 2003) explained that the diffusivity of CO_2 was approximately 1.8×10^{-5} m^2/s in the N_2 gas and 1.3×10^{-9} m^2/s in the liquid (30 wt% aqueous MEA), which indicated the mass transfer would then be limited by molecular diffusion through a liquid layer with diffusivities 10000 times lower than in the gas. The gas resistance contribution was calculated to be roughly 5-6% of the overall resistance, which was also in agreement of the reported value of roughly 5-10% (deMontigny et al., 2006; Khaisri et al., 2009; Khaisri et al., 2011; Simioni et al., 2011). Our previous parametric study also confirmed that gas velocity was not a significant factor for this process. Membrane resistance contribution was found to be from 0.5% to 4%. Scrutinizing the values, $PP_{0.1}$, $PP_{0.22}$, $PP_{0.45}$ (GE) membranes accounted for very little resistance, much smaller than the rest membranes acquired from Millipore. The differences were due to different pore size, porosity and tortuosity values. Physically, the differences of membrane pore shape, surface morphology and support structures were visualized in Figure 6-4.

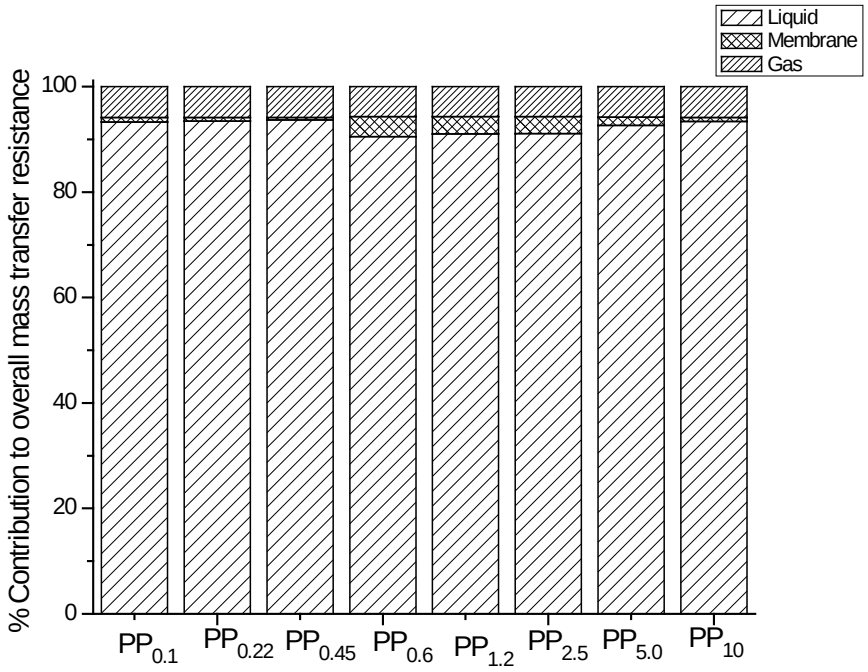

Figure 6-9 Percentage comparison of individual mass transfer resistance to overall resistance for membranes with different pore size

Table 6-7 Summary of percentage of individual resistance to overall resistance for membranes with different pore size.

Membrane	**k_L (%)**	**k_M (%)**	**k_G (%)**
$PP_{0.1}$	93.3	0.9	5.8
$PP_{0.22}$	93.5	0.7	5.8
$PP_{0.45}$	93.7	0.5	5.9
$PP_{0.6}$	90.6	3.8	5.7
$PP_{1.2}$	91.1	3.3	5.7
$PP_{2.5}$	91.1	3.2	5.7
$PP_{5.0}$	92.7	1.5	5.8
$PP_{10.0}$	93.4	0.7	5.8

6.4. Chapter Conclusion

For the membrane pore size study, the membranes with best selectivity have been identified. Membrane $PP_{0.6}$ allowed substantial CO_2 flux and blocked liquid flux through the membrane pores thus showed excellent selectivity and great potential for this application. Membrane with pore size smaller than 2.5 μm showed excellent hydrophobicity; and no wetting and fouling was found during the run. Membranes with pore size of 5 μm and 10 μm were wetted during the process. The mass transfer coefficients were calculated under the assumption that all the porous membranes were operating in non-wetted mode. The results confirmed the controlling mass transfer resistance was from the liquid phase layer, accounting for roughly 90%-93% of the overall mass transfer resistance. Membrane mass transfer resistance accounted for roughly 0.5%-4% and gas phase mass transfer resistance contributed 5% to 6% of the overall resistance, respectively.

7. CONCLUSIONS

Membrane contactors were studied as an alternative format to conventional column contactors for CO_2 regeneration from CO_2 loaded aqueous MEA solutions. An experimental system with CO_2 absorption unit and regeneration unit based on membrane contactors was designed; constructed and validated. This study appeared to be an early and unique one in this field and successfully proved the concept of using polymeric membranes for CO_2 regeneration to be technically possible.

7.1. Summary of Findings

The following are the highlights of research findings from this study:

- The capability of absorbing CO_2 and recovering CO_2 using a porous membrane system in the experimental setup have been verified.
- Porous membranes of polypropylene (PP), polytetraflouroethylene (PTFE) were able to strip CO_2 from an MEA solution with high selectivity.
- Cellulose acetate, PVDF, PES and nylon were found to be unsuitable for this application without further modifications.
- Solvent temperature increase improved CO_2 flux through the membrane and thus improved CO_2 recovery. However, higher solvent loss was also observed with increased temperatures. Solvent temperature was confirmed to be a significant

factor for this process by an individual parametric study and by design of experiment methodologies.

- Retentate-side pressure increase showed a decreased in CO_2 recovery. The higher trans-membrane pressure increased the mass transfer resistance of the liquid film in contact with the membranes. The liquid mass transfer resistance was found to be the major resistance of this process.
- Faster flow rate of retentate solution increased CO_2 flux. A sharp decrease, related to the membrane wetting caused by the high liquid partial pressure at high retentate flow rate, was found at the flow rate of 300mL/min. Increased retentate flow rate decreased regeneration efficiency but not at a linear rate. This can be explained as a combined effect of the shortened residence time and increased CO_2 availability.
- Recovery of CO_2 in this study was low due to the limited membrane surface area provided by the lab-scale membrane unit. A large membrane surface area will be needed to obtain the regeneration rate required for this process to be commercially viable.
- Varying sweep gas rate showed no clear trend on the regeneration performance and did not influence solvent regeneration significantly.
- Multiple phases of gas, vapor, and liquid co-exist within the membrane unit. Most CO_2 gas enters the membrane unit took the less resistance exit and did not flow towards the membrane. Most CO_2 recovered at the permeate side was from the solvent in contact with membrane pores.

- Liquids in the membrane unit take the form of laminar flow across the membrane. This laminar flow liquid layer adds significant resistance for the lighter gas phase to diffuse through.
- Solvent temperature influences the TPC of the system significantly. Retentate flow rate and sweep gas flow rate had no significant effect. At process temperatures of 80ºC and above, the measured TPC was approximately 0.5. This value suggests that roughly half of the heat energy provided by the heater is used for the separation process. The TPC value is close to that the reported for laminar flow in membrane distillation.
- Degradation residues of the MEA are observed to adsorb into the membrane when operating pressures are higher than the membrane breakthrough pressure. Altered surface properties, reduced hydrophobicity of the membrane, and slower CO_2 mass transfer are also observed.
- Membrane module design and configuration are important factors affecting membrane performance. Unlike other membrane process whose performance is indifferent to the operating orientation, CO_2 regeneration performance is sensitive to membrane orientation. Gravity assisted operation is preferred for improved separation performance and yield.
- The PP membrane with pore size 0.6 μm had the best selectivity of the membranes studied. Substantial CO_2 flux and high rejection of liquid flux through the membrane was observed.
- Membranes within the study with pore size smaller than 2.5 μm showed excellent hydrophobicity, as well as no wetting or fouling during experiments. Membranes

with pore size of 5 μm and 10 μm were wetted during the process and fouling was not observed.

- Mass transfer coefficients were calculated under the assumption that all the porous membranes are operated in non-wetted mode. Results confirmed that the controlling mass transfer resistance originates from the liquid phase layer. Roughly 90%-93% of the overall mass transfer resistance is from the liquid phase layer. Membrane mass transfer resistance accounts for roughly 0.5%-4% and gas phase mass transfer resistance contributes 5% to 6%.

7.2. Recommendations

Recommendations for future work in this field are varied. The largest limitation encountered during this research undertaking was limited membrane surface area. A membrane module with much larger surface area should be utilized in future studies. This will allow the economic feasibility of the process to be understood and compared with other CO_2 capture methodologies.

Other research aspects, such as finding novel membrane materials, materials modification techniques for improved membrane performance, solvent selection and optimization, process modeling, process development and energy integration, economic feasibility study, are important for commercialization and represent areas where further contributions could be made. Priority should also be given to the design and fabrication of the membrane module in any future undertaking. Results from this study have laid a foundation, and provided directions, for continued use of membrane contactors for CO_2 recovery from chemical solvents.

8. APPENDICES

Appendix A Equipment List

Appendix B Membrane Material Candidates

Appendix C Mass Transfer Coefficient Calculation

Appendix A Equipment List

A detailed list of equipment and materials is given below:

Equipment:

- Membrane unit: Millipore 47mm Stainless Steel Membrane Holder XX4404700
- Pump: Cole-Parmer digital gear pump, pumping speed 0- 330ml/min, ± 1ml/min
- Two Cartridge heaters: Stainless steel construction, 3 feet leads, ¼" diameter, 8" length, ¼" NPT thread, 600 W from Omega engineering Inc.
- Alternative heater: Low flow air process and liquid circulation heater AHPF-121, 120VAC, 1200W, stainless stain, outlet temperature up to 430 C, flow rate up to 15CFM, pressure up to 100 psi from Omega.
- Heater controller: Cal controller 9400
- Pressure transducer: Omega, 0-300psi, 5 VDC regulated input, 0-100mV output.
- Pressure gauges: Omega 0-300psi, unknown origin
- Thermocouple: 1/8", 1/4" diameter, K type from Omega
- Mass flow controller: Brooks 4800 series, CO_2 (0-10 SLPM), N_2 (0-10 SLPM).
- Swagelok tubing and fittings
- Liquid and particulate filter: Parker coalescing filter (Cole Parmer)

Data logger:

- National Instruments USB-9219 4-Channel Universal Analog Input Module

CO_2 analyzers:

- Li-cor 820 Non-Dispersive Infrared CO_2 analyzer, 0-20,000ppm, ± 1ppm
- Agilent 7850A GC- FID with methanizer, TCD

Computers and Software:

- Computer: Dell Precision T3200, Microsoft™ Windows 7
- Data acquisition: Labview™ software, version 2010 from National Instruments
- GC control and analysis: Chemstation, Agilent
- CO_2 analyzer: LI-820 v2.0.0

Materials:

- Ethanolamine, 99% ACS reagent 2.5L (Sigma- Aldrich)
- PTFE 47 mm membranes (Sartorius Stedim), pore size: 1.2 μm
- Polyamide 47 mm membranes (Sartorius Stedim), pore size: 0.45 μm
- Laminated Teflon 47 mm membranes (GE Water & Process Technologies), pore size: 0.45 μm
- Polyester (PETE) 47 mm membranes (GE Water & Process Technologies) pore size: 0.4 μm
- Polypropylene 47 mm membranes (GE Water & Process Technologies), pore size: 0.4 μm

- Cellulose Acetate 47 mm membranes (Advantec), pore size: 5.0 μm
- PES 47 mm membranes (Millipore), pore size: 0.22 μm;
- PVDF 47 mm membranes (Millipore), pore size: 0.45 μm;
- Mixed Cellulose Ester 47 mm membranes (Advantec), pore size:5.0 μm;

Appendix B Membrane Material Candidates

Table 8-1 Membrane Material Candidates

Rank	Polymer	Abbreviation	$P(CO_2)$ (barrer)	T_g (C)	T_m(C)	Water Absorption (%)	Solvents	Vender	Notes
1	poly(1-trimethylsilyl-1-propyne)	PTMSP	3520[2]	262[2]	323[2]				
2	polydimethylsiloxane	PDMS	3100[5],4553 [7]	-128[4]	-40[3]		Benzene, Toluene		Rubbery Polymer
3	6FDA-based polyimides	6FDA–durene	456[1], 24.2[5]	300-350[9]	N/A				
4	Poly(phenylene oxide)	PDMPO (60.0% brominated)	159.9[1]	184[2]	279-285[2]				
5	cis-polyisoprene	cis-PIP	134[5],191[7]	99[2]	156[2]		Hydrocarbon		Rubbery Polymer
6	Polycarbonates	TMHFPC	111[1]	217[2]	270[2]			GE,	
7	Polysulfones	PSF	110[1], 5.6[5]4.6[7]	237[2]186-190[9]	N/A		HPLC grade reagent alcohol (Fisher Sci)	Amoco Performance Products	P-1700
8	Poly(ether-b-amide)	PEBAX[6]	30-104[15]	-60 to -70[2] -30to 160[9]	120-210[2]		3:1 by weight mixture of 1-propanol and 1-butanol at 80C [6]	ATOFINAChemical, Inc. (Philadelphia, PA.)	grade 2533,hydrophobic
9	Polyarylates	TBHFBPA/tBIA	85.1[1]	N/A	N/A				Similar to polyester aromatics

Table 8-1 Membrane Material Candidates continued

Rank	Polymer	Abbreviation	$P(CO_2)$ (barrer)	T_g (C)	T_m(C)	Water Absorption (%)	Solvents	Vender	Notes
10	Poly(4-methyl-1-pentene)	PMP	83[5]	151-162[2]	270[2]		Xylene (>100C)		
11	Polyester	PE	HDPE 76.4[12] LDPE 13.4[12]	-20[8]	166-249[2]	0.1-0.5[2]		GE, Sigma-Aldrich	
12	Poly(2,6-dimethyl phenylene oxide)	PPO	61[5]	249-259[2]	282[2]		Benzene, Toluene		
13	Poly(pyrrolone)	6FDA–TAB	54.0[1]	N/A	273(?)[2]				
14	Polypropylene	PP	13.4,34[11]	-10[8]	135-165[8]				P477
15	Poly(arylene ether)	6FPPy–6FBPA	29.46 [1]	N/A	82-96[8]	0.06[2]			Similar to Poly(phenylene ether) V13P21
16	poly(tertbutyl acetylene)	PTBA	5.0-27.4[13]	-77[13]	126-204[13]		isopropanol		
17	Poly(tetrafuoroethylene)	PTFE	21.3[11]	204[2]	316[2]		Perfluorinated Materials, >573K	GE, Dupont-NEN, Millipore,Advantec,	
18	Polystyrene	PS	12.4	98[8,9]			Acetone, Benzene		

Table 8-1 Membrane Material Candidates continued

Rank	Polymer	Abbreviation	P(CO_2) (barrer)	T_g (C)	T_m(C)	Water Absorption (%)	Solvents	Vender	Notes
19	Polyimides	PMDA–BAPHF	11.8[1]	230-330[9]	N/A				
20	Cellulose acetate	CA	5.5[7]	117-245[2]	304[2]	0.6[2]			
21	polyethersulfone	PES	4.2[2]	259[2]	N/A		0.43	GE	
22	Poly(vinyl acetate)	PVAC	3.1[10]	150[2]34.8[9]	231[2]	3-6[2]	Acetone,ethanol, methanol, benzene, toluene		
23	Polyamide	Nylon Hydrophobic	1.5[11]	160[2]	231-234[2]	1.0[2]		GE	Nylon 12
24	Poly(vinyl chloride)	PVC	1.3[12]	71[9]173-188[2]			Toluene, Acetone		Poisonous, p157
25	poly(ethylene terephthalate)	PET	0.5[12]	172-198[2]	281[2]	0.5[2]			
26	Polyvinyl fluoride	PVF	0.06[11]					GE	
27	Polyvinylidene fluoride	PVDF	0.05[14]	114[2]	227[2] 155-192[8]	0.025[2]	Acetone	GE, Dupont-NEN, Millipore,	V17P537

Table 8-1 Membrane Material Candidates continued

Rank	Polymer	Abbreviation	$P(CO_2)$ (barrer)	T_g (C)	T_m(C)	Water Absorption (%)	Solvents	Vender	Notes
28	poly(amide-imide)	PAI		287[2]	N/A	0.33[2]			
29	Nitrocellulose	cellulose nitrate CN	2.1[2]	163[2]	N/A	1.0[2]	Acetone, water	GE,Bio-Rad,Dupont-NEN, Millipore, S&S	
30	Polyvinylpyrrolidone	PVP		194-233[2]	N/A		Water,alcohol	Fluka Chemika	
31	Polyvinyl alcohol	PVA	161[10]	181[2]	281[2]		water		
32	Poly(acetylene)	Poly(trimethyl-prop-1-ynyl-silane)	19000 [1]	145[2]	420[2]				Degrades, not stable
33	Poly(ethylene oxide)	PEO	773[1]	70-112[2],-60[6]	99-171[2]		water	Sigma-Aldrich	Hydrophobic, Flash point 270C

Section references:

[1] Clem E. Powell, Greg G. Qiao, Polymeric CO_2/N_2 gas separation membranes for the capture of carbon dioxide from power plant flue gases, Journal of Membrane Science 279 (2006) 1-49

[2] James E. Mark, Polymer Data Handbook, Oxford University Press, USA (February 25, 1999)

[3] Knovel Critical Tables, http://web.mit.edu/6.777/www/matprops/pdms.htm

[4] Robert Martin Sok, Permeation of Small Molecules across a Polymer Membrane: a Computer Simulation Study, Dissertation, RIJKSUNIVERSITEIT GRONINGEN, 1994, page 20

[5] Nikunj Pragjibhai Patel, Nanostructured Polymeric Membranes for Selective CO_2 Removal from Light Gas Mixtures, Dissertation, North Carolina State University, 2004, page 29

[6] Jennifer Chih-Yi Chen, Evaluation of Polymeric Membranes for Gas Separation Processes: Poly(ether-b-amide)(PEBAXR2533) Block Copolymer, MS thesis, University of Waterloo, 2002

[7] Jennifer Run-Hong Du, Studies on Poly(N,N-dimethylaminoethyl methacrylate) Composite Membranes for Gas Separation and Pervaporation, Dissertation,University of Waterloo, 2002, page 16

[8] Herman F. Mark, Norbert Bikales, etc, Encyclopedia of Polymer Science and Engineering, Wiley-Interscience; 2 Edition (May 12, 1986)

[9] James E. Mark, Physical Properties of Polymer Handbook, American Institute of Physics Press, 1996

[10] Colin A. Scholes, Sandra E. Kentish and Geoff W. Stevens, Carbon Dioxide Separation through Polymeric Membrane Systems for Flue Gas Applications, Recent Patents on Chemical Engineering, 2008, 1, 52-66

[11] Liesl K. Massey, Permeability properties of plastics and elastomers: a guide to packaging and barrier materials, William Andrew, 2003

[12] Stuart Patrick, Practical guide to polyvinyl chloride, iSmithers Rapra Publishing, 2005, p79

[13] Li Liu, Gas Separation by Poly(Ether Block Amide) Membranes, Dissertation, the University of Waterloo ,2008, p54

[14] http://www.westlakeplastics.com/pdf/film_pvdf.pdf

[15] Benny Freeman, Yuri Yampolskii, Membrane Gas Separation, John Wiley and Sons, 2010, p27

Appendix C Mass Transfer Coefficient Calculation

C.1. Physical Liquid Phase Mass Transfer Coefficient (k_L)

The CO_2 diffusivity in liquid phase can be determined by the following equation (Khaisri et al., 2011):

$$D_{CO_2} = D_{N_2O}\left(\frac{D_{CO_2,H_2O}}{D_{N_2O,H_2O}}\right)$$

Equation 8-1

T = 77ºC = 350 K, C_{MEA} = 15 wt.% = 2.45 mol L^{-1}, α = 0.45 mol CO_2/ mol amine, and μ_{H_2O}= 1 mPa·s

$$D_{CO_2,H_2O} = 2.35 \times 10^{-2} \exp\left(\frac{-2119}{T}\right) = 2.35 \times 10^{-2} \exp\left(\frac{-2119}{350}\right) = 5.5 \times 10^{-5} cm^2 s^{-1}$$

Equation 8-2

$$D_{N_2O,H_2O} = 5.07 \times 10^{-2} \exp\left(\frac{-2371}{T}\right) = 5.07 \times 10^{-2} \exp\left(\frac{-2371}{350}\right) = 5.8 \times 10^{-5} cm^2 s^{-1}$$

Equation 8-3

$$D_{N_2O,MEA} = (5.07 \times 10^{-2} + 8.65 \times 10^{-3} C_{MEA} + 2.78 \times 10^{-3} C_{MEA}^2) \exp\left(\frac{-2371 - 93.4 C_{MEA}}{T}\right)$$

$$= (5.07 \times 10^{-2} + 8.65 \times 10^{-3} \times 2.45 + 2.78 \times 10^{-3} \times 2.45^2) \exp\left(\frac{-2371 - 93.4 \times 2.45}{350}\right)$$

$$= 5.3 \times 10^{-5} cm^2 s^{-1}$$

Equation 8-4

$$D_{CO_2} = D_{N_2O}\left(\frac{D_{CO_2,H_2O}}{D_{N_2O,H_2O}}\right) = 5.3 \times 10^{-5}\left(\frac{5.5 \times 10^{-5}}{5.8 \times 10^{-5}}\right) = 5.0 \times 10^{-5} cm^2 s^{-1}$$

Equation 8-5

$$\frac{\mu_{MEA}}{\mu_{H_2O}} = \exp\frac{[21.186\Omega + 2373][\alpha(0.01015\Omega + 0.0093T - 2.2589) + 1]\Omega}{T^2} = 1$$

$$\mu_{MEA} = 1 \text{ mPa·s}$$

Equation 8-6

v_L = 120 mL/min = 120 cm^3/[π(0.25 inch/2) ^{2}]/60 s = 6.3 cm s^{-1}

d_h = 2.45 mm = 0.245 cm

L = 4.7 cm (The average liquid path approximate the diameter of the membrane)

$$k_L = \frac{D_L}{d_h} 1.62\left(\frac{d_h^2 v_L}{L D_L}\right)^{\frac{1}{3}} = \frac{5.0 \times 10^{-5} cm^2 s^{-1}}{0.245 \text{ cm}} 1.62\left(\frac{0.245 \text{ cm } \times 6.3 \text{ cm } s^{-1}}{5.0 \times 10^{-5} cm^2 s^{-1}}\right)^{\frac{1}{3}}$$
$$= 1.037 \times 10^{-2} \text{ cm} \cdot s^{-1} = 1.037 \times 10^{-4} \text{ m} \cdot s^{-1}$$

Equation 8-7

C.2. Physical Gas Phase Mass Transfer Coefficient (k_G)

The CO_2 diffusivity in gas phase can be determined by the following equation (Khaisri et al., 2011):

$$D_G = \frac{0.001858 T^{3/2}[(1/M_A + 1/M_B)]^{1/2}}{P\sigma_{AB}^2 \Omega_G}$$

Equation 8-8

Parameters included can be calculated accordingly (Bird et al., 2006).

T = 65ºC = 338 K

M_A = 44, M_B = 28, and P = 1 atm = 1.01325 bar

$\sigma_{AB} = 0.5(\sigma_A + \sigma_B) = 0.5(4.63\text{Å} + 3.76\text{Å})$ = 4.195 Å

$\varepsilon_{AB}/\kappa=[(\varepsilon_A/\kappa)(\varepsilon_B/\kappa)]^{1/2} = [195.2\times 71.4]^{1/2}$ = 118 K

$T^* = \kappa T/\varepsilon_{AB}$ = 338 K/118 K = 2.8

$$\Omega_G = \frac{1.06036}{(T^*)^{0.15610}} + \frac{0.19300}{\exp(0.47635T^*)} + \frac{1.03587}{\exp(1.52996T^*)} + \frac{1.76474}{\exp(3.89411T^*)}$$

$$= \frac{1.06036}{(2.8)^{0.15610}} + \frac{0.19300}{\exp(0.47635 \times 2.8)} + \frac{1.03587}{\exp(1.52996 \times 2.8)} + \frac{1.76474}{\exp(3.89411 \times 2.8)} = 0.97$$

Equation 8-9

$$D_G = \frac{0.001858T^{3/2}[(1/M_A + 1/M_B)]^{1/2}}{P\sigma_{AB}^2\Omega_G} = \frac{0.001858 \times 338^{3/2}[(1/44 + 1/28)]^{1/2}}{1 \times 4.195^2 \times 0.97}$$
$$= 0.164\ \text{cm}^2\text{s}^{-1}$$

Equation 8-10

$$\frac{k_G d_h}{D_G} = 0.023\left(\frac{d_h \rho v_G}{\mu_G}\right)^{0.8}\left(\frac{\mu_G}{D_G \rho}\right)^{0.33}$$

Equation 8-11

$\rho_{mixture} \approx 1.0101\ \text{kg}\cdot\text{m}^{-3} = 10^{-3}\ \text{g}\cdot\text{cm}^{-3}$ (at 338 K, 1 atm)

$\mu_{mixture} \approx 19\times 10^{-6}$ Pa·s = $19\times 10^{-5}\ \text{g}\cdot\text{cm}^{-1}\cdot\text{s}$ (at 338 K, 1 atm, and 1 Pa·s = 10 $\text{g}\cdot\text{cm}^{-1}\cdot\text{s}$)

$v_G = 500\ \text{cm}^3\cdot\text{min}^{-1} = 500\ \text{cm}^3/[\pi(0.25\ \text{inch}/2)^2]/60\ \text{s} = 26.25\ \text{cm}\cdot\text{s}^{-1}$

$$k_G = \frac{D_G}{d_h} \times 0.023\left(\frac{d_h \rho v_G}{\mu_G}\right)^{0.8}\left(\frac{\mu_G}{D_G \rho}\right)^{0.33}$$

$$= \frac{0.164\ \mathrm{cm^2 s^{-1}}}{0.245\ \mathrm{cm}} \times 0.023\left(\frac{0.245\ \mathrm{cm} \times 10^{-3}\ \mathrm{g \cdot cm^{-3}} \times 26.25\ \mathrm{cm \cdot s^{-1}}}{19 \times 10^{-5}\ \mathrm{g \cdot cm^{-1} \cdot s^{-1}}}\right)^{0.8}\left(\frac{19 \times 10^{-5}\ \mathrm{g \cdot cm^{-1} \cdot s^{-1}}}{0.164\ \mathrm{cm^2 s^{-1}} \times 10^{-3}\ \mathrm{g \cdot cm^{-3}}}\right)^{0.33} = 0.27\ \mathrm{cm \cdot s^{-1}} = 2.7 \times 10^{-3}\ \mathrm{m \cdot s^{-1}}$$

Equation 8-12

C.3. Membrane Mass Transfer Coefficient (k_M)

$$k_M = \frac{D_e \varepsilon}{\tau \delta}$$

Equation 8-13

$$\frac{1}{D_e} = \frac{1}{D_k} + \frac{1}{D_G}$$

Equation 8-14

where D_e is the combination of Knudsen and molecular diffusivity coefficient. D_k is the Knudsen diffusivity coefficient, and D_G is the diffusivity of CO_2 in the gas phase (Khaisri et al., 2011).

$D_G = 0.164\ cm^2\ s^{-1}$, T =0.5(77 +65) = 71ºC = 344 K

Equation 8-15

$$D_k = 4850\ d_{pore} \sqrt{\frac{T}{M_A}}$$

Equation 8-16

For $PP_{0.1}$, d_{pore} = 0.5×0.1 μm = 0.5×10^{-5} cm, ε = 0.76, τ = 2.04, δ = 0.1 mm = 0.01 cm,

$$D_k = 4850\ d_{pore} \sqrt{\frac{T}{M_A}} = 4850 \times 0.5 \times 10^{-5}\ \mathrm{cm} \times \sqrt{\frac{344}{44}} = 0.0678\ \mathrm{cm^2 s^{-1}}$$

Equation 8-17

$$D_e = \frac{1}{\frac{1}{D_k} + \frac{1}{D_G}} = \frac{1}{\frac{1}{0.0678} + \frac{1}{0.164}} = 0.0479\ cm^2 s^{-1}$$

Equation 8-18

$$k_M = \frac{D_e \varepsilon}{\tau \delta} = \frac{0.0479\ cm^2 s^{-1} \times 0.76}{2.04 \times 0.01} = 1.78\ cm \cdot s^{-1} = 1.78 \times 10^{-2} m \cdot s^{-1}$$

Equation 8-19

C.4. Enhancement Factor

The enhancement factor can be determined by equation as shown below (Khaisri et al., 2011):

$$E = 1 + \frac{(D_{MEACOO^-}/D_{CO_2})\sqrt{K} C^B_{MEA}}{\left(1 + 2(D_{MEACOO^-}/D_{MEA})\sqrt{K C_{CO_2,i}}\right)\left(\sqrt{C_{CO_2,i}} + C^B_{CO_2}\right)}$$

Equation 8-20

where C^B_{MEA} and $C^B_{CO_2}$ are the bulk concentration of free MEA and CO_2.

$C^B_{MEA} = 2.45\ mol/L$

$C^B_{CO_2} = 1.10\ mol/L$

D_{CO_2} is the CO_2 diffusivity in MEA solution.

$D_{CO_2} = 5.0 \times 10^{-5} cm^2 s^{-1}$

D_{MEACOO^-} and D_{MEA} are diffusivity of carbamate and MEA.

$D_{MEACOO^-} \approx D_{MEA} = 5.3 \times 10^{-5} cm^2 s^{-1}$

K is the equilibrium constant

$$K = \frac{1}{C_{CO_2,e}}\left(\frac{\alpha}{1-2\alpha}\right)^2$$

Equation 8-21

$C_{CO_2,e} \approx C^B_{CO_2} = 1.10$ mol/L, α = 0.45

K = 18.4 L/mol

Assume $C_{CO_2,e} \approx C_{CO_2,e} \approx C^B_{CO_2} = 1.10$ mol/L

Therefore,

$$E = 1 + \frac{\left(\frac{5.3\times10^{-5}\text{cm}^2\text{s}^{-1}}{5.0\times10^{-5}\text{cm}^2\text{s}^{-1}}\right)\sqrt{18.4\frac{\text{L}}{\text{mol}}}\times 2.45\ \text{mol/L}}{\left(1+2(1)\sqrt{18.4\frac{\text{L}}{\text{mol}}\times 1.1\ \text{mol/L}}\right)\left(\sqrt{1.1\ \text{mol/L}}+\sqrt{1.1\ \text{mol/L}}\right)} = 1.53$$

Equation 8-22

C.5. Henry's Constant

The Henry's constant can be described as following equation(Khaisri et al., 2011):

$$H_{CO_2} = H_{N_2O}\left(\frac{H_{CO_2,H_2O}}{H_{N_2O,H_2O}}\right)$$

Equation 8-23

The unit of H_{CO2} is kPa·L·mol^{-1}

T = 65°C = 338 K

$$H_{CO_2,H_2O} = 2.82 \times 10^6 \exp\left(\frac{-2284}{T}\right) = 2.82 \times 10^6 \exp\left(\frac{-2284}{338}\right) = 3277\ \text{kPa} \cdot \text{dm}^3 \cdot \text{mol}^{-1}$$

Equation 8-24

$$H_{N_2O,H_2O} = 8.55 \times 10^6 \exp\left(\frac{-2284}{T}\right) = 8.55 \times 10^6 \exp\left(\frac{-2284}{338}\right) = 9935\ \text{kPa} \cdot \text{dm}^3 \cdot \text{mol}^{-1}$$

Equation 8-25

$$H_{N_2O,MEA} = 1.207 \times 10^5 \exp\left(\frac{-1136.5}{T}\right) = 1.207 \times 10^5 \exp\left(\frac{-1136.5}{338}\right)$$

$$= 4188\ \text{kPa} \cdot \text{dm}^3 \cdot \text{mol}^{-1}$$

Equation 8-26

The two body interaction parameter for MEA and H_2O is calculated as below, where Φ_{H_2O} is volume percentage of water.

$$\lambda_{H_2O-MEA} = 4.793 - 7.44 \times 10^{-3}T - 2.201\Phi_{H_2O}$$

$$= 4.793 - 7.44 \times 10^{-3} \times 338 - 2.201 \times 0.85 = 0.32$$

Equation 8-27

The excess Henry's constant is calculated as below:

$$H^E = \Phi_{MEA}\Phi_{H_2O}\lambda_{H_2O-MEA} = 0.15 \times 0.85 \times 0.32 = 0.041$$

Equation 8-28

$$\ln H_{N_2O} = H^E + \Phi_{MEA}H_{N_2O,\text{pure MEA}} + \Phi_{H_2O}\ln H_{N_2O,H_2O}$$

$$= 0.041 + 0.15 \times \ln 4188 + 0.85 \times \ln 9935 = 9.1$$

Equation 8-29

$$H_{N_2O} = 9092\ \text{kPa} \cdot \text{dm}^3 \cdot \text{mol}^{-1}$$

Therefore,

$$H_{CO_2} = H_{N_2O}\left(\frac{H_{CO_2,H_2O}}{H_{N_2O,H_2O}}\right) = 9092\left(\frac{3277}{9935}\right) = 1381\ \text{kPa} \cdot \text{dm}^3 \cdot \text{mol}^{-1}$$

$$= 3000\ \text{kPa} \cdot \text{dm}^3 \cdot \text{mol}^{-1} = 3000\ \text{kPa} \cdot \text{L} \cdot \text{mol}^{-1}$$

Equation 8-30

The dimensionless H of CO_2 is

$$H = \left(\frac{1}{H_{CO_2}}\right)RT = \left(\frac{8.314\ \text{kPa} \cdot \text{L} \cdot \text{K}^{-1} \cdot \text{mol}^{-1} \times 338\ \text{K}}{3000\ \text{kPa} \cdot \text{L} \cdot \text{mol}^{-1}}\right) = 0.94$$

Equation 8-31

9. REFERENCES

Aaron, D., & Tsouris, C. (2005). Separation of CO_2 from flue gas: A review. *Separation Science and Technology, 40*(1-3), 321-348.

Adnan, S., Hoang, M., Wang, H., & Xie, Z. (2012). Commercial PTFE membranes for membrane distillation application: Effect of microstructure and support material. *Desalination, 284*, 297-308.

Alklaibi, A., & Lior, N. (2005). Membrane-distillation desalination: Status and potential. *Desalination, 171*(2), 111-131.

Alvarez, E., Rendo, R., Sanjurjo, B., Sanchez-Vilas, M., & Navaza, J. M. (1998). Surface tension of binary mixtures of water N-methyldiethanolamine and ternary mixtures of this amine and water with monoethanolamine, diethanolamine, and 2-amino-2-methyl-1-propanol from 25 to 50 C. *Journal of Chemical & Engineering Data, 43*(6), 1027-1029.

Bird, R. B., Stewart, W. E., & Lightfoot, E. N. (2006). *Transport phenomena* Wiley.

Buckley-Smith, M. (2006). *The use of Solubility Parameters to Select Membrane Materials for Pervaporation of Organic Mixtures,*

Carapellucci, R., & Milazzo, A. (2003). Membrane systems for CO_2 capture and their integration with gas turbine plants. *Proceedings of the Institution of Mechanical Engineers, Part A: Journal of Power and Energy, 217*(5), 505-517.

Cath, T. Y., Adams, V. D., & Childress, A. E. (2004). Experimental study of desalination using direct contact membrane distillation: A new approach to flux enhancement. *Journal of Membrane Science, 228*(1), 5-16.

Chen, S., Lin, S., Chien, R., & Hsu, P. (2010). Effects of shape, porosity, and operating parameters on carbon dioxide recovery in polytetrafluoroethylene membranes. *Journal of Hazardous Materials, 179*(1), 692-700.

Curnow, O. J., Krumdieck, S. P., & Jenkins, E. M. (2005). Regeneration of carbon dioxide saturated monoethanolamine-glycol aqueous solutions at atmospheric pressure in a packed bubble reactor. *Industrial & Engineering Chemistry Research, 44*(4), 1085-1089.

Davis, J. D. (2009). *Thermal degradation of aqueous amines used for carbon dioxide capture*, The University of Texas at Austin, Dissertation.

deMontigny, D., Tontiwachwuthikul, P., & Chakma, A. (2006). Using polypropylene and polytetrafluoroethylene membranes in a membrane contactor for CO_2 absorption. *Journal of Membrane Science, 277*(1), 99-107.

Ding, Z., Liu, L., Li, Z., Ma, R., & Yang, Z. (2006). Experimental study of ammonia removal from water by membrane distillation (MD): The comparison of three configurations. *Journal of Membrane Science, 286*(1), 93-103.

DOE. (2007). *Carbon sequestration technology roadmap and program plan.* U.S. Department of Energy, Office of Fossil Energy, National Energy Technology Laboratory:

EIA. (2013a). *Annual energy outlook 2013.* Energy information administration.

EIA. (2013b). *Short-term energy outlook.* Energy information administration.

Erbil, H. Y., Demirel, A. L., Avcı, Y., & Mert, O. (2003). Transformation of a simple plastic into a superhydrophobic surface. *Science, 299*(5611), 1377-1380.

Favre, E. (2007). Carbon dioxide recovery from post-combustion processes: Can gas permeation membranes compete with absorption? *Journal of Membrane Science, 294*(1), 50-59.

Figueroa, J. D., Fout, T., Plasynski, S., McIlvried, H., & Srivastava, R. D. (2008). Advances in CO2 capture technology—The US department of energy's carbon sequestration program. *International Journal of Greenhouse Gas Control, 2*(1), 9-20.

Franco, J. A., deMontigny, D., Kentish, S. E., Perera, J. M., & Stevens, G. W. (2009). Effect of amine degradation products on the membrane gas absorption process. *Chemical Engineering Science, 64*(18), 4016-4023.

Freeman, S. A., Davis, J., & Rochelle, G. T. (2010). Degradation of aqueous piperazine in carbon dioxide capture. *International Journal of Greenhouse Gas Control, 4*(5), 756-761.

Fu, D., Xu, Y., Wang, L., & Chen, L. (2012). Experiments and model for the surface tension of carbonated monoethanolamine aqueous solutions. *Science China Chemistry, 55*(7), 1467-1473.

Garcıa-Payo, M., Izquierdo-Gil, M., & Fernandez-Pineda, C. (2000). Wetting study of hydrophobic membranes via liquid entry pressure measurements with aqueous alcohol solutions. *Journal of Colloid and Interface Science, 230*(2), 420-431.

Goff, G. S., & Rochelle, G. T. (2006). Oxidation inhibitors for copper and iron catalyzed degradation of monoethanolamine in CO_2 capture processes. *Industrial & Engineering Chemistry Research, 45*(8), 2513-2521.

Hoff, K. A. (2003). *Modeling and Experimental Study of Carbon Dioxide Absorption in a Membrane Contactor,* Trondheim: Norwegian University of Science and Technology, Dissertation.

Hook, R. J. (1997). An investigation of some sterically hindered amines as potential carbon dioxide scrubbing compounds. *Industrial & Engineering Chemistry Research, 36*(5), 1779-1790.

Hrdlicka, J. A., Seames, W. S., Mann, M. D., Muggli, D. S., & Horabik, C. A. (2008). Mercury oxidation in flue gas using gold and palladium catalysts on fabric filters. *Environmental Science & Technology, 42*(17), 6677-6682.

Ji, L., Miksche, S., Rimpf, L., & Farthing, G. (2009). CO_2 chemical solvent screening. Paper presented at the *8th Annual Conference on Carbon Conference and Sequestration. Pittsburgh, PA, USA*, 4-7.

Khaisri, S., deMontigny, D., Tontiwachwuthikul, P., & Jiraratananon, R. (2009). Comparing membrane resistance and absorption performance of three different membranes in a gas absorption membrane contactor. *Separation and Purification Technology, 65*(3), 290-297.

Khaisri, S., deMontigny, D., Tontiwachwuthikul, P., & Jiraratananon, R. (2011). CO_2 stripping from monoethanolamine using a membrane contactor. *Journal of Membrane Science, 376*(1), 110-118.

Khayet, M. (2011). Membranes and theoretical modeling of membrane distillation: A review. *Advances in Colloid and Interface Science, 164*(1), 56-88.

Kittel, J., Idem, R., Gelowitz, D., Tontiwachwuthikul, P., Parrain, G., & Bonneau, A. (2009). Corrosion in MEA units for CO2 capture: Pilot plant studies. *Energy Procedia, 1*(1), 791-797.

Koonaphapdeelert, S., Wu, Z., & Li, K. (2009). Carbon dioxide stripping in ceramic hollow fibre membrane contactors. *Chemical Engineering Science, 64*(1), 1-8.

Kosaraju, P., Kovvali, A., Korikov, A., & Sirkar, K. (2005). Hollow fiber membrane contactor based CO2 absorption-stripping using novel solvents and membranes. *Industrial & Engineering Chemistry Research, 44*(5), 1250-1258.

Lawson, K. W., & Lloyd, D. R. (1997). Membrane distillation. *Journal of Membrane Science, 124*(1), 1-25.

Li, J., & Chen, B. (2005). Review of CO_2 absorption using chemical solvents in hollow fiber membrane contactors. *Separation and Purification Technology, 41*(2), 109-122.

Mackie, J., & Meares, P. (1955). The diffusion of electrolytes in a cation-exchange resin membrane. I. theoretical. *Proceedings of the Royal Society of London.Series A.Mathematical and Physical Sciences, 232*(1191), 498-509.

Mansourizadeh, A., & Ismail, A. (2009). Hollow fiber gas–liquid membrane contactors for acid gas capture: A review. *Journal of Hazardous Materials, 171*(1), 38-53.

Mansourizadeh, A., & Ismail, A. F. (2011). CO_2 stripping from water through porous PVDF hollow fiber membrane contactor. *Desalination, 273*(2), 386-390.

Mccabe, W. L., Smith, J. C., & Harriott, P. (2005). *Unit operation of chemical engineering* (6th ed.)

Naim, R., Ismail, A., & Mansourizadeh, A. (2012). Preparation of microporous PVDF hollow fiber membrane contactors for CO_2 stripping from diethanolamine solution. *Journal of Membrane Science, 392*, 29-37.

Nakao, S. (1994). Determination of pore size and pore size distribution: 3. filtration membranes. *Journal of Membrane Science, 96*(1), 131-165.

Oyenekan, B. A. (2007). *Modeling of Strippers for CO_2 Capture by Aqueous Amines,* The University of Texas at Austin, Dissertation

Phattaranawik, J., Jiraratananon, R., & Fane, A. (2003). Effect of pore size distribution and air flux on mass transport in direct contact membrane distillation. *Journal of Membrane Science, 215*(1), 75-85.

Rabiller-Baudry, M., Le Maux, M., Chaufer, B., & Begoin, L. (2002). Characterisation of cleaned and fouled membrane by ATR—FTIR and EDX analysis coupled with SEM: Application to UF of skimmed milk with a PES membrane. *Desalination, 146*(1), 123-128.

Rochelle, G. T. (2009). Amine scrubbing for CO_2 capture. *Science, 325*(5948), 1652-1654.

Simioni, M., Kentish, S. E., & Stevens, G. W. (2011). Membrane stripping: Desorption of carbon dioxide from alkali solvents. *Journal of Membrane Science, 378*(1), 18-27.

Srisurichan, S., Jiraratananon, R., & Fane, A. (2006). Mass transfer mechanisms and transport resistances in direct contact membrane distillation process. *Journal of Membrane Science, 277*(1), 186-194.

Stanojevi, M., Lazarevi, B., & Radi, D. (2003). Review of membrane contactors designs and applications of different modules in industry. *FME Transactions, 31*, 91-98.

Veldman Ray. (1989). How to reduce amine losses. *Petroenergy.*

Wallace, J. S. (2006). Development of a carbon dioxide continuous scrubber (CDOCS) system for alkaline fuel cells. University of Canterbury, Dissertation.

Wijmans, J., & Baker, R. (1995). The solution-diffusion model: A review. *Journal of Membrane Science, 107*(1), 1-21.

Yamaguchi, T., Nakao, S., & Kimura, S. (1993). Design of pervaporation membrane for organic-liquid separation based on solubility control by plasma-graft filling polymerization technique. *Industrial & Engineering Chemistry Research, 32*(5), 848-853.

Yang, H., Xu, Z., Fan, M., Gupta, R., Slimane, R. B., Bland, A. E., & Wright, I. (2008). Progress in carbon dioxide separation and capture: A review. *Journal of Environmental Sciences, 20*(1), 14-27.

Yeh, J. T., Pennline, H. W., & Resnik, K. P. (2001). Study of CO_2 absorption and desorption in a packed column. *Energy & Fuels, 15*(2), 274-278.

Zhang, J. (2011). *Theoretical and Experimental Investigation of Membrane Distillation,* Victoria University, Dissertation.

Zhang, J., Dow, N., Duke, M., Ostarcevic, E., Li, J., & Gray, S. (2010). Identification of material and physical features of membrane distillation membranes for high performance desalination. *Journal of Membrane Science, 349*(1), 295-303.

Zhao, C., Zhou, X., & Yue, Y. (2000). Determination of pore size and pore size distribution on the surface of hollow-fiber filtration membranes: A review of methods. *Desalination, 129*(2), 107-123.